SCRATCH BEHAVIOR OF MULTIPHASE STYRENIC COPOLYMERS AND THE

INFLUENCE OF ENVIRONMENTAL CONDITIONING


A Dissertation

by

EHSAN MOGHBELLI


Submitted to the Office of Graduate and Professional Studies of
Texas A&M University
in partial fulfillment of the requirements for the degree of

DOCTOR OF PHILOSOPHY


| | |
|---|---|
| Chair of Committee, | Hung-Jue Sue |
| Committee Members, | Terry Creasy |
| | David Bergbreiter |
| | Hong Liang |
| Head of Department, | Ibrahim Karaman |

August 2014

Major Subject: Materials Science and Engineering

ABSTRACT

Scratch-induced surface deformation is a tribological research area that falls under the abrasive wear category. A variety of factors including high strain rate, large-scale deformation, non-linear material response, heat dissipation, and the evolution of a complex stress field, renders scratch a complex mechanical process. The dependence of polymers on testing rates, temperature, and pressure, along with the surface characteristics of the two materials in contact bring the rate, time, temperature, and pressure dependent behaviors of polymers, and the surface condition of the interacting surfaces also add to the complications of scratch analysis. In order to gain an in-depth understanding of polymer scratch behavior, this dissertation focuses on the scratch response of multiphase systems made up of a plastic matrix and a dispersed rubber phase. The introduction of a rubber phase and the effect it has on scratch behavior is explored through a number of factors including rubber size and type, environmental conditioning through heat processing, moisture exposure, and water immersion.

A standardized progressive load scratch test (ASTM D7027/ISO 19252) is used to examine the mechanical response to scratch deformation in ASA and ABS systems with varying rubber particle size. Previous simulation results from finite element methods are used to assess the scratch response of the multiphase systems and comparisons are made to results based on single phase plastics and their respective scratch behavior. The key scratch damage transitions identified and studied are: (1) the onset of scratch groove formation, (2) the onset of periodic cracking, (3) the onset of material removal (plowing), and (4) the onset

of scratch visibility. The onset of groove formation is generally related to the secant modulus at the point of compressive yielding. The onsets of crack formation and plowing are more complex to quantitatively evaluate, and are strongly influenced by the material tensile and/or shear strength.

For ASA copolymers, enhanced scratch performance is observed in systems with rubber particles the size of 1 micron relative to 100 nm sized rubber particle systems, while ABS copolymers containing 100 nm sized rubber particles are more scratch resistant than ASA copolymer systems with similar rubber particle size and distribution. The fact that these three model systems exhibit similar mechanical properties in uniaxial tension and compression bulk testing does not explain their differences in scratch resistance based on our previous FEM modeling and experimental results for single phase systems. The local stress state generated by the rubber particles and the scratch process at the surface, along with changes in surface coefficient of friction, are used to explain these findings.

In order to minimize orientation and residual stress effects from the injection molding process, heat treatments at temperatures above and below $T_g$ were carried out on ASAs with varying rubber content, rubber size, and rubber type. Low temperature annealing (LTA) was seen to reduce rubber orientation while having no impact on bulk mechanical properties, surface characteristics, or scratch resistance. On the other hand, high temperature annealing (HTA) minimized orientation and residual stress and showed no impact on bulk mechanical properties or surface characteristics, while also leading to a significant improvement in scratch resistance for high rubber content systems.

# DEDICATION

To:

My Loving Mother and Father:

Zohreh Eslami and Hassan Moghbelli

&

My Mentor, Professor Hung-Jue Sue

# ACKNOWLEDGEMENTS

TABLE OF CONTENTS

Page

LIST OF FIGURES

xi

# LIST OF TABLES

CHAPTER I

INTRODUCTION & LITERATURE REVIEW

## 1.1 Outline

This chapter provides a brief background on the origins of scratch testing and analysis, the standardization of scratch testing methods, and the research methods used to explore this topic. An extensive literature review of related research studies has been detailed in each corresponding section along with an overview on polymer scratch research. Motivations and goals for the current study will then be stated and explored to a small extent. An outline of this dissertation and a brief overview of the research will be provided as well.

## 1.2 Polymer Scratch Significance

Surface quality retention in durable polymer parts, from both a functional and an aesthetic point of view, has recently become one of the critical property attributes in material selection for many engineering applications. While producing a desirable surface finish for a polymer has an inherent level of difficulty, the true challenge lies in preserving the surface quality over the entire service life cycle. Scratch, which is a form of surface deformation, can be considered one of the primary causes for reductions in polymer surface quality upon frequent usage which necessitates research on the topic.

For polymer applications, the surface quality properties concerned herein can be broadly classified into surface aesthetics, structural integrity, and durability [1, 2]. Surface aesthetics, such as automotive exteriors and interiors or housing for electronic products and telecommunication devices, are important due to the fact that surface

scratches may reduce the product's value even though their intended functionality is still generally unaffected. As for applications like food packaging, e.g., military MRE's (Meals Ready to Eat), retaining the structural integrity of the packaging films is a major concern for preservation of food quality and safety. Scratches, if formed on food packaging films, can cause them to tear prematurely or compromise its barrier properties, which in turn may spoil the food inside. In coating applications, a scratched surface may lead to corrosion or damage of the underlying metal or wood substrate. Therefore, a coating must maintain its mechanical integrity for the entire expected service life of a product. Surface durability is also appreciated in the data storage industry, where scratches on hard drives and optical storage devices can cause permanent loss of data. Another important concern, from a structural point of view, is that scratches can act as stress concentration points, leading to a reduction in load bearing capacity that will ultimately result in the premature fracture and failure of a structural component. Scratch is also relevant to micro-mechanical devices and up-and-coming nano-devices where scratch formation can easily result in a total loss of functionality due to the small scale of these devices.
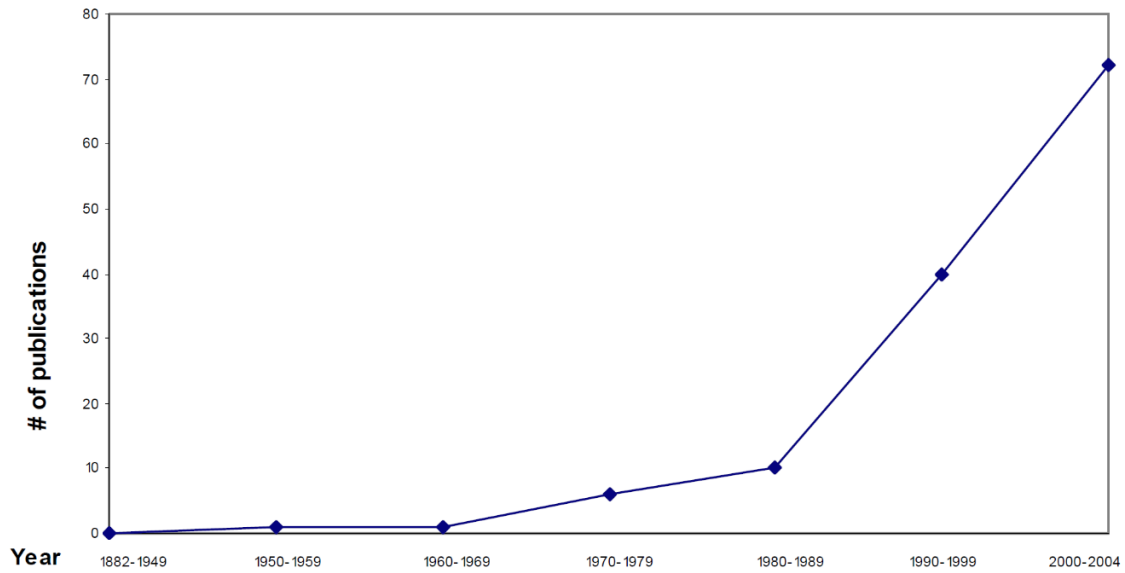
**Figure 1. Progress of scratch research over past few decades.**

In view of the critical issues mentioned above, it is evident that surface scratch is of particular concern for polymeric materials. To further illustrate this point, a graph of how much research studies relating to polymer scratch have increased over the past few decades is shown in Figure 1. The large jump in research topics related to polymer scratch can be seen especially in the last few decades. In this chapter, a brief review of polymer scratch research is given in order to highlight different aspects of polymer scratch behavior. Important factors and considerations that motivate the current study are also discussed. Finally, different components of this research and their arrangements are outlined.

**1.3 Polymer Scratch Research**

The science of tribology, which is the study of two surfaces in contact against one another, can be dated back to the 15th century with Leonardo da Vinci and his

3

documented experiments studying two surfaces in a relative sliding motion. Several hundred years later, Charles de Coulomb established the first fundamental laws of friction. A mineral hardness scale based on the fact that harder minerals can scratch softer minerals was developed by Friedrich Mohs in 1812. Amontons and Coulomb made significant progress in tribology within this time period by devising the laws of friction.

Tribology, defined specifically as the science of two contacting surfaces in relative motion, focuses on three major branches: (1) friction, (2) wear, and (3) lubrication. Wear can be a product of abrasion, adhesion, tribologically-assisted corrosion, or surface fatigue. Abrasive wear is the result of a single-pass or a multi-pass encounter between surfaces. The contact developed between two surfaces can either be a single asperity (car keys on a surface) or a multi-asperity (sandpaper polishing a surface) contact. Scratch, which falls under abrasive wear, will be designated as a single pass process with a single asperity contact using either a constant or increasing load in this study for simplification. This categorization, developed by Professor Klaus Friedrich, has been shown as a schematic in Figure 2(a) where the scratch definition is denoted by a red line in Figure 2(b).

**(a)**



**(b)**
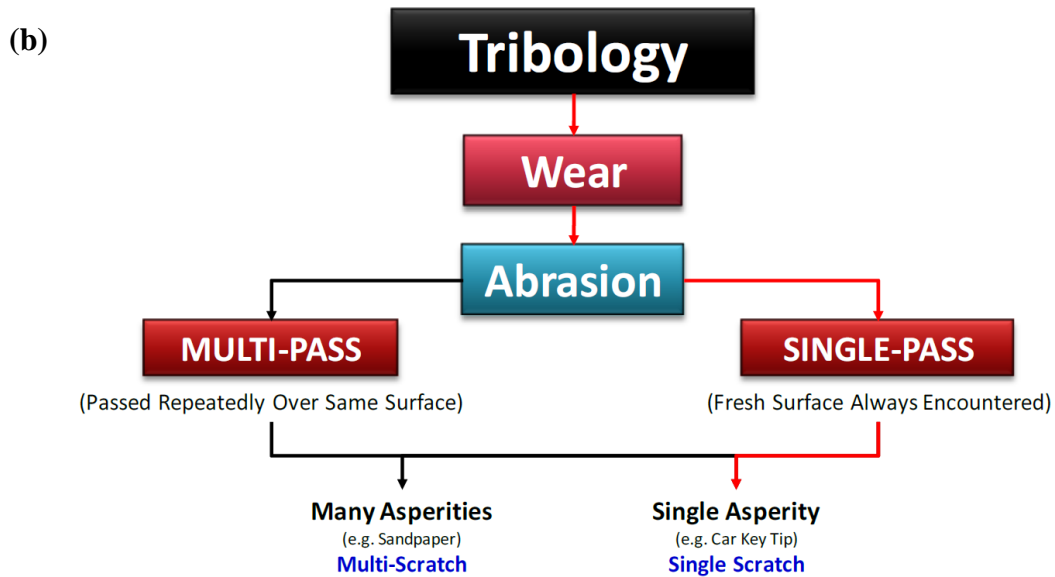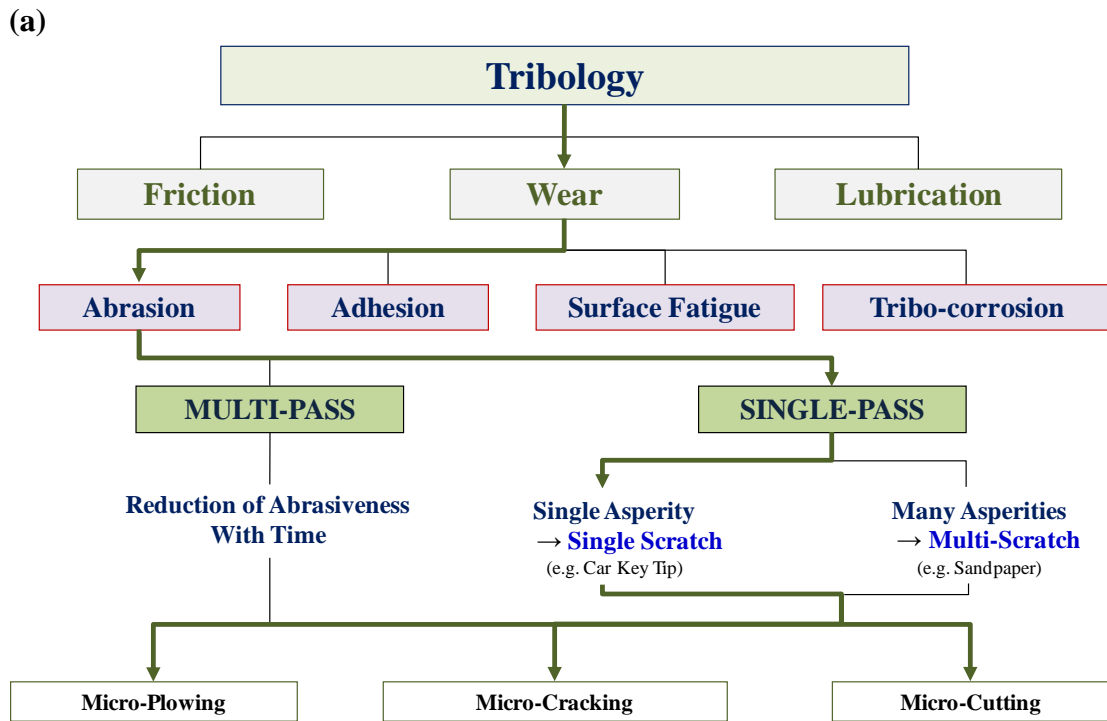


**Figure 2. Tribology a) classification schematic and b) definition of scratch in this study.**

5

A representation of a single pass, single asperity scratch deformation is shown in Figure 3, where a rigid spherical tip traverses across a polymer substrate at a specific velocity under a constant or changing normal load. Scratch resistance is generally determined by the ability of a material to resist surface deformation due to this sliding indentation of an asperity under the application of a prescribed normal load.
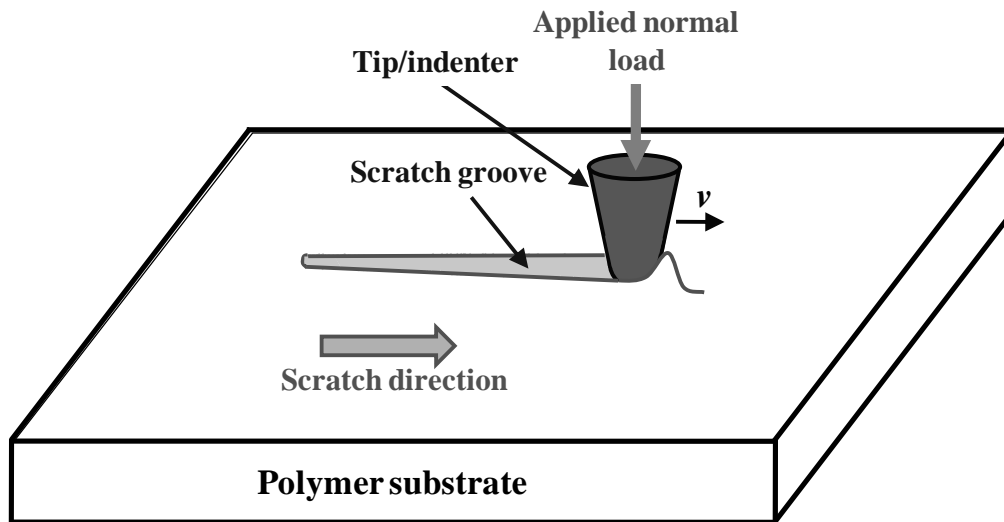


**Figure 3. Schematic of the scratching process.**

Although retention of surface quality in polymers has demanded attention, due to their susceptibility to surface deformation and damage under low contact loads when compared to metals and ceramics, significant breakthroughs in the fundamental knowledge of scratch behavior in polymers has only recently been achieved. Prior to that, there was a lack of standardized testing methodologies and equipment to administer adequate scratch experiments on polymers. As a result, researchers developed their own unique testing equipment to perform scratch experiments under a specific set of conditions. Methods that were used to evaluate scratch resistance ranged from simplistic

test methods, such as the pencil hardness test, to more sophisticated methods like the Taber test, pin-on-disc test, Ford five-finger test, and the single-pass pendulum sclerometer [3]. A complete list of the testing methods and equipment used by various researchers can be seen in these articles [1, 4].

Furthermore, other than the variation in testing techniques, the methodologies utilized for a quantitative evaluation of scratch performance also varied considerably. These ranged from subjective human observers to more objective optical instruments like high-resolution scanners, atomic force microscopy, and scanning electron microscopy. These factors unfavorably lead to a difficult situation for researchers to verify and compare experimental results published in the literature, thus inevitably hindering fundamental understanding of polymer scratch behavior. Fortunately, recent establishment of the ASTM/ISO scratch test standard [5], has led to significant progresses in understanding the fundamental nature of polymer scratch behavior. The test employs a linearly increasing normal load applied on a 1 mm diameter, spherical, stainless steel tip for scratch testing and generates a continuous progression of deformation and damage on the scratch path. This allows for a straightforward analysis and establishment of a structure-property relationship. An illustration of the scratch testing machine developed by Surface Machine Systems (SMS) in cooperation with the Polymer Scratch Consortium at Texas A&M University and an example of a scratch tested plastic plaque are shown in Figure 4. Furthermore, the combined usage of a commercially available software package (Automatic Scratch Visualization (ASV©) and the ASTM/ISO scratch test standard enables meaningful quantitative evaluation of the

onset of scratch visibility, which is a key criterion for polymers used in environments where they must be aesthetically pleasing. The corresponding physical origins of a scratch can also be investigated as it has been shown that the development of such deformation features is responsible for the scratch to become visible [6].
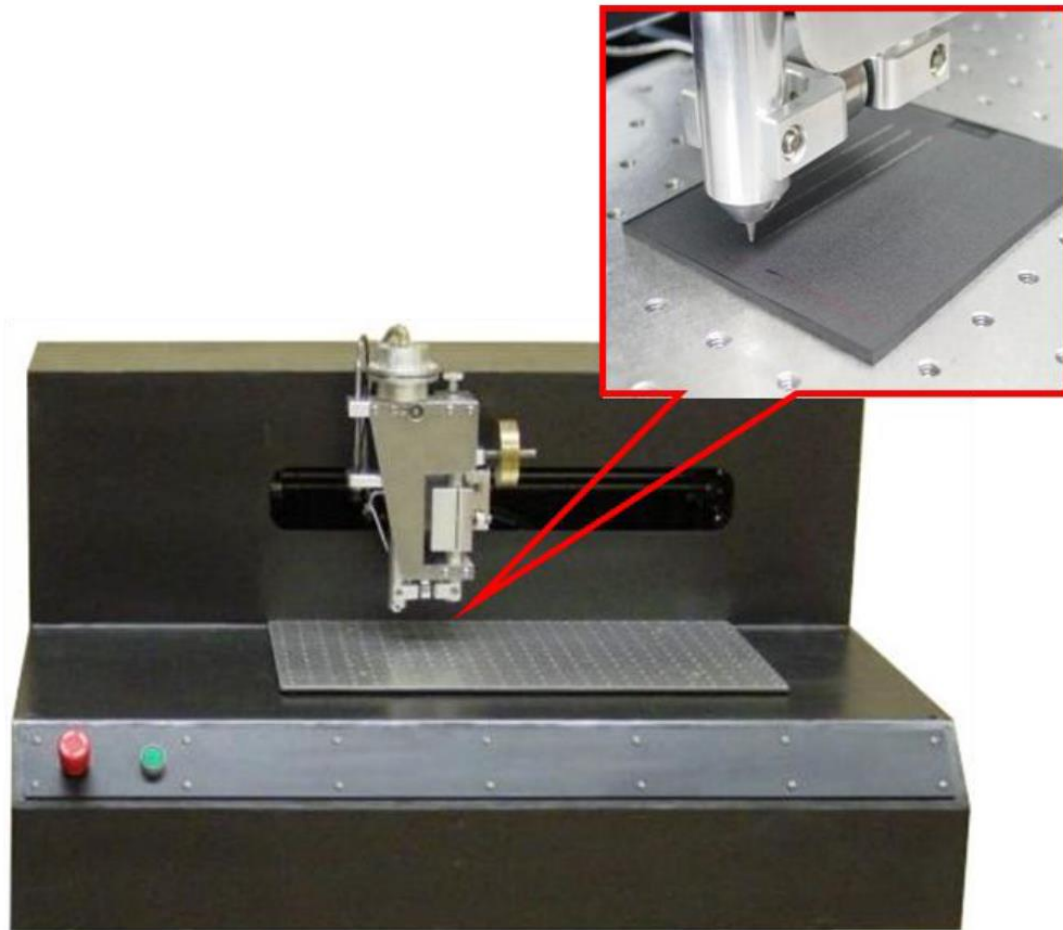


**Figure 4. Illustration of the scratch machine and testing process.**

The onset and extent of different scratch-induced deformation features, such as scratch depth, shoulder height and scratch width (shown schematically in Figure 5), micro-cracks or crazes, fish-scale formation, and plowing, depends on a rather complex

surface deformation process that involves the following: a dynamic rate dependent deformation, surface contact between the tip and the substrate, friction interaction, heat dissipation, and large-scale material and geometrical nonlinearity. Another level of complexity is added when considering polymers due to their unique material and surface properties. Since the development of scratch-induced damage features in polymers involves deformation comparable to the bulk, extensive research work has been carried out to correlate the evolution of scratch-induced deformation features with the bulk mechanical and surface properties [7-14].
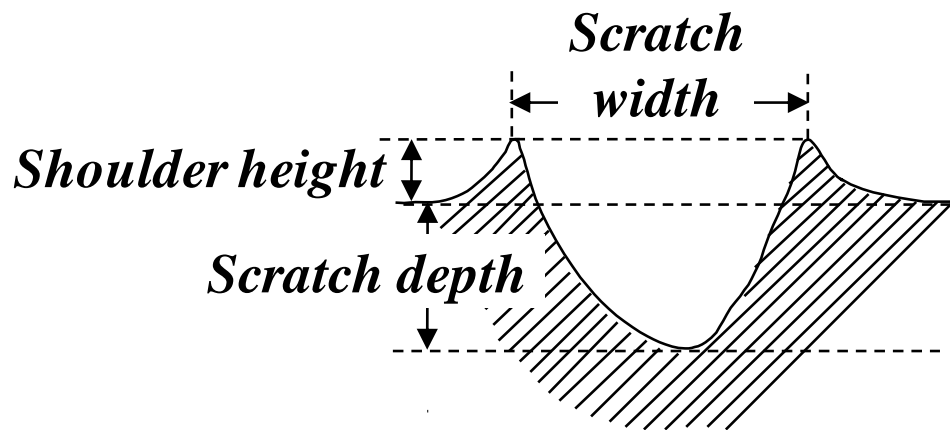


**Figure 5. Schematic of the cross section of a scratch groove where the scratch direction is perpendicular to the page.**

Parametric studies of polymers using numerical methods such as finite element methods (FEM) simulations are possible unlike experimental methods. This advantage stems from the fact that in numerical methods parameters of interest can be decoupled in a systematic fashion and studied independently. Elastic modulus, tensile strength, and ductility are examples of such parameters which are not easily decoupled thus limiting

the capability of experimental methods. To better understand scratch behavior, it is important to complement experimental methods with proper modeling and simulation investigations for fundamental understanding of scratch. Addressing issues with numerical approaches also relate to the complex material and mechanical properties of polymers, including viscoelasticity, inelastic deformation, strain softening, and other mechanical responses.

To study the mechanics involved during the scratch process, FEM [15] has been widely used by the researchers due to its capability to formulate physical phenomena and unique material response into a single analysis. Even so, the research effort on scratch behavior using FEM remains scanty and mostly restricted to the study of indentation [16]. Lee et al. [17] performed FEM analysis by modeling a steel ball scratching a rotating polycarbonate (PC) disk using ABAQUS®. Although a realistic material law was adopted for the PC substrate, they over-simplified a three-dimensional problem into a two-dimensional plane-strain problem. Bucaille et al. [18] and Subhash and Zhang [19] performed 3-D simulations of a displacement-controlled scratch-induced deformation process by employing a rigid conical indenter on elastic-perfectly-plastic and bilinear materials. Unfortunately, their 3-D FEM models did not take into account the strain softening-strain hardening nature of the polymers. Researchers in the last decade have extensively used FEM along with accompanying experiments to study the underlying mechanics involving scratch deformation of polymers following the ASTM D7027-05 scratch test [2, 7, 9, 20-22] and other testing methods [12, 23-27].

To understand the development of the stress state and corresponding material response during the scratch process, FEM modeling along with the ASTM/ISO standard scratch tests was carried out by Jiang et al. [7]. The primary focus of the study was to investigate the evolution of scratch-induced deformation features in the scratch groove (i.e., the development of fish-scale, crack, etc.) not taking into account the scratch depth and shoulder height formation along the scratch path. The stress analysis using FEM simulation showed that as the scratch tip moves with an increasing normal load, the material in front of the tip experiences tensile stress, which quickly changes into compressive and then back to tensile again (Figure 4). Since the development of scratch-induced deformation features depends on both stress state and material type, variation in deformation features (fish-scale, micro-crack etc.) in the scratch groove for different polymers was observed experimentally. At a low scratch normal load, the scratch penetration depth was low due to small plastic deformation. The extent of this so-called "mar" region and the development of scratch-induced damage features in the scratch groove (fish-scale, crack etc.) were observed to vary with the material type (Figure 6). Based on the experimental data, they developed a polymer scratch damage evolution map (Figure 7) to qualitatively differentiate the scratch behavior based on the respective material constitutive relation. A similar scratch deformation map, developed by other researchers [28-30] using conical indenter and constant or dead weight scratch normal load, showed the evolution of different scratch-induced deformation to vary with the scratch speed due to the change in strain rate imposition.

11
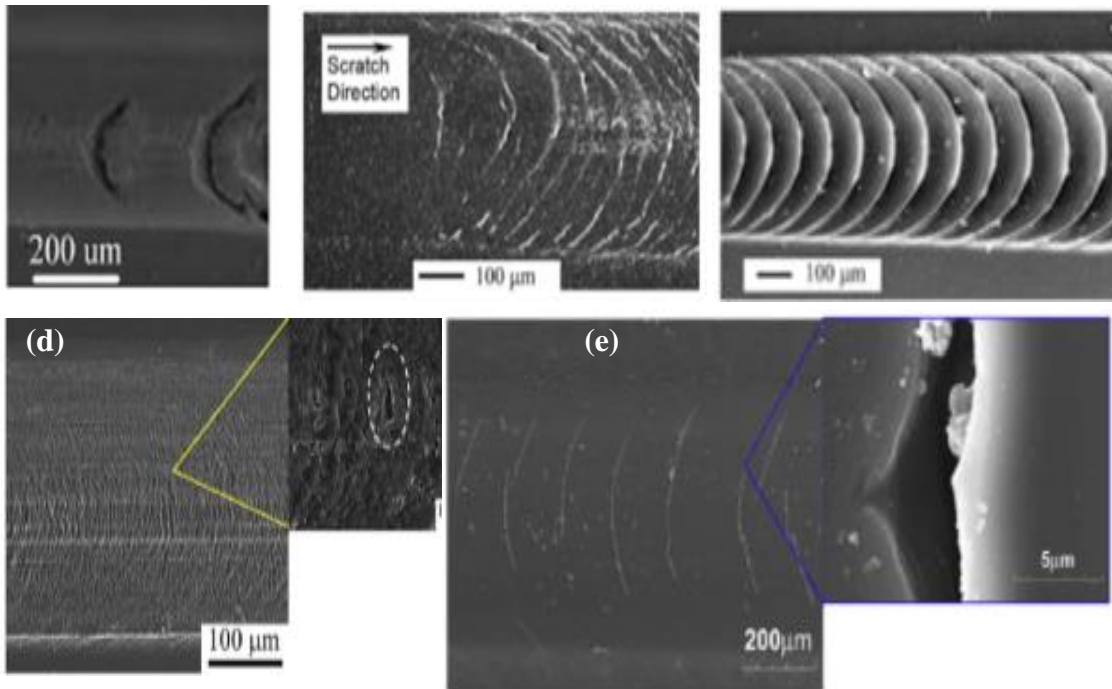
**Figure 6. SEM of - (a) Parabolic crack pattern in PC; (b) Onset of fish-scale formation in TPO; (c) Well developed fish-scale in TPO; (d) Pseudo fish-scale pattern mixed with crazes/voids in PS; (e) Parabolic crack pattern in Epoxy [7].**
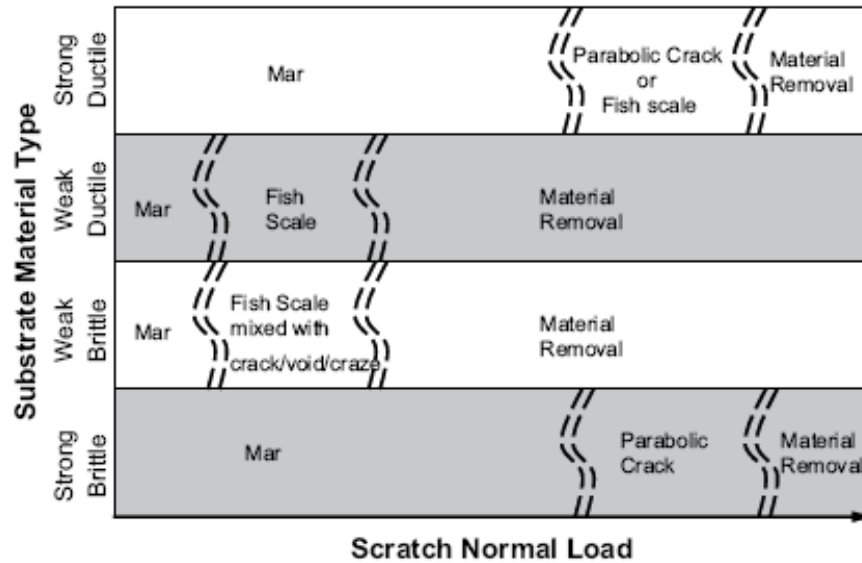
**Figure 7 Polymer scratch damage evolution map [7].**
**(Figure reprinted from Polymer, 50, Jiang, H., Browning, R.L., Sue, H.-J.,**
**Understanding of scratch-induced damage mechanisms in polymers, 4056-4065,**
**Copyright (2009), with permission from Elsevier)**

Parametric studies on scratch behavior of polymers using FEM have long been carried out to study the effect of various material and surface properties on scratch-induced deformation mechanisms. Simplified material models, not including mechanisms involving node or element separation during the scratch process, and rate, time, temperature and pressure dependent response of polymers, have been used to gain fundamental understating on the effect of various material constitutive parameters on scratch-induced deformation. In an earlier attempt, FEM parametric study was performed [9] by employing an elastic-perfectly-plastic model to investigate the effect of material and surface properties on scratch behavior of polymers. It was concluded that the yield stress and coefficient of surface friction are the most important parameters that have significant influence on the residual scratch depth of a polymer after the scratch

13

process. Increasing the yield stress and/or reducing the coefficient of friction induce a shallower residual scratch depth, thus improving the scratch performance of polymers. Poisson's ratio has shown not to influence the residual scratch depth. Furthermore, Young's modulus in the range of 1.65 to 4 GPa does not significantly affect the residual scratch depth, which was similarly studied by Xiang et al. [31] for 1 mm spherical tip based on the Hamilton and Goodman expression [32, 33].

Pelletier et al. [24] employed FEM for elastic-plastic contact and showed that the shape of the residual groove during scratching is related to the plastic strain field in the deformation beneath the indenter. Bucaille et al. [12] employed experimental work and FEM to study the effect of compressive strain hardening slope on piling-up phenomena during scratch. They concluded that a larger strain hardening led to greater elastic deformation and thus, less plastic strain [12, 27], which improved the scratch resistance. In case of metals and metallic alloys, Bellemare et al. [34] reported a decrease in pile-up height (shoulder height) with the increase in strain hardening exponent using pure Copper and Copper/Brass alloy. However, several factors including constitutive model simplicity, heat dissipation during scratch, rate and temperature dependence, complexities of tip/surface contact area, etc. limit the extensive scratch investigations using numerical methods such as FEM.

Extensive experimental work has also been carried out to study the effect of bulk mechanical and surface properties on the evolution of different scratch-induced deformation features. Hadal et al. [36] showed that both higher modulus and yield strength are responsible for superior resistance to scratch deformation using different

14

grades of ethylene-propylene copolymers and polypropylene. Unfortunately, only tensile properties were utilized in drawing these conclusions. Xiang, et al. conducted a study on the relationship between polymer scratch deformation phenomena and mechanical properties based on a variety of amorphous and semi-crystalline polymers [33]. Jardret and Morel studied the effects of temperature and strain rate on the scratch deformation of PMMA [34]. Their study found that as the temperature increases, the material around the scratch tip is deformed quite easily and also that if the scratch speed is increased, the brittleness of the material increases and fracture occurs earlier. A similar study was carried out by Browning, et al. to investigate the effect of scratch speed on the scratch behavior of soft TPOs [35]. The findings were similar in that, even though the TPOs were soft and rubbery, the material behaved in a more rigid and brittle fashion at higher testing speeds. In particular, the surface tensile stresses were used to gauge the scratch resistance of the polymers with respect to onset of plastic flow or brittle surface fracture. However, no detailed knowledge was gained in addressing correlation between the material properties and scratch damage mechanisms. Browning et al. [8] investigated the effect of acrylonitrile (AN) content and molecular weight (MW) on scratch behavior of styrene-acrylonitrile (SAN) random copolymers by employing ASTM/ISO standard scratch test. The critical load for onset of scratch groove formation, periodic micro-cracking, and plowing were measured and correlated with the compressive and tensile properties of the model SAN systems. Since the compressive properties of the chosen model SAN systems were virtually the same, they concluded that increasing the AN content or MW can have a positive effect on improving the scratch resistance as it

increases the tensile strength and ductility. Furthermore, Jiang et al. probed the effects of surface roughness on frictional behavior and its relationship to scratch behavior [36]. Their findings show that if the surface roughness increases, the friction during scratching is reduced, leading to improved scratch resistance.

The effect of coefficient of friction on scratch behavior of polymers has also been investigated experimentally by employing the ASTM D7027-05 standard scratch test on four model thermoplastic olefin (TPO) systems, with and without slip agent and talc fillers [36]. Through the standard scratch test and microscopy, it was shown that a reduction in coefficient of friction delays the fish-scale formation in the TPO systems. Also, reduction in coefficient of friction induces shallower scratch depth, which corroborates the FEM findings described above [9]. Using their analytical expressions for stress field due to a circular contact region carrying a hemispherical Hertzian normal pressure and a proportionally distributed shearing traction, Hamilton and Goodman [32, 33] showed that an increase in surface friction intensifies and move the maximum yield parameter from subsurface toward the surface, and, thus, inducing greater deformation. According to the study, a maximum tensile stress also develops at the rear end of the circular contact when increasing the surface friction, which can be thought of responsible for the ring crack in brittle materials.

**1.4 Research Scope**

One way many researchers have attempted to enhance the mechanical properties of polymers is by adding nanoscale fillers to make polymer nanocomposites. Indeed, the mechanical properties of polymer nanocomposites were greatly improved over those of

16

the neat systems and studies in polymer nanocomposite scratch behavior followed suit [37- 41]. In a study on nanoclay-reinforced polypropylene (PP) and polyethylene, Yuan et al. found that incorporation of the nanocomposites decreased the susceptibility of the systems to micro- and nano-scale deformation in the form of surface ripples [40]. They attributed this improvement to increases in crystallinity, elastic recovery, modulus, and yield strength. In a comprehensive review of nanocomposite scratch, Dasari et al. points out that incorporation of nanofillers does not necessarily bring on improvements [41]. This was also shown in work carried out by Moghbelli et al. on epoxy nanocomposites [38]. The incorporation of $\alpha$-Zirconium Phosphate or core-shell rubber particles into epoxy matrices was found to improve the mechanical properties which should lead to enhanced scratch resistance, but the resulting scratch resistance of the composites were actually lower. This method of improving mechanical properties is not very sound because the incorporation of fillers into a polymer matrix alters its physical nature and limits the understanding of microstructural parameters on tribological behavior. Browning et. al. [31] studied a soft (TPO) composed of EPR and PP at 70/30 ratio where scratch behavior depended on EPR internal phase morphology and crystallinity of the ethylene part. Epoxy nanocomposites containing hard and soft particles in the study by Moghbelli et. al. [32] were shown to be at a disadvantage compared to the neat epoxy resin in terms of scratch resistance and their corresponding critical normal loads for crack formation. This shows us improved tensile properties or fracture toughness alone do not lead to enhanced scratch resistance as expected. These previous studies on scratch behavior of multi-phase polymers which exhibited similar scratch damage transitions to

single phase polymers, imply the importance of surface and subsurface morphology and other undetermined factors which must be explored. However, the multi-axial nature of the scratch stress field presents a challenge when attempting to relate the mechanical properties to the resulting scratch deformation. Numerous researchers have tried novel ways of relating scratch behavior to material properties.

Scratch behavior of multi-phase, non-homogeneous, or anisotropic polymer systems have been briefly investigated as listed above, while further studies are required to analyze and comprehend their scratch resistance and determine material characteristics and properties affecting scratch. The scratch behavior in two (rubber/plastic) phase systems is not fully understood and requires research attention. The purpose of this research effort is to determine the role of various blend parameters on scratch response. These studied parameters include: rubber concentration/size/type, thermal history, moisture content, and injection molding conditions. The nature of the scratch damage transitions for these systems is also examined.

In summary, the primary objective of this research is to examine the influence of introducing a dispersed rubber phase, in a polymer matrix, on the system's scratch behavior by better understanding the stress state alteration caused by the soft dispersed particles. When a better understanding of this subject is obtained, the optimization of a polymeric material's scratch performance may be achieved. Furthermore, the influence of environmental conditioning on scratch resistance, which is of paramount importance, will be examined through various moisture exposure setups (moisture chamber and water immersion). The findings of this study will lead to improved material selection

and design of polymeric products with respect to their scratch resistance and surface properties.

**1.5 Layout of the Dissertation**

The brief review of polymer scratch research and the corresponding literature review presented above in Chapter I, covering the fundamental aspects of polymer scratch behavior, provides the groundwork to perform a comprehensive study on the evolution of scratch-induced deformation features in multiphase polymers.

Extensive scratch investigations on rubber modified Styrenic plastics containing various types and size of rubber particles are provided in Chapter II. The corresponding damage features observed in these multiphase systems are discussed and compared to previous results for single phase polymers. In Chapter III, the rubber content was chosen as a variable to investigate the influence of heat treatment at temperatures above and below $T_g$ on scratch behavior of SAN based multiphase systems. The results indicate that annealing at high temperatures significantly enhances scratch resistance for systems with high rubber content, which through AFM and contact angle measurements, are related to the changes in rubber morphology and concentration at the surface. Environmental conditioning through high temperature annealing, moisture exposure, and water immersion, on the aforementioned multiphase systems, and the resulting effects on their scratch behavior is the focus of Chapter IV. The results indicate that the rubber size and type determine the influence of high temperature annealing on scratch resistance due to the rubber orientation and morphology at the surface and the corresponding surface shear strength. Water immersion was seen to significantly enhance scratch resistance in

19

ASAs while minimally impacting ABS. Water cluster formation at the surface of ASAs leading to a reduction of surface coefficient of friction is speculated to be the reason for this enhanced scratch resistance. In Chapter V, an extensive effort is made to understand the effect of moisture exposure and absorption on scratch resistance through three model PMMA systems. The effect of moisture on scratch performance is correlated with the type of water absorption theories indicating the possibility of water cluster formation in polar site bonding theory, in contrast to the free volume theory. Finally, a brief summary of this work and concluding remarks are given in Chapter VI where the significance of this research is summarized. Potential ideas and considerations for future complementing research work in this area are also included in this chapter.

CHAPTER II

EFFECTS OF RUBBER PARTICLE SIZE AND TYPE ON SCRATCH

BEHAVIOR OF MULTI-PHASE STYRENIC-BASED COPOLYMERS

## 2.1 Synopsis

Effects of rubber size and type on scratch performance of two styrenic copolymers, acrylonitrile styrene acrylate (ASA) and acrylonitrile butadiene styrene (ABS) were investigated. ASA with rubber particle sizes of 100 nm and 1 μm, and ABS with rubber particle size of 100 nm were examined. Linearly increasing normal load scratch tests were performed according to the ASTM D7027/ISO 19252 standard. A noticeable drop in scratch resistance is found in ASA containing nano-sized rubber particles when compared to ASA containing micron-sized rubber particles. ABS is observed to exhibit a higher scratch resistance when compared to ASA with comparable rubber particle size. Furthermore, ABS shows higher moisture sensitivity in terms of scratch resistance relative to ASA. Detailed deformation and damage mechanisms have been investigated to explain the observed differences in scratch performance of the model systems. Implication of the present findings for design of scratch resistant polymers is discussed.

Keywords: Rubber modification, acrylonitrile styrene acrylate, acrylonitrile butadiene styrene, scratch resistance, damage mechanisms.

## 2.2 Introduction

Polymeric materials are widely utilized for durable goods applications due to their low cost, high strength to weight ratio, and ease of fabrication. However, the scratch resistance of polymers is seen to be considerably less than that of competing ceramics and metals. Hence, polymer scratch resistance is a present day topic of research interest in industry and academia.

Scratch, which can be defined as a rigid tip indenting and traversing a polymer surface simultaneously, has been considered as a branch of abrasion in tribology [42, 43]. Various experimental techniques have been developed over the years to measure the scratch resistance of polymers with limited success [44-48]. Recently, a standardized test methodology, designated as the ASTM D7027-05/ISO 19252 standard [49, 50], has been established and used extensively for quantitative evaluation of polymer scratch resistance. By employing this ASTM standard, numerous quantitative scratch performance evaluation and structure–property relationship investigations have been carried out [49, 51-60]. The application of an increasing normal load, as prescribed in the standard, generates surface deformation with distinctive damage transitions throughout the scratch path, which may include onsets of groove formation, fish-scale development, microcracking, and plowing. Identification and analysis of these damage transitions are important for fundamental understanding of polymer scratch behavior.

Several attempts have been made to categorize the observed scratch damage features into scratch-deformation maps. Briscoe et al. [61, 62] concluded that the formation of scratch damage features in a specific polymeric system depends on the

normal load, testing speed, temperature, and cone angle of the scratch tip. Maeda et al. [63] emphasized the relationship between the frictional force and scratch damage by manipulating the cone angle of the scratch tips and viscoelastic properties of the formulated rubber compounds. More recently, Jiang et al. [56] investigated four distinctively different polymers and detailed the observed relationship between material properties and scratch-induced deformation features. Their efforts resulted in a scratch damage map which is useful for illustrating the importance of various material parameters and testing conditions on scratch-induced damage mechanisms. Jiang et al. [65] also provided an in-depth mechanistic description on how the scratch damage evolves. By using a three-dimensional finite element methods (FEM) analysis, they found that the material beneath the scratch tip experiences a compressive stress state while the material near the surface behind the scratch tip experiences a high magnitude of tensile stress. They also noticed an additional maximal tensile stress component develops in front of the scratch tip as the normal load increases, which eventually leads to plowing or cutting when the exerted tensile stress magnitude exceeds the strength of the material. The scratch studies mentioned above were largely based on single-phase polymers.

Although numerous studies on polymer scratch behavior have been carried out [42-69], significant research efforts are still needed to better understand the scratch-induced deformation and damage in polymers, specially, in multi-phase polymeric systems. For instance, in-depth analysis on the roles rubber particles play on scratch performance of rubber-modified polymers is still lacking. Even though rubber particles

23

can act as impact modifiers to increase toughness and ductility, they can also reduce modulus and strength of the polymeric system [64, 69], which complicates their influence on scratch behavior. Furthermore, choices of processing equipment and conditions can significantly affect their final phase morphology and skin-core characteristics.

In a recent study on a soft thermoplastic olefin (TPO) that consists of 70 wt.% ethylene-propylene rubber (EPR) and 30 wt.% polypropylene (PP), Browning et al. [54] observed that the crystallinity of the ethylene segment and the internal morphology of the EPR phase significantly affect the scratch behavior of the soft TPO. In another study, Moghbelli et al. [55] modified the skin-core morphology of PP thin sheets through post-processing thermal treatments. Their results suggest that the degree of surface crystallinity can significantly influence the scratch behavior. The above findings suggest that: 1) the surface or sub-surface phase morphology of semi-crystalline polymers, which can be modified by the processing conditions, plays an important role in polymer scratch behavior and 2) the material properties near the surface of a semi-crystalline polymer, which significantly affect the scratch performance, are likely to be different from those of the bulk. Moghbelli et al. [57] further showed that neat epoxy resin exhibits a higher resistance to crack formation during scratching compared to nanocomposites of the same epoxy filled with either synthetic clay nanoplatelets or core-shell rubber (CSR) nanoparticles. This implies that the improvements in tensile strength and modulus alone (i.e., epoxy/clay scenario) or fracture toughness and ductility alone (i.e., the epoxy/CSR scenario) may not necessarily lead to enhancement of scratch

performance. It should be noted that the surface damage mechanisms observed in this study [57] were consistent with single phase systems as the localized damage mechanisms due to inclusion of nanoparticles seemed not to influence the surface deformation features significantly.

The present research focuses on investigating how the rubber type and size influences scratch behavior of styrenic-based copolymers. Both acrylonitrile styrene acrylate (ASA) and acrylonitrile butadiene styrene (ABS) are composed of styrene–acrylonitrile (SAN) matrix containing rubber phase. The core of ABS is butadiene rubber, while that of ASA is acrylic elastomer. Our previous study [43] indicates that the scratch performance of ASA generally deteriorates with increasing rubber content, and is strongly related to their reduction in tensile and compressive yield strengths. The effect of moisture exposure on scratch performance of the above model systems was also probed. Implication of the present study for designing scratch resistant rubber-modified polymers is discussed.

## 2.3 Experimental

### 2.3.1 Materials

The ASA copolymers utilized in this study were provided by Styrolution GmbH (Frankfurt, Germany). They consist of a random copolymer SAN matrix and grafted polybutyl-acrylate (PBA) rubber particles with an average nominal diameter of 100 nm or 1 μm. In the SAN phase, the acrylonitrile content was controlled to be at 35 wt%, and the weight-average molecular weight (Mw) of SAN was chosen to be 104 kg/mol [43]. The test specimens were fabricated by injection molding with a fan gate design to spread

and slow the melt as it enters the mold cavity to ensure near-uniform molecular orientation across the width of the plaques. The plaques were 150 mm × 150 mm in rectangular shape and 6 mm in thickness. Nomenclature and physical characteristics of each system are listed in Table 1.

*2.3.2 Environmental Conditioning*

The ASA and ABS plaques were initially dried in a vacuum oven overnight at 80°C and a vacuum pressure of 30 mmHg. After drying, some of the plaques were placed into a moisture chamber with controlled relative humidity of 75% at 23°C for a duration of 28 days in which equilibrium water content was achieved. In addition to the dried samples, these moisture absorbed plaques were also scratch tested and analyzed to determine the effect of moisture on scratch performance of the model systems.

*2.3.3 Scratch Testing*

Scratch tests were carried out according to the ASTM D7027-05/ISO 19252 standard by using a progressive load range of 1–70 N at constant scratch speeds of 1 and 100 mm/s for a length of 100 mm. A stainless steel scratch tip with spherical geometry was used. The diameter of the scratch tip was 1 mm. A minimum of five scratch tests, oriented in the same direction as the melt flow direction, were performed on each plaque.

*2.3.4 Post Scratch Analysis*

Scratch damage analysis was carried out 24 hours after completion of scratch tests to allow for any viscoelastic recovery. The critical normal loads for the onsets of groove formation, cracking, and plowing were measured using a Keyence VK9700

Violet Laser Scanning Confocal Microscope (VLSCM). The onset points for microcracking and plowing were directly observed under the microscope. The onset of groove formation was determined using the height profile obtained from topographical imaging *via* VLSCM.

Longitudinal sections along the scratch direction were also examined to determine the sub-surface damage using an optical microscope. The samples were carefully cut in half using an Isomet® saw equipped with a diamond-tipped blade. The surface corresponding to the center-line axis of the longitudinal cut was wet-polished with a Struers Abramin disk polisher using a succession of P1200, P2400, and P4000 grit sandpapers (Struers, Buehler) and then affixed to a glass slide using epoxy adhesive. The glass slide was subsequently mounted in the diamond saw to cut the sample as close to the glass slide as possible. After this, the slide-mounted specimen was wet-polished to achieve a thickness of around 80 μm to allow for transmitted light observation under crossed-polars using the Olympus BX60 microscope.

## 2.3.5 Atomic Force Microscopy (AFM)

The characterization of sample morphology using AFM (Dimension, Veeco) was carried out by BASF SE. The AFM imaging and analyses were performed in Tapping Mode. The cantilever was excited at its resonance frequency and moved at a defined height over the sample surface. Thus, interaction forces cause a variation in the oscillation amplitude of the lever. Furthermore, a phase shift between the excitation and response oscillation can be induced by different material properties like stiffness or adhesiveness. In addition to the height, this effect provides the material contrast

information on the sample (Phase images). An Olympus silicon tip was used with cantilever spring constant of 40 N/m. The smooth cross-section surfaces of the samples were prepared using microtome technique at -80°C. The AFM measurements were carried out at room temperature.

*2.3.6 Tensile and Compressive Analysis*

Dog-bone shaped specimens for tensile testing based on ASTM D638 type I geometry were prepared by BASF SE (Ludwigshafen, Germany). The nominal length, thickness, and width of the narrow section were 170, 4, and 10 mm, respectively. The test was performed at constant crosshead speeds of 5 and 50 mm/min under ambient temperature using a screw-driven Sintech2 load frame equipped with a 30 kN load cell and MTS632 extensometer.

Specimens for uniaxial compression testing were prepared using plaques with 6 mm thickness. The compression specimens were precisely cut by an Isomet VR Precision Saw 1000 into prisms with sharp, clean edges. The surfaces of the specimens were carefully polished using 4000 grit silicon carbide polishing paper. The nominal dimensions of the prisms were 12.7 mm $\times$ 6 mm $\times$ 6 mm, and the actual dimensions were measured by a digital caliper. The uniaxial compression tests were performed following the ASTM standard D695-10 using a screw-driven load frame (MTSVR Insight) and an MTSVR extensometer with a gauge length of 25.4 mm. During compression testing, adequate lubricant (DupontVR TeflonTM Silicone Lubricant spray) was applied on the contact surfaces to reduce surface friction. The compression tests were performed at a crosshead speed of 2.5 mm/min.

*2.3.7 Coefficient of Friction Measurement*

To determine the coefficient of friction, $\mu$, between the Styrenic plaques and stainless steel surface, a flat smooth stainless steel tip with dimensions of 10 mm $\times$ 10 mm was used. The flat tip was installed on the scratch machine and tests were conducted at 5 N constant normal load for a distance of 60 mm at a velocity of 100 mm/s. Three tests were conducted for each system to obtain an average value of $\mu$.

**Table 1. Rubber particle size/type in each system**

|  | Rubber Type | Structure Type | Rubber Size | Color |
|---|---|---|---|---|
| **ASA100** | ASA | SAN grafted PBA rubber | $\approx$ 100 nm | Black |
| **ABS100** | ABS | SAN grafted PBD rubber | $\approx$ 100 nm | Black |
| **ASA1000** | ASA | SAN grafted PBA rubber | $\approx$ 1000 nm | Black |

**2.4 Results and Discussion**

AFM study of both sub-surface and midsection of each model system reveals the size and shape of the rubber particles (Figure 8). It can be seen that in both ASA100 and ABS100, the approximate rubber size is 100 nm; while in ASA1000, the rubber is 1 μm in size. The rubber phase close to surface is oriented in the mold flow direction. The variation in rubber shape throughout the thickness for each system is attributed to the injection molding process. A graphic description of rubber particle size distribution in each system is shown in Figure 9.
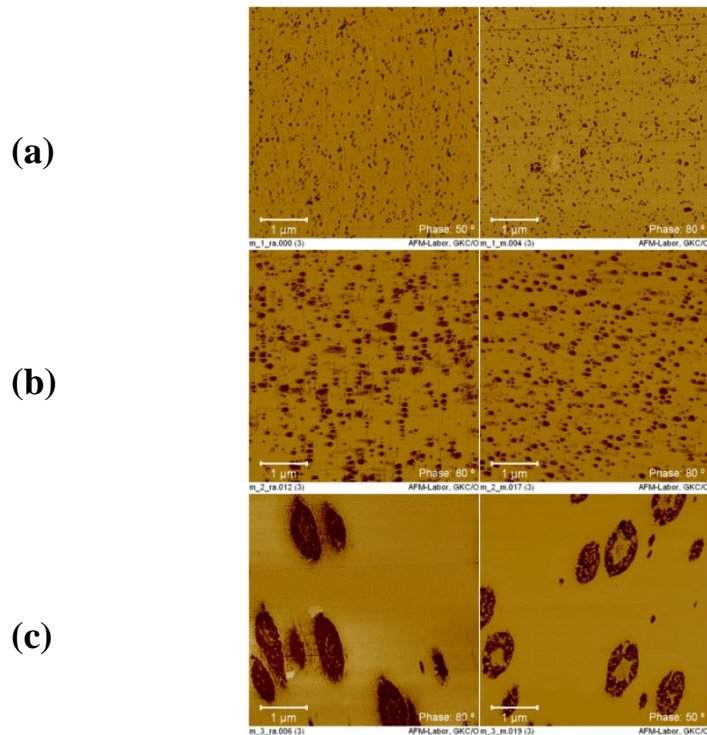
**Figure 8. AFM micrographs of the samples cross-sections: left – close to the surface, right – in the middle of the plaque, (a) ASA100 (b) ABS100 and (c) ASA1000.**

To study the influence of rubber particle size and type on scratch behavior, scratch-induced deformation in dry-conditioned samples were analyzed first. Critical normal loads for various scratch damage transitions including onsets of groove formation, cracking, and plowing for ASA100, ABS100, and ASA1000 are shown in Figure 10. ASA1000 exhibits a noticeable improvement in scratch resistance based on the onsets of groove formation, cracking, and plowing. In other words, inclusion of micron-sized rubber particles is more beneficial for scratch performance compared to the nano-sized counterparts in the systems investigated. Furthermore, as can be seen in the figure, the rubber type also significantly influences the scratch resistance as ABS100 shows a better scratch resistance compared to ASA100. Periodic crack formation along

30

the scratch path is a known scratch damage mechanism in styrenic polymers [42, 43]. Optical and surface topographical micrographs of the cracking transitions with the corresponding normal load for all three systems are shown in Figure 11.
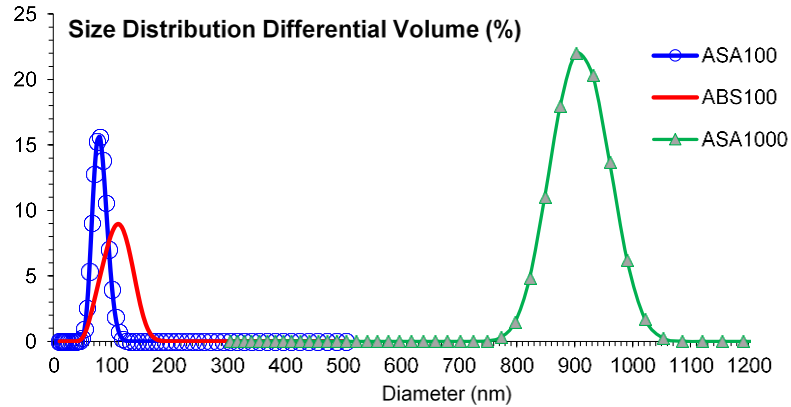


**Figure 9. Size distribution of rubber particles in each model system.**
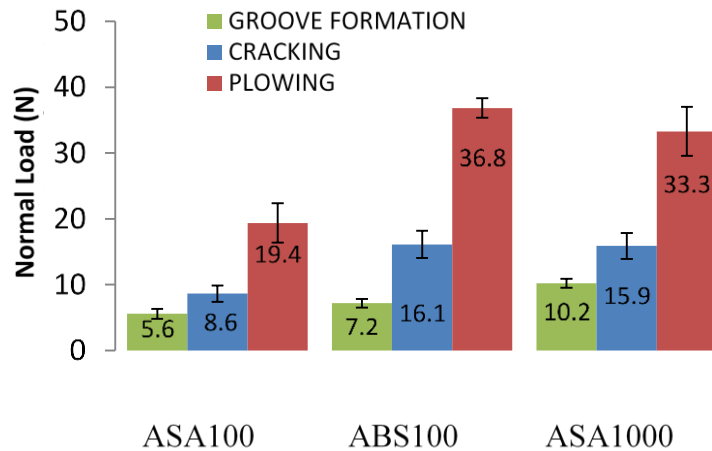


**Figure 10. Critical normal loads for ASA100, ABS100, and ASA1000 under dry conditions at scratch speed of 100 mm/s: onsets of groove formation, cracking, and plowing.**
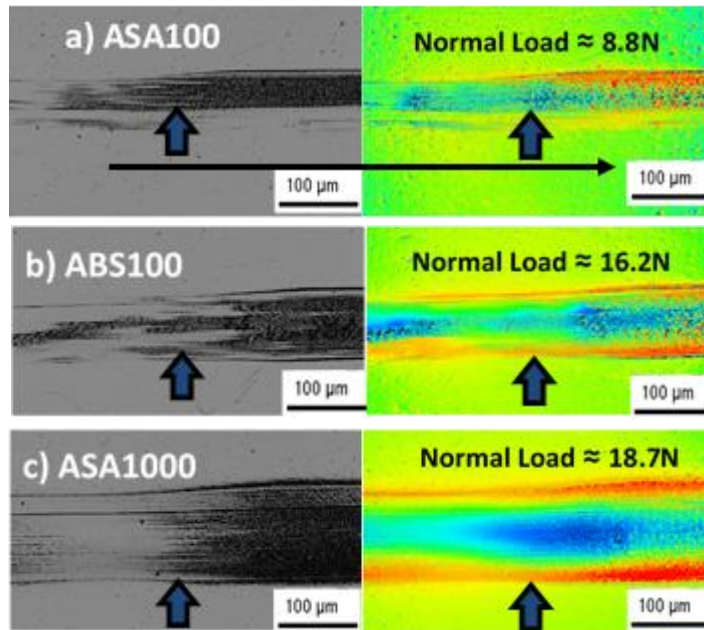
**Figure 11. Onset of cracking optical image (left), height profile (right), and corresponding normal loads for a) ASA100, b) ABS100, and c) ASA1000. Scratch is from left to right.**
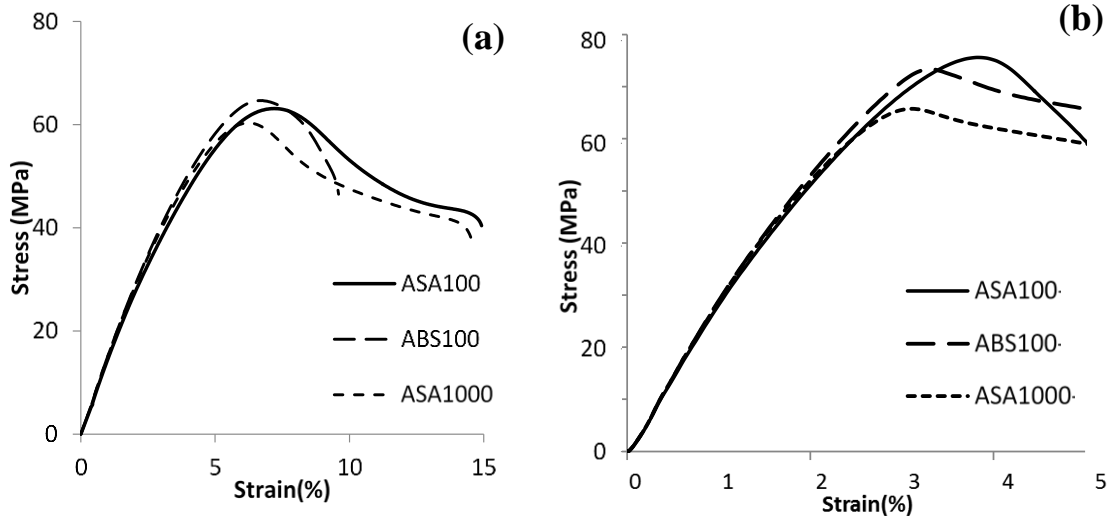


**Figure 12. Tensile curves of ASA and ABS in dry condition at (a) 5 and (b) 250 mm/min.**

To explain the scratch performance of the model systems, the corresponding mechanical properties in uniaxial tension and compression were determined. As discussed elsewhere [42, 52, 58-60], various aspects of the mechanical behavior and surface properties can influence the development of scratch depth, shoulder height, onsets of groove formation, cracking and plowing. For crazing-prone polymers, it has been shown that tensile strength and friction coefficient are most critical to scratch resistance [42, 56, 60]. Tensile behavior of the model systems at different crosshead speeds are compared in Figure 12 and compressive behavior of each system at a standard strain rate is shown in Figure 13. Based on Figures 12 and 13, all three model systems show almost identical uniaxial tension and compression behavior. To compare scratch behavior and mechanical response in tension at similar strain rates, a slow speed scratch test at 1 mm/s was also carried out to correlate with the tensile test speed at 250 mm/min (Figure 14). The results suggest that no correlation between the tensile behavior and onset of crack formation during scratching can be established, indicating that the crack formation in rubber-modified SAN may be more complicated than single-phase polymers as has been discussed in the literature [42, 57].
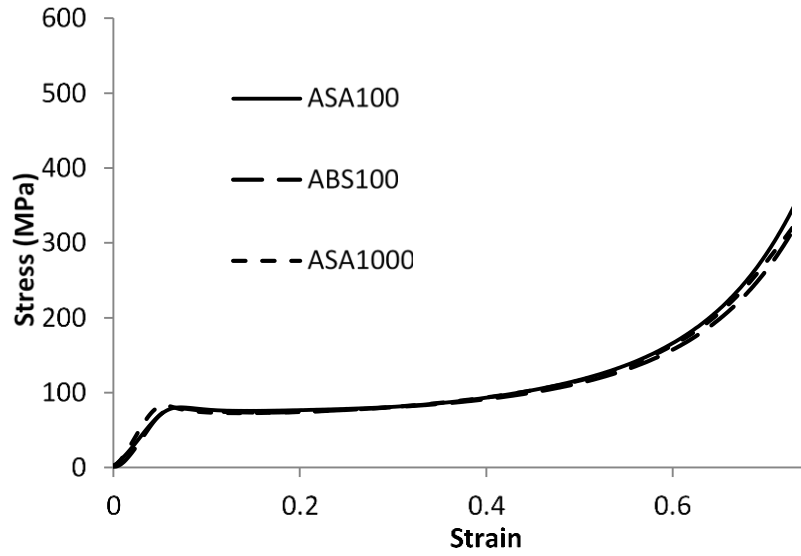
**Figure 13. Compression curves of ASA and ABS grades in dry condition at 2.5 mm/min.**
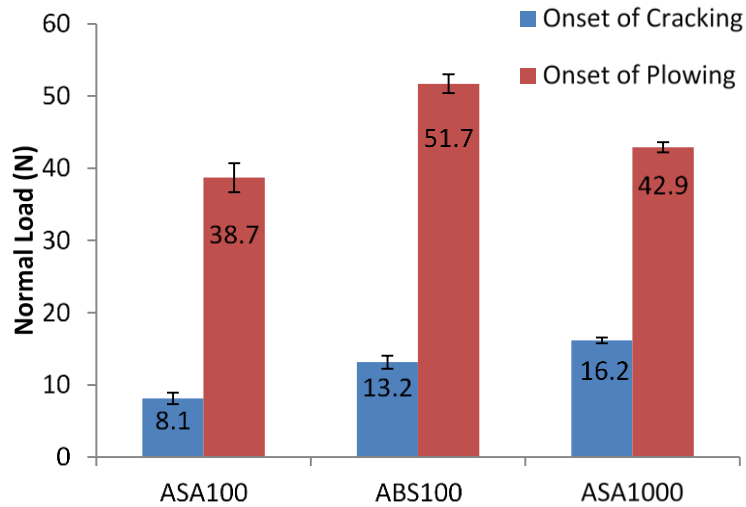


**Figure 14. Critical normal loads for ASA100, ABS100, and ASA1000 in dry conditions at scratch speed of 1 mm/s.**

Figure 15 shows the $\mu$ for each system measured using the flat tip. As can be seen in the figure, ASA100 shows higher $\mu$ compared to that of ASA1000. It has been

shown that [60, 70, 71] the increase in $\mu$ intensifies the stress magnitude towards the surface leading to more severe damage and an earlier onset of groove formation and cracking. This could be an explanation for the observed difference in scratch resistance between ASA100 and ASA1000 (Figure 10). Similar conclusion can be made when comparing the scratch resistance of ASA100 with ABS100 (Figure 10). It should be noted that the $\mu$ values for ABS100 and ASA1000 are comparable (Figure 15) which reflects in their comparable scratch resistance (Figure 10). Thus, the variation in $\mu$ values can be at least partially considered responsible for the observed difference in scratch resistance among the systems.

To examine the deformation and damage mechanisms during scratch, the induced subsurface damage must also be taken into account. Longitudinal sections of the scratch deformation were carefully prepared to analyze the permanent damage beneath the scratch path at the onset of cracking. It can be observed in Figure 16 that all three systems undergo significant subsurface plastic deformation which can be seen through the bright birefringent zones under cross polarization. The extent of subsurface damage in the systems was compared with the relative scratch resistance of the polymers. The longitudinal subsurface examination of the scratch deformation in multiphase systems reported previously [57] indicate that microcracks were formed due to predominantly tensile stress development immediately behind scratch tip during scratching, which is in agreement with the modeling work of Chu et al. and Jiang et al. [47, 56]. However, in this case, the systems show a noticeable difference in crack shape and angle compared to the previous studies [55, 57]. The depth of the subsurface plastic zone is seen to vary

among the systems, where ASA1000 has the largest plastic deformation zone of approximately 80 microns in depth compared to ABS100 and ASA100 where the plastic deformation depth is approximately 60 and 30 microns, respectively. This subsurface plastic deformation zone is formed to reflect their propensity to deform plastically during scratch.
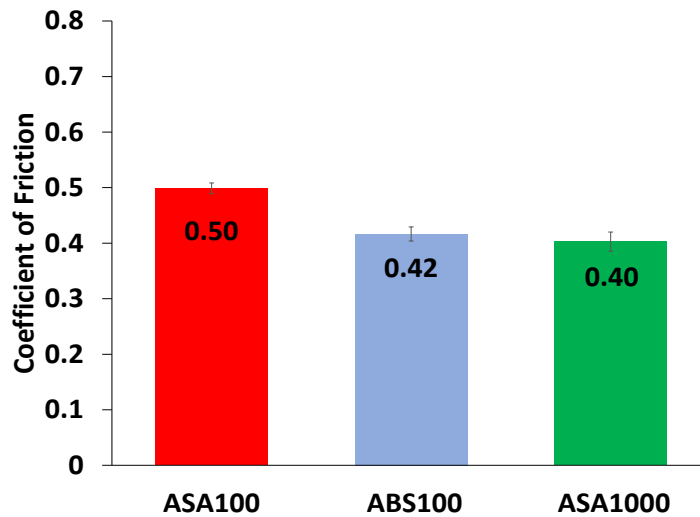


**Figure 15. Coefficient of friction comparison for model systems.**

SEM micrographs of the scratch deformation around the onset of crack formation in each system are shown in Figure 17. It can be observed that the onset of cracking for each system has introduced permanent damage on the surface while the crack characteristics seem different for each scenario. For instance, the onset of cracking is a sharp transition for ASA1000 from no apparent damage to visible crack patterns along the scratch; while in ABS100 and ASA100, the onset of cracking is a more gradual process where small microcracks on the scratch surface and subsurface increase in size, frequency, and continuity, which eventually leads to visible crack formation. Figure 18

shows micrographs of a scratch in the longitudinal direction using reflective OM and SEM for ASA100 and ASA1000. The angle of crack formation suggests different crack shapes, i.e., different degrees of mixed-mode stress induced crack formation for different systems. Based on Figures 17 and 18, the type of cracks observed in ASA1000 look similar to previously observed tensile cracks perpendicular to the scratching direction [55, 57]. This cracking feature indicates a tensile dominated fracture, which is known to be a common scratch mechanism for single phase brittle polymers. However, in the nanophase systems, i.e., ASA100 and ABS100, the crack formation appears to be at an angle away from being perpendicular to the scratching direction, suggesting significant mix-mode fracture. Also, the cracks appear to be more "flaky" than from ASA1000.

To better understand the scratch deformation mechanisms in these rubber-modified systems, the influence of rubber particles on stress field development during a deformation process must be considered. Based on the previous studies, the introduction of a soft phase in a polymer matrix is expected to alter the stress state near the rubber particles significantly, especially if the rubber particles would cavitate or initiate crazing [72-77], which could render in modifying deformation mechanisms. This could ultimately result in changes in mode of fracture. Also, the adhesion between the rubber particles and matrix may play an important role in altering the stress state during the scratch process. As shown by Jiang et. al. [56], the magnitude and direction of the maximum principle stress behind the scratch tip is altered at the interface of the two phases. The direction of tensile stress behind the scratch tip can be changed from in-

37

plane to out-of-plane of the scratch path at the interface. This could lead to change in shapes of cracks formed during the scratching process.
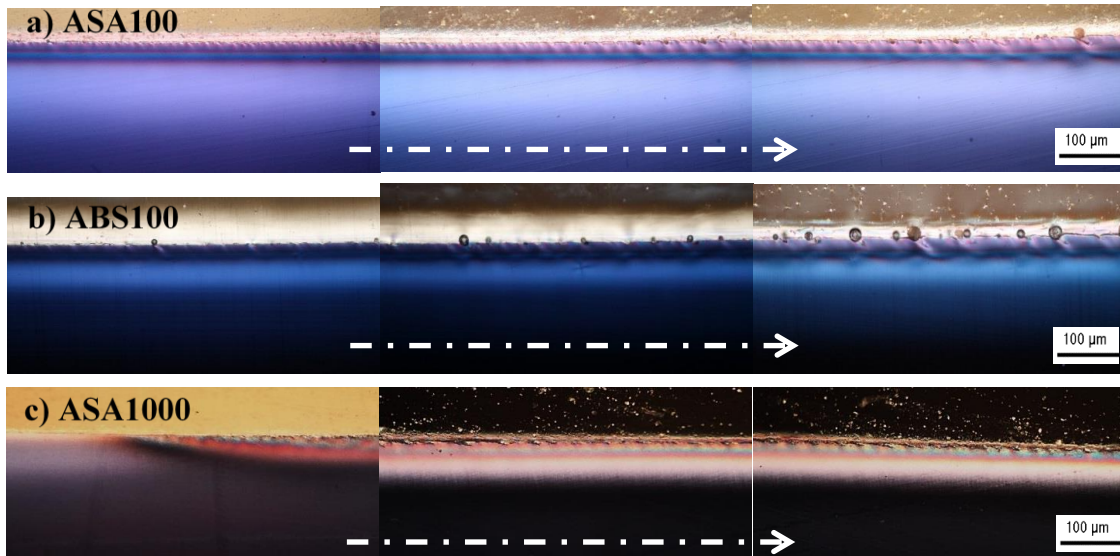


**Figure 16. Longitudinal view of subsurface damage at onset of crack formation under cross polarized light for a) ASA100, b) ABS100, and c) ASA1000.**

Crazing, shear yielding, and cracking are the three most commonly known deformation mechanisms for polymers [75, 76]. It has been shown that ASA and ABS with larger rubber particles within the micrometer range show higher impact strength due to more effective craze formation compared to the smaller nanosized rubber particles, which are too small to induce effective crazing [35]. Larger rubber particles in ASAs can induce a larger scale of shear plastic deformation compared to the shear deformation caused by smaller particles [77, 78], which in turn may explain the differences in subsurface damages observed in ASA systems in Figure 16. Furthermore, the larger plastic deformation zone observed in ASA1000 leads to higher energy dissipation during the scratch process which in turn increases the resistance to crack formation.
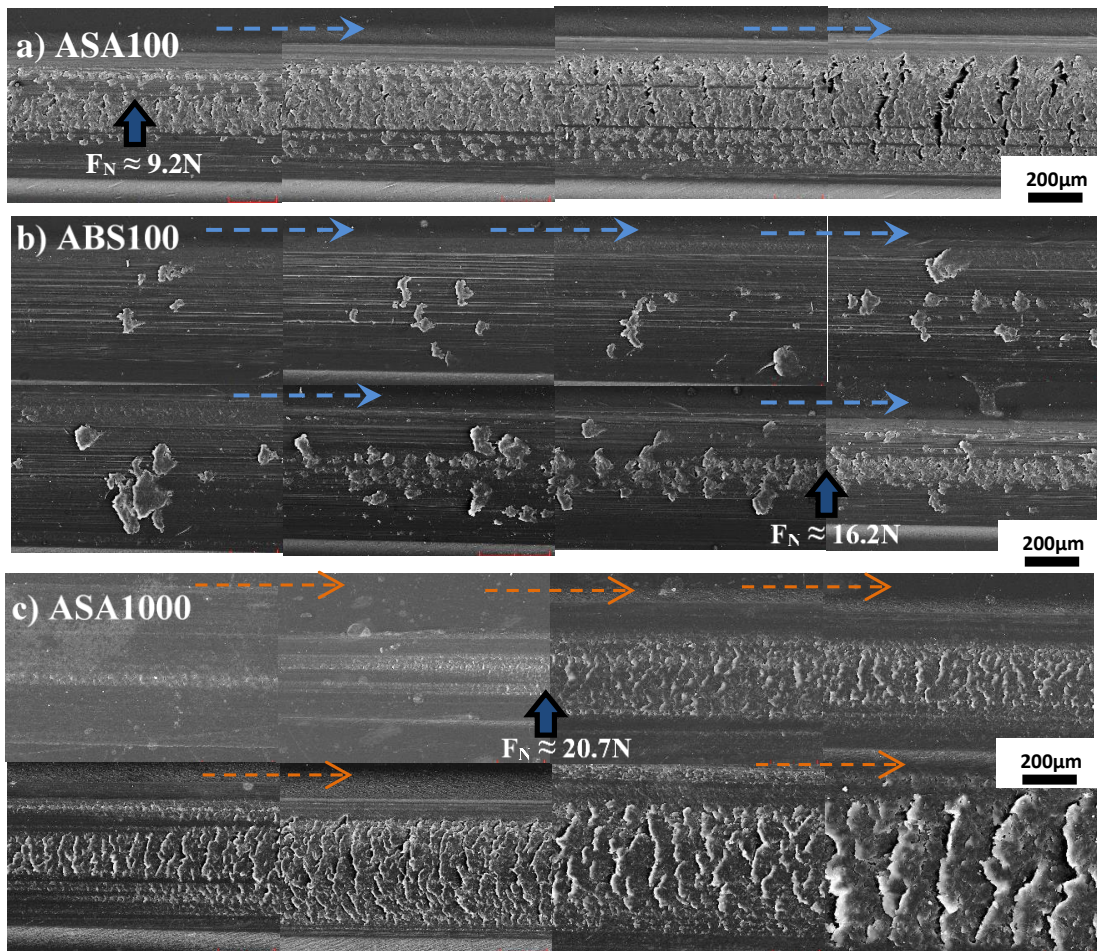
**Figure 17. SEM micrographs of scratch surface around onset of cracking for a) ASA100, b) ABS100, and c) ASA1000.**
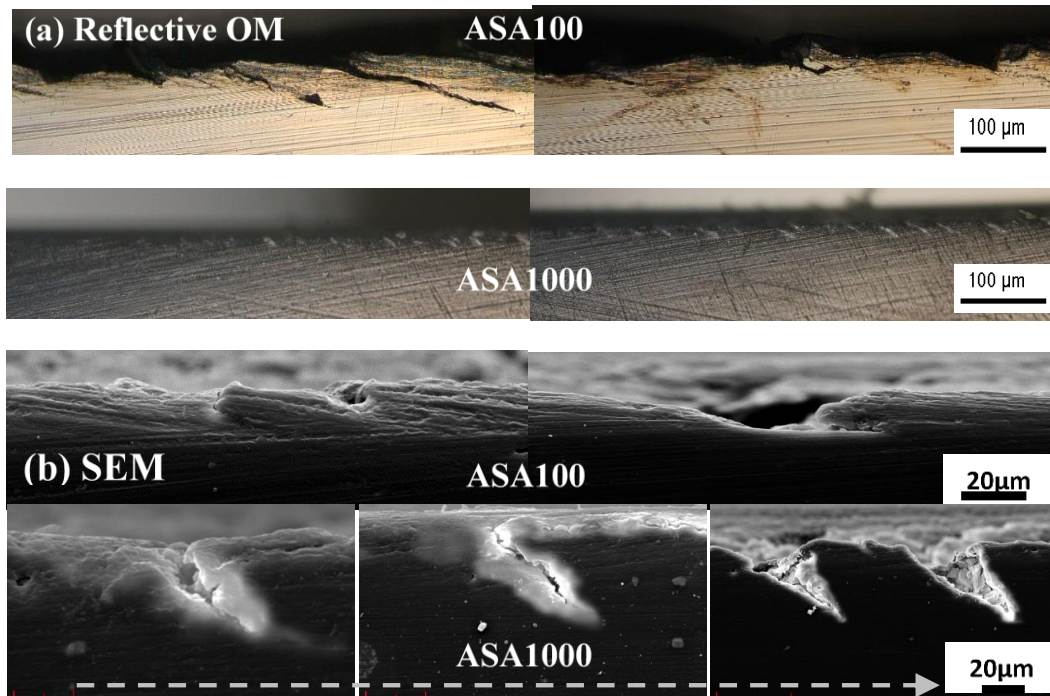
**Figure 18. (a) Reflective OM of scratch longitudinal sections for ASA100 and ASA1000 (b) SEM micrographs of phase and surface morphology for ASA100 and ASA1000.**
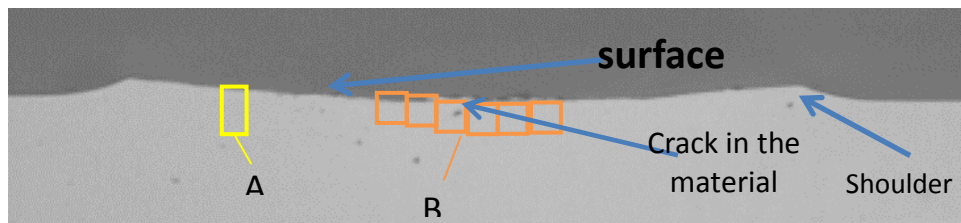


**Figure 19. Optical micrograph of the scratch cross section indicating subsurface regions where AFM measurements were performed. Scratch direction is perpendicular to the page.**
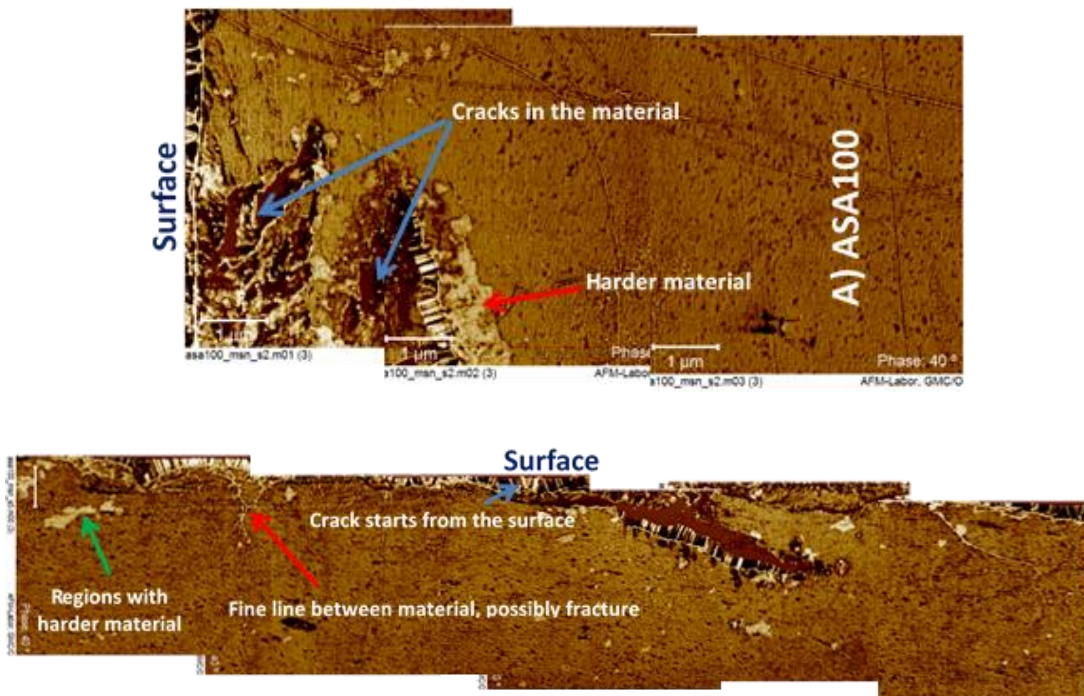
**Figure 20. AFM micrographs of scratch cross sections in ASA100 after onset of crack formation: a) region where subsurface crack has initiated b) middle of scratch groove and more subsurface cracking, compiled images.**

To better comprehend the scratch deformation in these systems, AFM analysis was performed on various locations on cross-sections of the scratch damage beyond the onset of crack formation. Figure 19 gives a representation of the locations chosen for AFM analysis. These micrographs were compiled to further analyze subsurface damages of each system. In Figure 20, a detailed AFM map of scratch damage cross-section is shown for ASA100. In this image, a profile of the material on and beneath the surface of a scratch deformation provides insightful details. Cracks caused by scratch can be seen in Figure 20, while small regions of material with brighter contrast, indicating higher hardness seem to form around these cracks and in other regions. These bright regions

around the crack tips can be strain-hardened material. However, further investigation is necessary to confirm the validity of this finding. The crack seen in Figure 20(b) initiates and propagates from surface through subsurface and its angle must also be noted as in agreement with the crack formation observed in OM (Figure 18(a)) as discussed earlier.

An AFM map of the scratch deformation cross-sectional view for ABS100 is shown in Figure 21. In Figure 21(a), large dark areas can be observed throughout the depth of the measurement, which increases closer to the surface. These dark areas are most probably voids caused by scratching in subsurface regions and possible debonding of the rubber particles. Figure 21(b) shows two regions of varying morphologies at different depths from the surface in ABS100. The bottom region has a similar morphology to non-deformed regions prior to scratching, while the top region closer to the surface appears to be highly deformed, making it difficult to identify the rubber particle phase. This could be a result of the scratch deformation compressing perpendicular to the scratch direction and stretching of the rubber phase along the scratch direction. This rubber stretching feature has previously been observed in scratch tested injection molded plaques by Tang et. al. [79]. The extent of rubber particle deformation in ASA1000 is seen in Figure 22(a) and shows much more rubber particle deformation toward the surface as expected. Fracture within the subsurface through crack formation is observed in Figure 22(b) while the harder regions (lighter color) previously seen in ASA100 can also be seen around cracks in ASA1000.

Areas with harder (brighter) and softer (darker) material



Crack goes along the material border

Different morphology above/under theoretical line
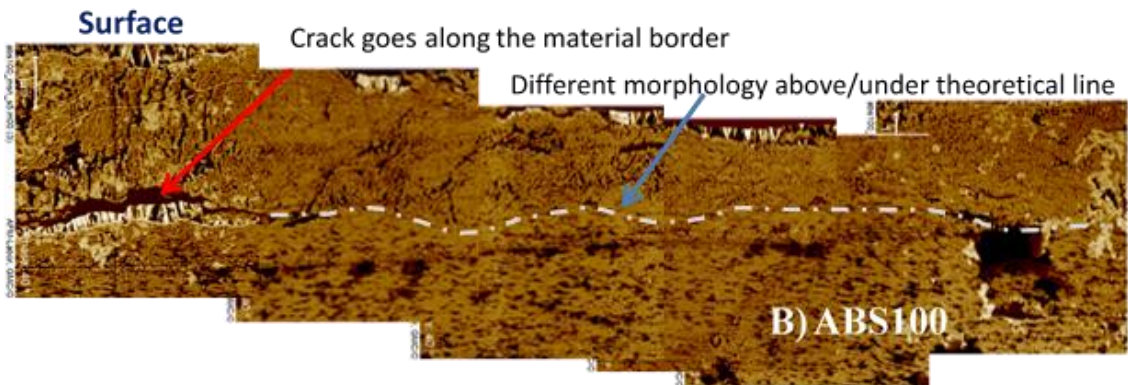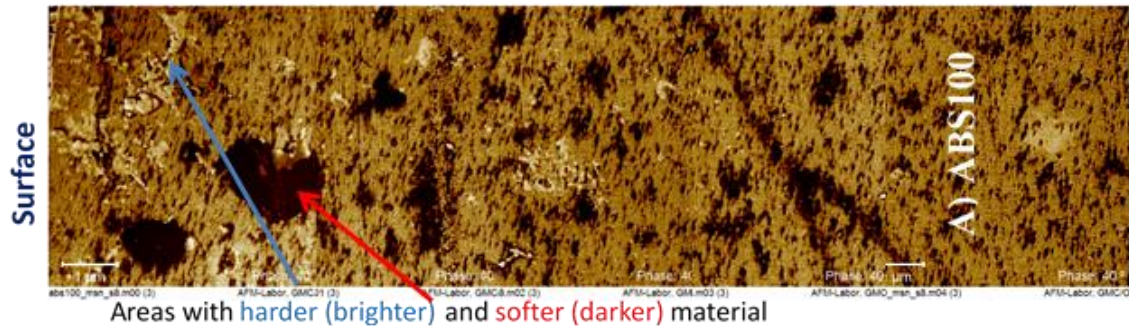
**Figure 21. AFM micrographs of scratch cross sections in ABS100 after onset of crack formation: a) region where subsurface crack has initiated b) middle of scratch groove with subsurface cracking, compiled images, showing bilayered morphology.**
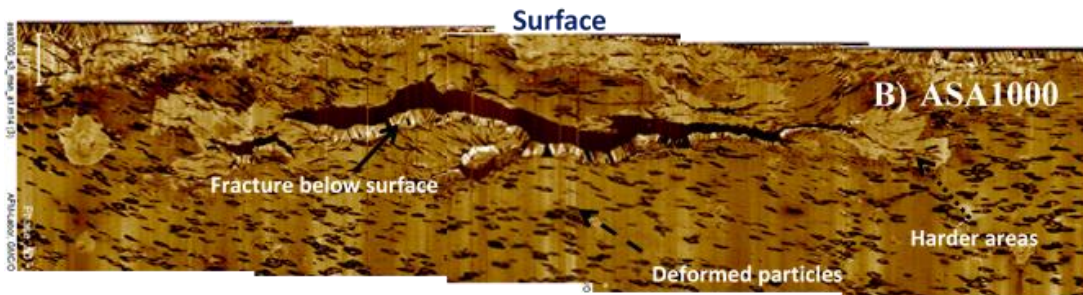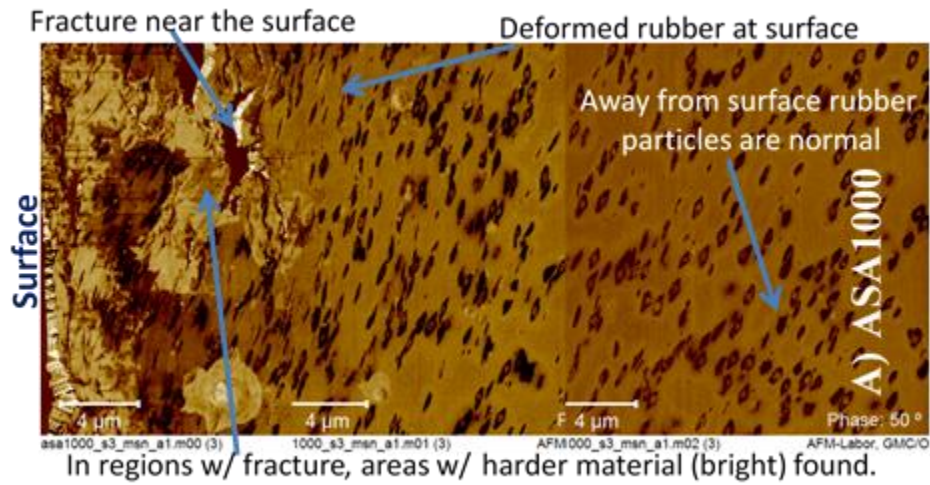
**Figure 22. AFM micrographs of scratch cross sections in ASA1000 after onset of crack formation: a) region where subsurface crack has initiated b) middle of scratch groove and more subsurface cracking, compiled images.**

Finally, the effect of moisture exposure on scratch behavior of the ABS and ASA systems was studied. The corresponding critical normal loads at the onset of cracking for ASA100, ABS100, and ASA1000 under dry and moisture saturated conditions are shown in Figure 23. As can be seen in the figure, only ABS100 system is affected by moisture exposure. Butyl acrylate rubber present in ASA is insensitive to moisture exposure compared to butadiene rubber in ABS, which is expected based on moisture affinity of the systems [70, 80].

44
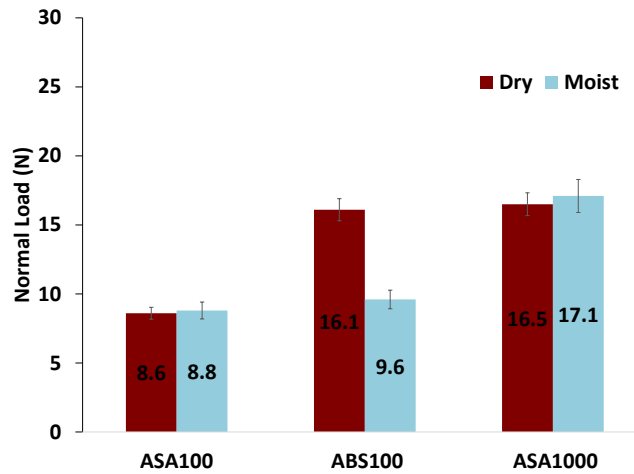
**Figure 23. Critical normal loads at onset of cracking for ASA100, ABS100, and ASA1000 under dry and moist conditions at scratch speed of 100 mm/s.**

The present study indicates that, under dry conditions, ABS shows a better scratch resistance than ASA when the rubber particle size of each is approximately 100 nm. As previously reported in the literature [78, 81], craze stabilization by the rubber phase is more effective in ABS compared to ASA with nanosized rubber particles, which could impact the scratch performance. Furthermore, micron sized rubber particles proved to be more effective than nanosized particles in ASAs. The difference in $\mu$ values among the systems can be used to explain the observed difference in scratch resistance. The ability of each system to undergo subsurface plastic deformation and the related energy dissipation based on rubber particle size [82-85] can partially explain for this effect, as well. The crack damage feature in single phase polymers appearing on the scratch surface were previously considered to be due to tensile dominated stress immediately behind the scratch tip on the scratch path; whereas, more complex mode of deformation is found in these multiphase systems.

Therefore, in multiphase materials subjected to complex stress field during scratching, crack formation can vary in shape from previously defined tensile cracks to mixed mode flake-like cracks. Although the scratch-induced cracks in multiphase systems vary in shapes, the coefficient of friction variation can partially be used to explain the observed differences in scratch resistance among the systems. As such, the bulk material and surface properties can still be used to understand the scratch resistance of multiphase systems. However, to explain the type of cracks observed in the systems investigated, extensive study on localized stress and strain field development during scratching process due to interaction between the particles and matrix is needed. Theses aspects of study will be subject to our future investigation.

## 2.5 Conclusion

In this study, influences of rubber size and type on scratch performance of ASA and ABS model systems were investigated. Our findings suggest that micron-sized rubber particles are more scratch resistant than nano-sized rubber in styrenic copolymers. It has also been found that in dry condition butadiene rubber offers better scratch resistance than butyl acrylate rubber. The basic mechanical properties of the three model systems were almost identical while scratch behavior were noticeably different. The difference in coefficient of friction among the systems can be used to explain the observed difference in scratch resistance. Based on the multiphase nature of the systems investigated, scratch deformation is more complicated compared to that of single phase material. In multiphase ASA and ABS rubber containing materials, the

crack formation caused by scratching can vary in nature from a predominantly tensile to

mixed mode damage and exhibit flake like crack features.

CHAPTER III

EFFECT OF HIGH TEMPERATURE ANNEALING ON SCRATCH BEHAVIOR OF

ACRYLONITRILE STYRENE ACRYLATE COPOLYMERS

## 3.1 Synopsis

The scratch behavior of butyl-acrylate rubber modified styrene-acrylonitrile (ASA) upon high temperature annealing is investigated following the ASTM D7027/ISO 19252 linearly increasing normal load test methodology. The critical normal loads at the onset of the major deformation transitions along the scratch path, such as groove formation, scratch visibility, microcrack formation, and plowing, are reported and quantitatively analyzed. It is found that the scratch resistance improves with high temperature annealing, i.e., 30°C above $T_g$, as compared to annealing below or around $T_g$. Microscopic investigation suggests that the increase in scratch resistance is related to the changes in surface morphology of the polymer. It is concluded that performing high temperature annealing enhances the scratch performance without compromising ASA bulk properties. Implication of the present study for improving scratch resistance of polymers is discussed.

## 3.2 Introduction

Demands for scratch resistant polymers have rapidly increased in anti-corrosion coatings, consumer electronics housings, food packaging films, automobile interior and exterior components, and many other applications [86]. However, the lack of

48

fundamental knowledge in polymer scratch behavior has limited our ability to effectively design and optimize material systems for scratch resistance. Significant research efforts are therefore still needed to improve the scratch resistance of polymers.

A popular method to assess polymer scratch resistance employs a rigid tip indenting and moving across a polymer surface simultaneously. A noticeable progress in the evaluation of polymer scratch performance was an establishment of a standardized test methodology, i.e., the ASTM D7027-05/ISO 19252 method. This testing methodology applies a progressive normal load to generate scratch damage from low to high level through a single scratch path [87]. In such a fashion, the test will be effective not only for quantitative evaluation of scratch performance but also for generation of fundamental knowledge for development of scratch resistant polymers [88-95]. The generation of scratch-deformation map is an effective way to categorize those deformations and concurrently illustrate the influence of different testing and material parameters on scratch mechanisms [96-98].

Through the aid of finite element methods (FEM) modeling, more in-depth understanding of scratch deformation and damage has been reported. Jiang et al. [94] isolated the influences of four material parameters on the residual scratch depth, and concluded the yield strength and the coefficient of adhesive friction are most relevant to scratch resistance. Subsequently, an insightful mechanics description of multi-axial stress state involved during the scratch process was provided [99]. It was found that the material beneath the scratch tip experiences a compressive stress state while the material element behind the scratch tip experiences a tensile stress state, which promotes either

fish-scale formation in the case of ductile polymers or crazing/microcracking in the case of brittle polymers. Moreover, an additional maximal tensile stress component develops in front of the scratch tip as the normal load increases, and its stress magnitude eventually overwhelms the material and causes cutting and plowing to take place. The above findings imply that surface constitutive behavior, not their bulk properties, of a given polymer governs the scratch performance.

Post processing heat treatment of polymers has been shown to significantly affect their physical and mechanical properties. Depending on the composition and processing conditions, noticeable changes in mechanical properties have been observed through heat treatment of styrenic copolymers [100, 101]. While partial residual stresses were relieved, a noticeable drop in impact resistance and ductility were observed after long term annealing of acrylonitrile-butadiene-styrene (ABS) at temperatures below $T_g$. This is due both to the physical aging effect and to degradation of the C=C double bond in the backbone of ABS [100]. In contrast, the heat treatment of butyl-acrylate rubber-modified styrene-acrylonitrile (ASA) copolymers caused no deterioration in mechanical properties at temperatures below or above $T_g$ even for extended periods of time [101]. In the same study, it was also shown that relief of injection molding residual stresses as well as molecular orientation could be achieved to a varying degree, depending on the ASA annealing process.

Interesting findings on how the scratch behavior is affected by surface morphology and post-processing annealing have also been reported. In a soft thermoplastic olefin (TPO) that consists of ethylene-propylene rubber (EPR) and

50

polypropylene (PP), Browning et al. [92] found that the crystallinity of the ethylene segment and the internal morphology of the EPR phase significantly affect the scratch behavior of the soft TPO. In addition, through post-processing thermal treatments, Moghbelli et al [93] investigated the correlation between skin-core morphology in PP and its scratch performance. Their results suggest that annealing, which increases the crystallinity level near the surface, enhances the scratch resistance of PP. The above findings imply that: 1) the surface or sub-surface phase morphology of semi-crystalline polymers, which can be manipulated by the processing conditions, plays an important role in polymer scratch behavior and 2) the surface properties of a semi-crystalline polymer, which significantly affect the scratch resistance, are likely to be different from those of the bulk. However, it is uncertain if the above observations hold true for amorphous polymers.

In this study, a series of amorphous ASA systems, which are butyl-acrylate rubber-modified styrene acrylonitrile (SAN) and neat SAN, were chosen as model systems for investigating how an above-$T_g$ high temperature annealing affects its scratch behavior. Our previous study indicates that the scratch performance of ASA generally deteriorates with increasing rubber content, and is strongly related to their reduction in tensile and compressive yield strengths [102]. It is hoped that the present study can further our fundamental understanding of structure-property relationship in polymer scratch, and also establish an approach to enhance the scratch resistance without compromising bulk properties through high temperature annealing.

51

### 3.3 Experimental

*3.3.1 Materials*

The ASA polymers utilized in this study were provided by BASF SE (Ludwigshafen, Germany). They consist of a random copolymer SAN matrix and grafted polybutyl-acrylate (PBA) rubber particles with an average nominal diameter of 475 nm. The PBA rubber content in ASAs was varied from 0 to 30 wt% (Table 2). In the SAN phase, the acrylonitrile content was controlled to be at 35 wt%, and the weight-average molecular weight (Mw) of SAN was chosen to be 104kg/mol [103]. Color pigments of 0.325% of anthrachinone and 0.15% of pyrazolone yellow were blended into the resins to provide adequate color background for the scratch visibility investigation. The test specimens were fabricated by injection molding with a fan gate design to spread and slow the melt as it enters the mold cavity to ensure near-uniform molecular orientation across the width of the plaques. The plaques were 150 mm x 150 mm in rectangular shape and were 6 mm in thickness.

*3.3.2 Heat Treatment*

Prior to the post-processing annealing, the specimens were dried in a vacuum oven at 86°C for 24 hrs to remove any pre-absorbed moisture [106]. The annealing experiment was carried out by sandwiching ASA plaques with two tempered glass plates. An external weight of about 10 KPa in stress was applied to the sandwiched samples during annealing and cooling to prevent potential warping due to uneven residual stress relief of the plaques. Two annealing processes, the low temperature annealing (LTA) and high temperature annealing (HTA), were individually performed

on all the ASA and SAN plaques. For the LTA process, the ASA plaques were annealed at 108 °C for 2 hrs under vacuum and allowed to slowly cool in a vacuum oven to minimize any residual stresses caused by the injection molding process. The HTA process was conducted at 140 °C, which is about 30°C higher than the measured $T_g$ [102], for 2 hrs under vacuum. Afterwards, the samples were cooled to ambient temperature by shutting off the oven power. The scratch tests were performed at ambient temperature and relative humidity of 50% and were completed within an hour after annealing to minimize moisture adsorption from atmosphere.

### 3.3.3 Surface Finish Measurement

A 60° specular gloss and the root-mean-square surface roughness ($R_q$) measurements of all the plaques were obtained by using BYK Gardner® Micro-TRI Glossmeter and Keyence® VK9700 violet laser scanning confocal microscope (VLSCM), respectively. The reported values were calculated based on an average of three scratches.

### 3.3.4 Mechanical Properties Characterization

The tensile tests were performed using a screw-driven Sintech 2 load frame and a MTS® 632 extensometer. The dog-bone shape specimens for tensile tests were based on the ASTM D638 type I specimen [104]. The nominal overall length, thickness and width of the narrow section were 170, 4, and 10 mm, respectively. The test was performed at a constant speed of 50 mm/min under ambient temperature in order to compare the results with one of our previous studies [102].

*3.3.5 Scratch Testing*

Scratch tests were performed under ambient temperature following the standardized ASTM D7027-05/ISO 19252:08 test method [87, 107]. The scratch tip was made of stainless steel and had a 1 mm diameter spherical geometry. The scratch direction was chosen in the same direction as the melt flow for all the tests. A progressive load of 1–80 N at constant scratch speeds of 100 mm/s was used to evaluate the scratch performance in a length of 100 mm. Note that a 10 mm lead distance at 1N constant load was used at 100 mm/s scratch speed to reduce the inertial effect from the scratch tip movement at low applied normal loads portion of the test.

*3.3.6 Post Scratch Analysis*

In order to provide sufficient time for viscoelastic recovery after the scratch test, the sample damage features were characterized after 24 hrs upon completion of the scratch tests. The optical microscopy images and the topographical information were obtained by using the aforementioned VLSCM and its accompanied image analysis software (VK Analyzer, 2.1.0, Keyence). For the scratch visibility analysis, a commercially available software ASV® (Automatic Scratch Visualization, http://www.surfacemachines.com) was applied. The scanned scratch images for analysis were obtained by using a PC scanner (Epson® Perfection Photo 4870) at 300 dpi resolution under "no color correction" mode. For all scanned images, the scratch direction was aligned perpendicular to the scanner light source movement. Additional characterization details can be found elsewhere [104].

*3.3.7 Contact Angle Measurement*

The surfaces of the ASA samples were cleaned using a pressurized $N_2$ nozzle head. Samples were then placed on a flat surface and a minimum of six droplets of deionized water were deposited on each surface. Droplet images were acquired using the super macro mode of an Olympus SP-570UZ Image Stabilization 10.0 Megapixels digital camera with an Olympus ED Lens AF Zoom attached to it. Images were inverted and sharpened using Image-J analyzer. The angle measurement tool in Image-J was used to measure the contact angles from each side of each droplet with respect to the sample surface. Twelve measurements were conducted for each sample and the average was calculated and reported.

*3.3.8 Fourier Transform Infra-Red Spectroscopy*

In order to determine surface chemical composition of all ASA systems a Nicolet Avatar 360 was utilized under attenuated-total-reflectance (ATR) mode at room temperature. Spectra were obtained at various locations of each specimen and the resulting FTIR spectra of LTA vs. HTA samples were compared.

*3.3.9 Image-J Analysis*

In order to determine the fraction of rubber particles to matrix at the surface of specimens, image-j analysis was performed on the AFM images. The color threshold was adjusted for the AFM micrographs automatically using the filtered mode. The images were then processed to binary mode and the fraction of rubber particles to surface area was determined using the particle analysis tool.

**3.4 Results**

*3.4.1 Annealing Effect on Chemical Composition and Surface Finish*

Figure 24 contains the FTIR-ATR (Attenuated Total Reflectance) setting spectra of ASA5 processed by LTA and HTA treatments, respectively. The typical IR adsorption peaks due to C≡N triple bonds and C=O double bonds [105] were highlighted. Note that the spectra are considered to represent the chemical compositions of the testing surface within several microns of depth [108]. The identical spectra between the two annealing conditions suggest no observable degradation is detected even after the HTA treatment. Although it is known that long-term aging at 90°C in air causes oxidation of butadiene in the rubbery phase of ABS [99], ASA appears to hold well against HTA annealing. It appears that the lack of C=C double bonds in ASAs, short annealing time under a vacuum chamber reasonably minimizes the potential of ASA degradation on the surface [100].
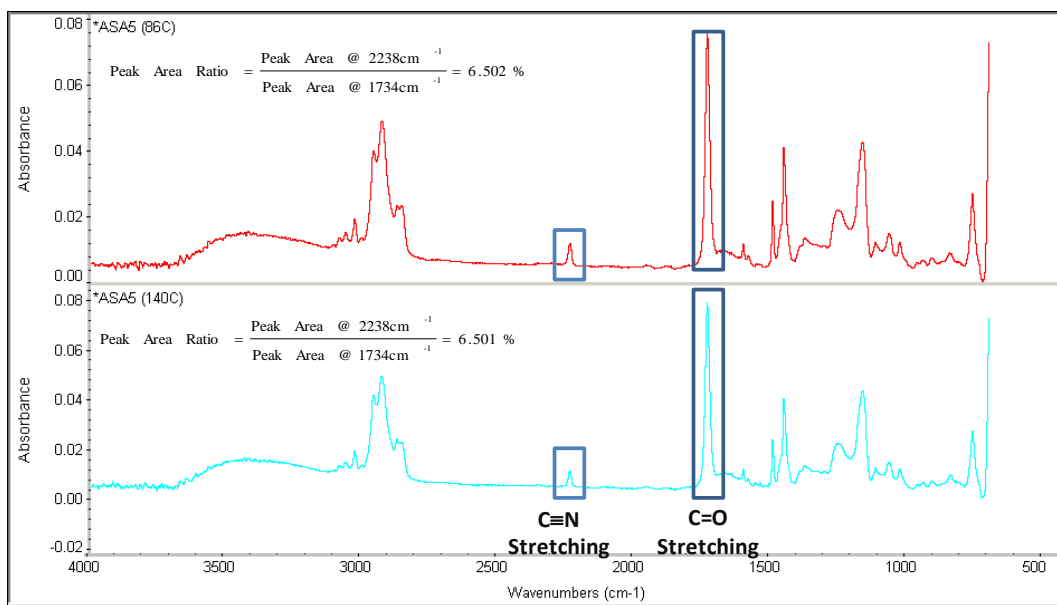
**Figure 24. FTIR spectrum of ASA5 annealed at low(bottom) and high(top) temperatures.**

Previous study showed that the LTA process brings a trivial impact on the surface finish of the testing plaques since its annealing temperature was slightly below the measured $T_g$ of ASA [100, 102]. Nonetheless, the ASA plaques treated by HTA in the present study were in their rubbery state during annealing. Hence, a considerable influence by HTA on the surface finish is expected. As shown in Table I, the change in 60° specular gloss and root-mean-square roughness indicate the surfaces of HTA processed plaques became smoother than those of as-received samples. The applied stress on the glass plates facilitates better contact between the ASA specimens and the smooth glass plate, resulting in a better surface finish of the plaques.

57

**Table 2. The rubber content and surface characteristics of the model ASA systems. Rq denotes the root-mean-square surface roughness, which is based on the measurement performed using VLSCM in a sampling area of 1.3x1.0 mm$^2$**

| Denotation | Rubber Content (wt%) | 60° specular gloss (%, n=3) | | $R_q$ (µm , n=3) | |
|---|---|---|---|---|---|
| | | As Received | Post ATT | As Received | Post ATT |
| ASA1 | 6 | 95.1±0.6 | 98.2±1.0 | 0.95±0.11 | 0.51±0.01 |
| ASA2 | 12 | 91.7±0.5 | 97.2±1.6 | 0.96±0.12 | 0.74±0.02 |
| ASA3 | 18 | 86.1±0.9 | 96.0±0.5 | 1.04±0.54 | 0.75±0.06 |
| ASA4 | 24 | 77.2±1.4 | 94.1±0.6 | 1.22±0.02 | 0.79±0.06 |
| ASA5 | 30 | 71.3±1.1 | 89.8±1.3 | 1.56±0.05 | 0.88±0.06 |

*3.4.2 Annealing Effect on Bulk Mechanical Properties and Phase Morphology*

Figure 25 demonstrates the uniaxial tensile behavior of both as-received samples (dash lines) and HTA processed samples (solid lines). It can be observed that the HTA process only shows a trivial impact on the bulk tensile property in terms of yield strength, Young's modulus, and elongation at break.

In order to illustrate the annealing effect on the rubber phase morphology on the surface, the AFM phase contrast maps of ASA5 with visible PBA rubber particles (dark spots shown in the figures) are presented in Figures 25 and 26. The AFM image obtained from LTA specimens appears to show a less smooth surface, which correlates well with the findings provided in the surface-finish investigation. The less elongated features of the dispersed rubber particles shown in the image of HTA specimen also suggest the

residual stress due to the injection molding has at least been partially relaxed and the molecular orientation in HTA specimen would be different from that in LTA specimen (Figure 25). Moreover, the same specimens processed by HTA show higher concentration of rubber particles on the surface when comparing to the "as-received" and LTA processed (Figures 25 and 26) ones. In fact the rubber/surface area fraction which was measured by image-j analysis of the AFM micrographs indicate an increase in rubber concentration from 13% to 18.9% at the surface due to annealing above $T_g$. A similar trend is also observed in ASA1 through ASA4. This finding strongly suggests that the annealing at above $T_g$ may promote migration of polar PBA rubber phase toward the surface. This in turn causes the rubber content at the surface to become higher than that of the bulk. Alternatively, the above phenomena can also be caused by the relaxation of the highly oriented SAN molecules and retraction of PBA rubber near the skin of the injection-molded sample. Upon high temperature annealing, the relaxation and retraction of the SAN molecules and PBA rubbers leads to exposure of the PBA rubber on the sample surface and roughens the surface somewhat. The above conjectures still await further experimental validation. It is worth mentioning that our preliminary results in nanoindentation as well as macroindentation did not show a significant difference in the indentation behavior between "as-received" specimens and HTA specimens.

**Table 3. Contact angle measurements for ASA1 and ASA5 systems (HTA vs. LTA)**

| Contact Angle | LTA | HTA |
|---|---|---|
| ASA1 | 66.23 ± 0.75 | 62.81 ± 0.82 |
| ASA5 | 65.70 ± 1.02 | 59.63 ± 0.61 |

Furthermore, the results obtained from the contact angle measurements further support this claim. It is known that the PBA phase has a higher surface energy in comparison to SAN matrix. It can be observed in Table 3 that the HTA leads to higher contact angles compared to LTA in both ASA1 and ASA5 systems. This in fact can be due to migration of the PBA particles to the surface of the molded plaques after annealing above $T_g$. The increase in contact angle due to high temperature annealing in ASA5 is more significant compared to ASA1 which is expected due to the rubber content concentrations of the systems. Therefore, the contact angle measurements support the previous assumptions. More study is needed to further clarify the impact of HTA process on the ASA surfaces.
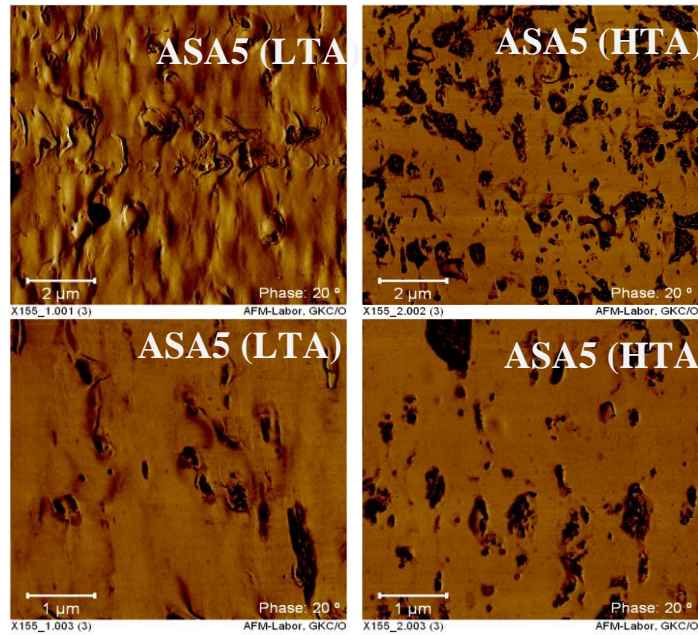
**Figure 25. AFM micrographs of ASA5 (LTA vs. HTA)**

*3.4.3 Scratch Damage Analysis*

Our previous findings have demonstrated that the typical scratch-deformation transitions observed in these ASAs and neat SANs contain (1) the onset of groove formation, (2) the onset of periodic cracking, (3) the onset of plowing, and (4) scratch visibility. The onset of groove formation represents a subtle plastic deformation feature developed during an early stage of the scratch process. Both the onsets of cracking and plowing are indicators of material failure on the surface beyond which material removal begins to take place. Note that the onset of scratch visibility is always found to be between the onset of groove formation region and the periodic cracking region, which will be discussed below.
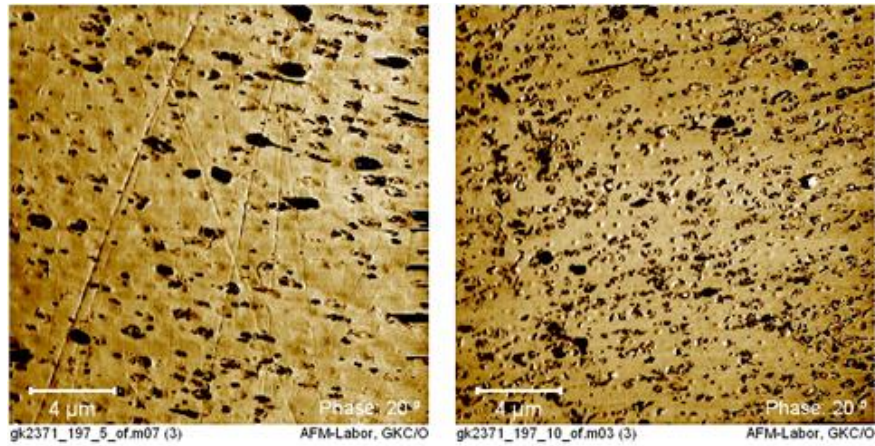
**Figure 26. AFM micrographs of ASA5 (as received vs. HTA)**
    (a) As received                               (b) HTA
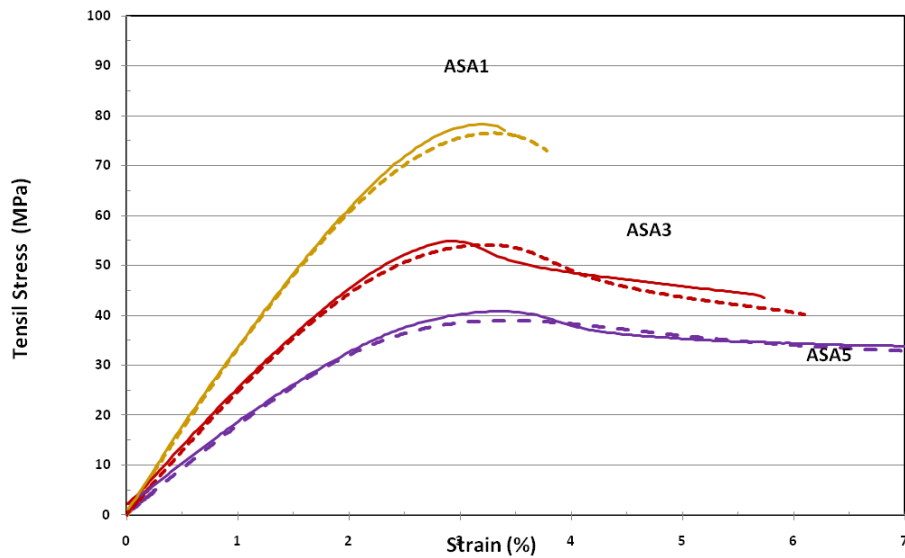


**Figure 27. Tensile behavior of LTA (dotted line) vs. HTA (solid line) for select systems.**

In order to determine the onset of groove formation, the depth profiles were precisely analyzed through laser confocal microscopy. The first sign of measured height

62

deviation between the scratch path and intact background surface was accurately determined and the corresponding normal load was reported as the critical load for the onset of groove formation. More details in the characterization can be found elsewhere [102].The critical normal load values at the onset of groove formation of LTA and HTA processed plaques are given in Figure 28(a). It has been shown in our previous study that the critical load for the onset of groove formation strongly depends on the rubber content, with a lower onset critical load for higher PBA rubber concentration. This is mainly due to the fact that a higher rubber addition causes a lower compressive yield stress of ASA, which makes it easier for the scratch groove to form [1-2]. In this study, no significant difference is observed in the onset of groove formation between LTA and HTA processed ASA plaques, which arises from the fact that compressive modulus is a bulk property not noticeably affected by heat treatment.

The onset of periodic crack damage for ASA1, ASA5 and neat SAN are shown in Figures 29-31, respectively. Note that the top pictures on each set show the laser confocal surface topographical images while the bottom ones represent the corresponding height profiles. Interestingly, the onset of periodic cracking begins right before the plowing damage, and is accompanied with a deep scratch deformation and wide groove width for those HTA processed ASAs (Figures 29a and 30a). This phenomenon is mainly due to the much higher corresponding load level imposed to generate periodic cracking. In contrast, the similar cracking transition appears much earlier in the LTA processed ASAs, with the periodic cracking features occupying a considerable length of the scratch path before the plowing takes place (Figures 29b and

30b). The aforementioned difference seen between LTA processed and HTA processed ASA is not seen in neat SAN system (Figures 31). Therefore, this difference in scratch behavior can be attributed to the presence and migration of the rubber particles to the ASA surfaces.
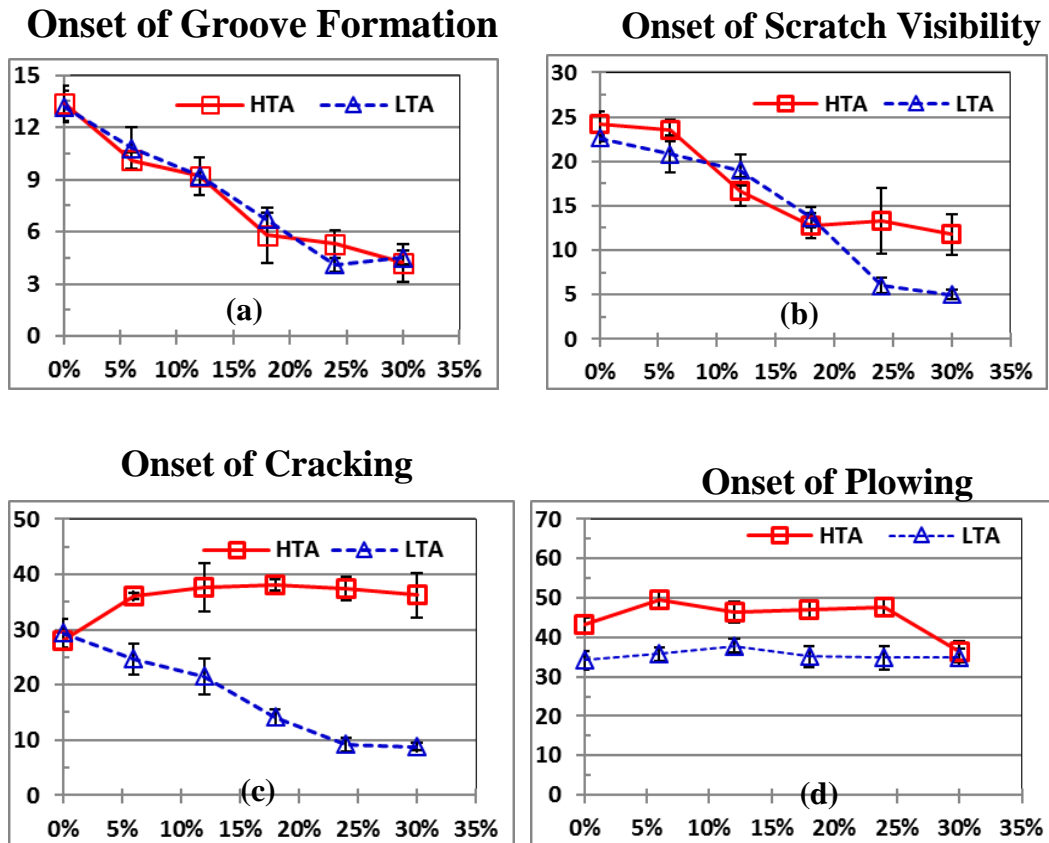


**Figure 28. Scratch resistance of LTA vs. HTA samples as a function of rubber content (a) critical load for onset of groove formation (b) critical load for onset of scratch visibility (c) critical load for onset of periodic cracking and (d) critical load for onset of groove formation.**

The critical normal load for the onset of periodic cracking for the testing materials is plotted against the rubber content in Figure 5(c). It is evident that the scratch

performance, particularly the resistance to the formation of periodic cracking, is significantly enhanced due to the HTA process. However, such improvement is only seen in ASAs, but not in the neat SAN system. Surprisingly, the critical normal load values obtained from the HTA processed ASAs are independent of the rubber content and do not follow the downward trend due to rubber introduction into the matrix. This observation is in contrast to the previous findings in LTA-treated ASA systems [102], where we concluded the scratch resistance of the crack formation generally deteriorates with increasing butyl-acrylate rubber content, and is strongly related with the bulk tensile yield stress, which indicates the influence of annealing conditions on ASA scratch performance. More discussion regarding these interesting findings will be presented later.

Figure 28(d) shows the critical normal load for the onset of plowing. At the final stages of the progressive load scratch test, the tensile stress components developed in front of the scratch tip possess the highest tensile magnitude among other stress components [94]. This high tensile stress component whose direction is tangential to the scratch tip facilitates the cutting of the pile-up material in front of the scratch tip and reduces the stick-slip motion. As a result, a deep surface penetration of the scratch tip along with massive material deformation and removal develops. As shown in Figure 33, the critical normal load at plowing transition is enhanced by HTA process by roughly 7 to 10 N, except in the case of ASA5 system. The exact cause(s) for this observed discrepancy is subject to future investigation.

The critical normal loads at the onset of scratch visibility for the ASA systems are plotted in Figure 5(b). The scratch visibility resistance is reduced with increasing rubber content in both LTA processed and HTA processed plaques. However, HTA processed ASA4 and ASA5 plaques show a superior visibility resistance than the LTA processed ones. Figures 32 and 33 illustrate the scratch groove depth and shoulder height of ASA1 and ASA5 at normal loads equivalent to 30N, respectively. It can be observed that in both cases the shoulder height of LTA is higher in comparison to that of HTA, resulting in the reduction in scratch visibility resistance.
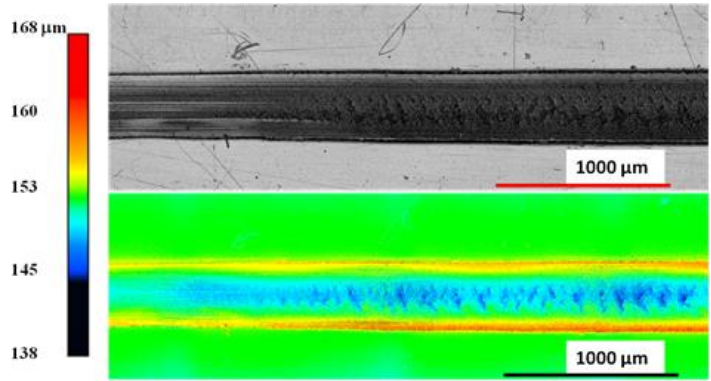


(a) LTA
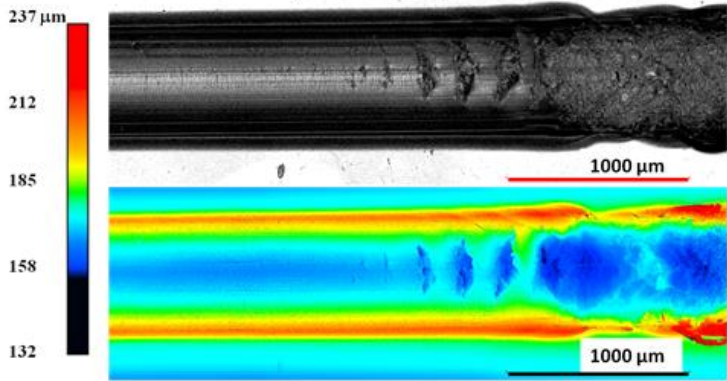


(b) HTA

**Figure 29. LCM Images of onset of cracking for ASA1 (HTA vs. LTA)**
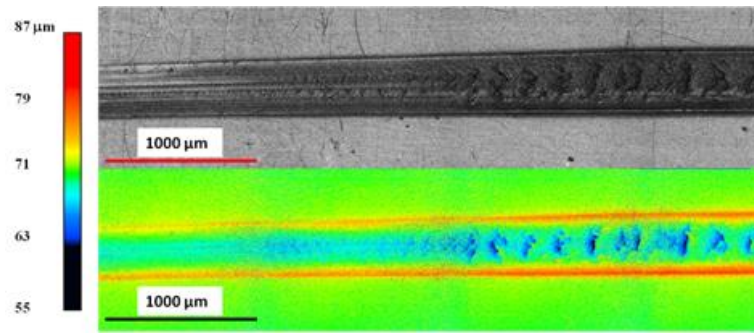
(a) LTA
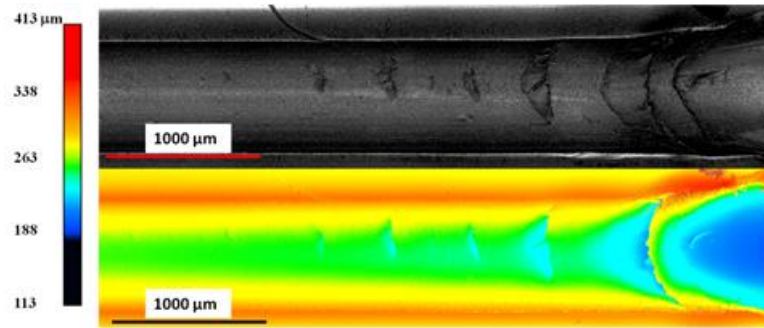


(b) HTA

**Figure 30.  LCM Images of onset of cracking for ASA5 (HTA vs. LTA)**
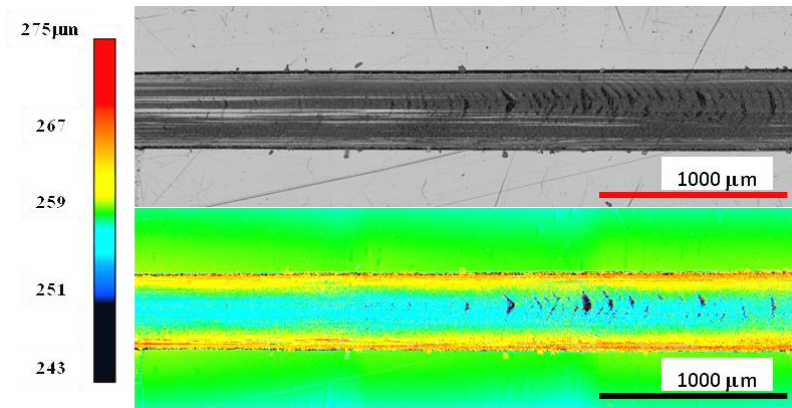
(a) LTA
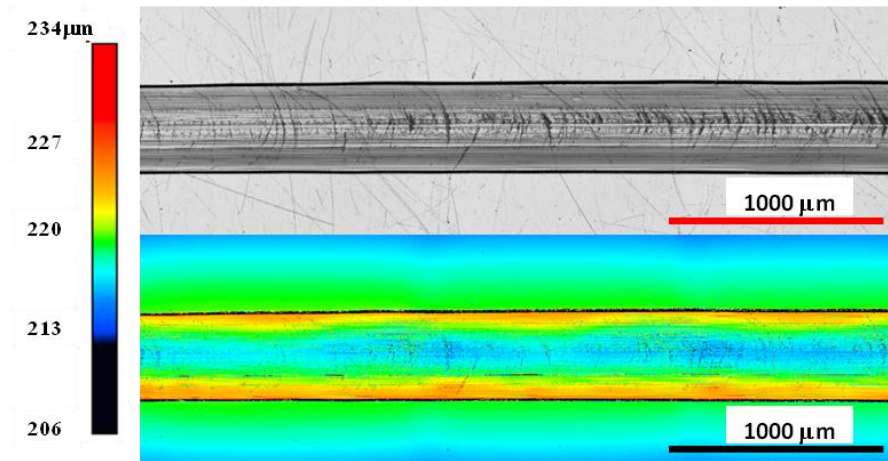


(b) HTA

**Figure 31. LCM Images Onset of Cracking for neat SAN.**
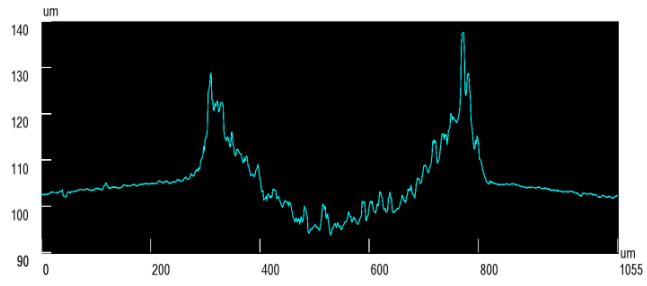
(a) LTA
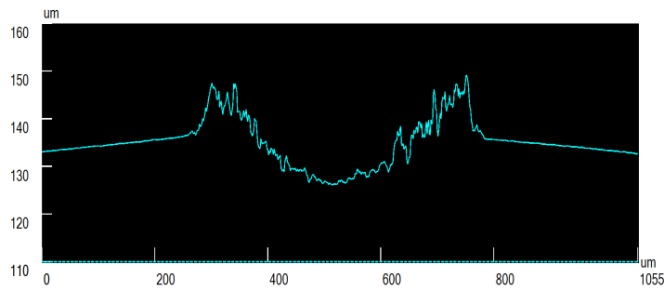


(b) HTA

**Figure 32**. **Evaluation of Scratch Groove Depth/Shoulder Height for ASA1 @30N normal load (LTA vs. HTA)**
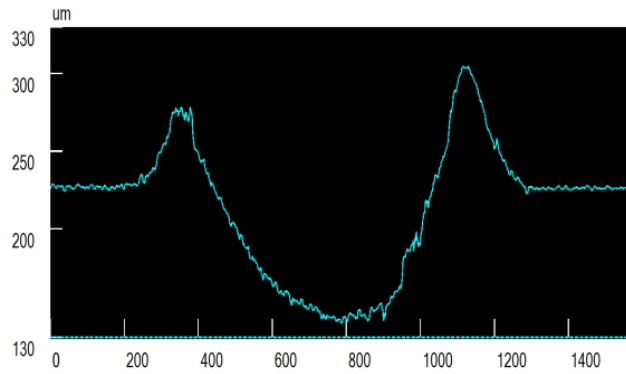
(a) LTA
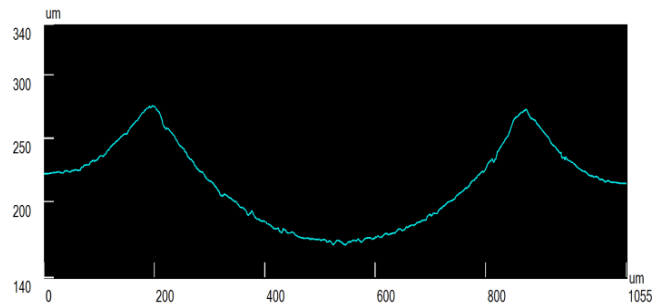


(b) HTA

**Figure 33. Evaluation of Scratch Groove Depth/Shoulder Height for ASA5 @30N normal load (LTA vs.HTA)**

## 3.5 Discussion

Heat treatment of styrenic copolymers has been shown to yield different results for different types of copolymers as well as their treatment conditions. It has been shown that in the case of long-term annealed ABS at temperatures below $T_g$, deterioration in mechanical properties, such as impact resistance and ductility, can be observed [100]. This is attributed to two factors. One is the presence of the C=C double bond on the butadiene segments resulting in change in chemical composition and degradation in

properties [100]. Another is the physical changes occurred during the aging process which can lead to decreases in ductility [100, 106]. However, in the case of ASA copolymers it was shown that heat treatment close to $T_g$ for an extended period of time does not cause any major deterioration in mechanical properties [101]. Considering the fact that the heat treatments in this study were performed under vacuum conditions and for a maximum of two hours, the possibility of lowered mechanical properties of ASA due to heat treatment is not expected. Comparison of the FTIR spectra in ATR mode of the ASA samples prior to and post HTA processing in fact confirm the fact that there are no observable changes in ASA chemical structure due to annealing. The comparison of the bulk mechanical properties also verifies this finding, as no signs of deterioration are observed after heat treatments.

Furthermore, the annealing process can also result in physical changes in the system, such as relaxing residual stress and the molecular orientation of the samples which were both results of the injection molding process. It is reasonable to assume that the changes in scratch behavior in the ASA systems are due to either PBA migration toward the surface or relief of surface residual stresses and molecular orientation, or a combination of both. However, the annealing conditions are seen to significantly alter the scratch performance of ASAs while having minimal effect on SAN. The sole difference between ASA and SAN copolymers is the presence of rubber phase in ASAs. Therefore, the changes in molecular orientation and relaxation of residual stress alone due to annealing are seen to have minimal effects on the scratch performance of these systems. It should be noted that the migration of rubber particles towards the surface of

71

an injection molded polymer blend has been observed in previous studies [112, 113] when heat treatment is performed at temperatures above $T_g$ which is in agreement to the basis of our findings. The results of image-j analysis on the surface mircographs indicating that rubber fraction per surface area of ASA5 increases from 13.0% to 18.9% due to annealing at high temperature further support this argument.

Based on the AFM images shown above, it can be observed that during the HTA process, the surface morphology of the ASA blends has been altered. Prior to the annealing, it can be detected that the observed concentration of the rubber particles on the surface is lower (13%) than that after annealing (18.9%) at high temperature (Fig. 25). This change in surface morphology because of increased concentration of rubber particles after being subjected to high temperature annealing is noteworthy. The morphology of the rubber phase also appears to vary due to the heat treatment, where the rubber phase in the as-received samples is more elongated; while, after the annealing process, the rubber particles tend to become a more spherical-like morphology. This is due to the effect of heat treatment on relaxation of thermal stress or variations in molecular orientation caused by the injection molding process, which has been shown to occur in previous studies [106].

Based on the findings of the onset of groove formation, it can be seen that an increase in rubber particle content in ASAs leads to a decrease in the critical normal load for groove formation which can be simply explained by the decrease in compressive strength due to increased rubber concentration. Based on the previous studies [94, 99, 100], it has been shown that groove formation during the scratch process typically

72

depends on the compressive yield strength of the material which is a bulk property. Since it is shown that the HTA treatment does not noticeably influence the bulk mechanical properties, it can be expected for the onset of groove formation to be independent of the heat treatment performed on the material, which validates the observation that onset of groove formation is not affected by heat treatment conditions. This is in agreement with the findings of this study.

Comparing the scratch visibility of the ASA systems prior to and after annealing processes, it shows that in most cases the onset of scratch visibility is delayed in HTA treated systems. Since it has been shown in previous studies that the onset of visibility depends mainly on the developed shoulder height of the scratch [108], it is concluded that the HTA treatment causes a reduction in the shoulder height of the scratch compared to LTA, leading to delayed scratch visibility. This in fact can be due to the rubber particle migration to the surface which may result in increased elastic and inelastic recovery after the scratch loads have been removed. The migrated rubber phase may not lead to a change in the bulk properties while enhancing the recovery of the scratch deformation, leading to a delay in scratch visibility.

Furthermore, it is evident that the onset of periodic cracking has been significantly delayed in the case of HTA treated ASA systems. The migration of the rubber particles to the surface as evidenced by the AFM images and supported by contact angle results can influence the scratch performance of the copolymer. While it has been shown that the bulk mechanical properties remain unchanged, the increase in rubber content at or near the surface can delay the cracking phenomena. Since periodic

73

cracking occurs at or near the surface of the ASA sample, the increased rubber content may lead to a localized toughening effect near the surface while maintaining the bulk properties of ASA. The possible change in rubber phase morphology due to stress relaxation must also be considered as a contributing factor in these phenomena. The fact that onset of crack formation for ASA systems is significantly affected by annealing conditions while in the case of SAN onset of cracking is independent of annealing conditions must be noted. The only variable between SAN and ASA is the presence of rubber particles in ASA systems. This in turn suggests that the improved scratch performance due to annealing significantly above $T_g$ in ASAs must be due to the presence of rubber particles, which can either migrate to the surface or facilitate relaxation of the SAN molecules and cause retraction of the stretched PBA rubber particles. However, to better comprehend the exact nature of this finding and also determine the influence and contribution of molecular orientation, further detailed studies are still needed.

## 3.6 Conclusion

In this study, the effects of two different heat treatments on the scratch behavior of ASA systems were investigated. It is found that, in comparison to annealing slightly higher then Tg (LTA), annealing well above Tg (HTA) caused a relative migration of rubber particles to the surface, which, in turn, leads to enhancement of the scratch behavior of ASAs. This improved scratch performance is evidenced by delays in the onset of periodic cracking, plowing deformation, along with scratch visibility. Interestingly, it is also shown that the bulk mechanical properties of the systems remain

the same after annealing, thus leading to the conclusion that the change in surface properties alone lead to this improved scratch resistance. These findings suggest that while keeping the bulk properties of a polymeric system unscathed, altering surface characteristics, such as phase morphology or molecular orientation, can lead to improved scratch behavior. This, in turn, introduces an interesting possibility of manipulating surface properties in order to achieve optimum scratch performance.

CHAPTER IV

ENVIRONMENTAL CONDITIONING EFFECT ON SCRATCH BEHAVIOR OF

MULTIPHASE STYRENIC COPOLYMERS

## 4.1 Synopsis

The effects of thermal history and moisture content on the scratch performance of two Styrenic copolymers, Acrylonitrile Butadiene Styrene (ABS) and Acrylonitrile Styrene Acrylate (ASA) with varying rubber size, is investigated through annealing at above $T_g$ temperatures and water immersion. ASA containing 100 nm and 1 micron sized rubber particles as well as ABS with 100 nm rubber particles were studied. Linearly increasing normal load scratch tests were performed according to ASTM D7027/ISO 19252 standards and the onsets of crack formation and plowing were the criteria used to investigate the scratch damage. Comparatively, the results for ASA and ABS indicate that the scratch resistance of ASAs are more dependent on thermal history than ABS, whereas ABS exhibits a higher sensitivity to moisture than ASA. When looking at the effect of rubber size, the results indicate a more pronounced effect from annealing with nano-sized rubber particles compared to the micron-sized scenario and the scratch resistance. Several deformation and damage mechanisms have been proposed to explain the observed differences in scratch performance based on the multiphase nature of these polymers that leads to localized deformation mechanisms during scratch.

## 4.2 Introduction

The widespread use of polymers in various industrial applications such as packaging films, coatings, electronic housings, structural components, etc. has led to a research emphasis on tribological investigations in order to determine the surface damage behavior of these polymers [114]. Scratch, which can be defined as an indentation and subsequent transverse movement of a rigid tip across a surface [114, 115], is considered one of the most common forms of surface damage and falls under the abrasive wear branch of tribology. Since 1950, various experimental techniques for polymer scratch testing have been proposed [116-120] and most recently one of these testing methodologies was standardized and designated as the ASTM D7027-05/ISO 19252 method [121, 122]. This standardized testing method consists of a progressively linearly increasing linear normal load generating distinct damage transitions, and has since been used extensively for industrial and academic scratch studies. Damage transitions along the scratch path may include groove formation, scratch visibility, fish-scale formation, cracking, and plowing, and have been essential in quantitative scratch performance evaluation as well as structure–property relationship investigations [121, 123-129].

Several attempts have been made to categorize the observed scratch damage features into scratch-deformation maps. Briscoe et al. [130, 131] explained that the formation of scratch damage features in a specific polymeric system depends on the normal load, testing speed, testing temperature, and the cone angle of the scratch tip. Maeda et al. [132] emphasized the relationship between the friction force and scratch

damages by manipulating the cone angle of the scratch tips and the viscoelastic properties of formulated rubber compounds. More recently, Jiang et al. [125, 128] investigated four kinds of distinctively different commercial polymers and detailed the observed relationship between a material's characteristics/properties and its scratch deformation features. Their efforts resulted in scratch maps, useful tools for illustrating the importance of various material parameters and testing conditions on scratch damage mechanisms. Jiang et al. [125, 128] also provided an in-depth mechanistic description of how scratch damage evolves. By using a three-dimensional finite element methods (FEM) analysis, they found that the material beneath the scratch tip experiences a compressive stress state while the material element behind the scratch tip experiences tensile stress during the early stages of a scratch, which either leads to fish-scale formation in the case of ductile polymers or crazing/microcracking in the case of brittle polymers. They also noticed an additional maximal tensile stress component develops in front of the scratch tip as the normal load increases which eventually leads to plowing or cutting as the exerted stress magnitude exceeds the strength of the material. The findings explained above imply that the constitutive behavior of a polymeric surface is what governs its scratch behavior, not its bulk mechanical properties.

Although numerous studies on polymer scratch have been carried out [114-131], significant research efforts are still needed to better understand and improve polymer scratch resistance. For instance, the role of rubber particles added to a thermoplastic matrix in terms of scratch performance isn't completely understood. Even though rubber particles can act as impact modifiers, increasing the material's toughness and/or

78

ductility, they can also reduce the modulus and strength [133, 134] of the system, which complicates their effect on scratch behavior. Polymeric materials usually consist of more than one chemical component and can be multi-phase in nature. As a result, choices in processing equipment and conditions can significantly affect their final phase morphology and skin-core characteristics. In a recent study on a soft thermoplastic olefin (TPO) that consisted of 70 wt % ethylene-propylene rubber (EPR) and 30 wt % polypropylene (PP), Browning et al. [126] found that the crystallinity of the ethylene segment and the internal morphology of the EPR phase significantly affect the scratch behavior of the soft TPO. In another study, Moghbelli et al. [127] manipulated the skin-core morphology of polypropylene (PP) thin sheets through post-processing thermal treatments. Their results suggest that the degree of surface crystallinity can significantly influence the scratch behavior. Moghbelli et al. [129] further showed that neat epoxy resin exhibits a higher scratch resistance than nanocomposites of the same epoxy filled with either ZrP nanoplatelets or core-shell rubber (CSR) nanoparticles. This implies that improvements in tensile strength and modulus alone (i.e., epoxy/nanoplatelet scenario) or fracture toughness and ductility alone (i.e., epoxy/CSR scenario) may not necessarily lead to the enhancement of scratch performance. The above findings imply that: 1) the surface or sub-surface phase morphology of semi-crystalline polymers, which can be manipulated by the processing conditions, plays an important role in polymer scratch behavior and 2) the surface properties of a semi-crystalline polymer, which significantly affect the scratch resistance, are likely to be different from those of the bulk. However, it is uncertain if the above observations hold true for amorphous polymers.

ASA copolymer was developed in 1970s and is considered to be a weather resistant counterpart of ABS [135, 136] and is employed in exterior applications such as automotive radiator grills and casings, electronics, etc. [135] because of its combination of high toughness, dimensional and thermal stability, and its aging and weathering properties. This terpolymer can be processed repeatedly over a wide temperature range without yellowing. ASA has a similar chemical structure to acrylonitrile–butadiene–styrene terpolymer (ABS), both of them were composed of styrene–acrylonitrile (SAN) matrix containing a rubber phase. However, there exist some differences between the two rubber phases. The core of ABS is butadiene rubber, while that of ASA is acrylic elastomer. This difference causes the difference in aging characteristics between the two polymers because the double bond in the repeat unit of ABS undergoes physical or chemical aging caused by oxygen conditions and UV radiation when used in exterior applications, resulting in: aging of the rubber phase, a continuous decline in mechanical strength, and color changes. As the acrylic rubber replaces the butadiene rubber in ABS, the aging of butadiene rubber is resolved. ASA closely resembles ABS but ASA is superior to ABS, because ASA presents better comprehensive properties; it enhanced the weather resistance of the polymer to great extent without nearly any loss of other properties, such as mechanical properties, processing properties, electric insulation, and chemical resistance. Our previous study indicates that the scratch performance of ASA generally deteriorates with increasing rubber content, and is strongly related to their reduction in tensile and compressive yield strengths [115]. It is hoped that the present

study can further our fundamental understanding of structure-property relationship in polymer scratch.

Post processing heat treatment of polymers has been shown to significantly affect their physical and mechanical properties. Depending on the composition and processing conditions, noticeable changes in mechanical properties have been observed through heat treatment of styrenic copolymers [128, 129]. While partial residual stresses were relieved, a noticeable drop in impact resistance and ductility were observed after long term annealing in acrylonitrile-butadiene-styrene (ABS) at temperatures below $T_g$. This is due both to the physical aging effect and to degradation of the Carbon double bond in the backbone of ABS [128]. In contrast, the heat treatment of butyl-acrylate rubber-modified styrene-acrylonitrile (ASA) copolymers caused no deterioration in mechanical properties at temperatures below or above $T_g$, even for extended periods of time [129]. In the same study, it was also shown that relief of injection molding residual stresses, as well as molecular orientation, could be achieved to a degree, depending on the ASA annealing process.

Our previous study indicates that the scratch performance of ASA generally deteriorates with increasing rubber content, which is also related to the reduction in tensile and compressive yield strengths [130]. It was also shown elsewhere [] that annealing above the glass transition temperature can significantly enhance scratch resistance of ASA copolymers with high rubber content while having no impact on SAN scratch performance. This finding was explained through increased rubber concentration at the surface after annealing and a possible localized toughening mechanism. It is hoped

that the present study can further our fundamental understanding of structure-property relationship in polymer scratch of multiphase systems, and also establish an approach to enhance scratch resistance without compromising bulk properties through high temperature annealing or moisture exposure.

In this study, a series of amorphous ASA and ABS systems, which are butyl-acrylate/butadiene rubber-modified styrene acrylonitrile (SAN), were chosen as model systems for investigating how post processing heat treatment and water immersion affects their scratch behavior. The multiphase nature of these polymers can lead to complexities in scratch behavior and must be emphasized to gain fundamental knowledge of their scratch behavior.

## 4.3 Experimental

### 4.3.1 Materials

The ASA copolymers utilized in this study were provided by Styrolution GmbH (Frankfurt, Germany). They consist of a random copolymer SAN matrix and grafted polybutyl-acrylate (PBA) rubber particles with an average nominal diameter of 100 or 1,000 nm. In the SAN phase, the acrylonitrile content was controlled to be at 35 wt%, and the weight-average molecular weight (Mw) of SAN was chosen to be 104 kg/mol [115]. The test specimens were fabricated by injection molding with a fan gate design to spread and slow the melt as it enters the mold cavity to ensure near-uniform molecular orientation across the width of the plaques. The plaques were 150 mm x 150 mm in rectangular shape and 6 mm in thickness. Nomenclature and physical characteristics of each system are listed in Table 4.

**Table 4. Rubber particle size and type in each examined system.**

|  | Rubber Type | Structure Type | Rubber Size | Color |
|---|---|---|---|---|
| **SAN** | none | 35% AN content; $M_w$=134000 g/mol | none | Black |
| **ASA100** | ASA | SAN grafted PBA rubber | ≈ 100 nm | Black |
| **ABS100** | ABS | SAN grafted PBD rubber | ≈ 100 nm | Black |
| **ASA500** | ASA | SAN grafted PBA rubber | ≈ 500 nm | Black |
| **ASA1000** | ASA | SAN grafted PBA rubber | ≈ 1000 nm | Black |

*4.3.2 Environmental Conditioning*

The ASA and ABS plaques were initially dried in a vacuum oven overnight at 85°C and a vacuum pressure of 30 mmHg. After drying, some of the plaques were immersed into water by being placed into a 10 liter deionized water bath at 23°C for a duration of 28 days in which equilibrium water content was achieved. In addition to the dried samples, these moisture absorbed plaques were also scratch tested and analyzed to determine the effect of moisture on the scratch performance of the model systems.

Furthermore, after drying, the annealing process was carried out on each system by sandwiching ASA and ABS plaques with two tempered glass plates 200 x 200 x 6 mm$^3$ in size. An external weight leading to stress of about 10 KPa was applied to the sandwiched samples during annealing and cooling to prevent the potential for uneven residual stress relief or warping of the plaques. The high temperature annealing (HTA) process was conducted at 140 °C, which is about 30°C higher than the measured $T_g$

[130], for 2 hrs under vacuum pressure of 30 mm Hg. Afterwards, the samples were slowly cooled to ambient temperature at approximately 2°C/min. The scratch tests were completed within an hour after annealing to minimize moisture adsorption from the atmosphere.

*4.3.3 Scratch Testing*

Scratch tests were carried out according to the ASTM D7027/ISO 19252 standard by using a progressive load range of 1–70 N at a constant scratch speed of 100 mm/s for a length of 100 mm. A stainless steel scratch tip with a spherical geometry was used. The diameter of the scratch tip was 1mm. A minimum of five scratch tests were performed on each scratch plaque oriented in the same direction as the melt flow.

*4.3.4 Scratch Deformation Analysis*

Scratch damage analysis was carried out 24 hours after completion of scratch tests to allow for any viscoelastic recovery. The critical normal load for the onsets of groove formation, cracking, and plowing were measured using a Keyence VK9700 Violet Laser Scanning Confocal Microscope (VLSCM). The onset points for micro-cracking and plowing were directly observed under the microscope. The onset of groove formation was determined using the height profile obtained from topographical imaging *via* VLSCM.

*4.3.5 AFM*

The characterization of sample morphology using AFM (Dimension, Veeco) was carried out by BASF SE. The imaging for AFM measurements were performed in Tapping Mode. The cantilever is excited at its resonance frequency and moved at a

84

defined height over the sample surface. Thus, interaction forces cause a variation in the oscillation amplitude of the lever. Furthermore a phase shift between the excitation and response oscillation can be induced by different material properties like stiffness or adhesiveness. In addition to the height, this effect provides the material contrast information on the sample (Phase images). An Olympus silicon tip was used with cantilever spring constant 40 N/m. The cross sections of the samples were prepared using microtome technique at -80°C. The AFM measurements were carried out at room temperature.

*4.3.6 Tensile and Compressive Analysis*

Dog-bone shaped specimens for tensile testing based on ASTM D638 type I geometry were prepared by BASF SE (Ludwigshafen, Germany). The nominal length, thickness, and width of the narrow section were 170, 4, and 10 mm, respectively. The test was performed at constant crosshead speeds of 5 and 50 mm/min under ambient temperature using a screw-driven Sintech2 load frame equipped with a 30 KN load cell and MTS632 extensometer.

Specimens for uniaxial compression testing were prepared using plaques with 6 mm thickness. The compression specimens were precisely cut by an Isomet VR Precision Saw 1000 into prisms with sharp, clean edges. The surfaces of the specimens were carefully polished using 4000 grit silicon carbide polishing paper. The nominal dimensions of the prisms were 12.7 mm x 6 mm x 6 mm, and the actual dimensions were measured by a digital caliper. The uniaxial compression tests were performed following the ASTM standard D695-10 using a screw-driven load frame (MTSVR Insight) and an

MTSVR extensometer with a gauge length of 25.4 mm. During compression testing, adequate lubricant (DupontVR TeflonTM Silicone Lubricant spray) was applied on the contact surfaces to reduce surface friction. The compression tests were performed at a crosshead speed of 2.5 mm/min.

*4.3.7 Friction Measurement*

To determine the coefficient of friction, $\mu_f$ at the interface between the Styrenic plaques and stainless steel surface, a flat smooth stainless steel surface with dimensions of $10x10$ mm$^2$ was used and tested using 5 N constant normal load for a distance of 60 mm at a velocity of 100 mm/s. Three tests were conducted for each system to obtain an average value of $\mu_f$.

*4.3.8 FTIR*

In order to determine surface chemical composition of all ASA systems a Nicolet Avatar 360 was utilized under attenuated-total-reflectance (ATR) mode at room temperature. Spectra were obtained at various locations of each specimen and the resulting FTIR spectra of samples before and after annealing were compared.

*4.3.9 Surface Shear Strength Measurements*

Surface shear strength was measured for each system using a SAICAS DN-20S apparatus at constant horizontal and vertical speeds of 5.0 and 0.5 μm/s using a 0.5 mm wide diamond blade and was repeated at least five times. A cutting depth of 100 microns from the surface was selected for analysis.

**4.4 Results and Discussion**

AFM micrographs throughout the sample thickness of each system before and after annealing is shown in Figure 34. These images indicate the size and shape of the rubber particles within each studied system throughout the cross sectional thickness before and after annealing. It can be seen that in both ASA100 and ABS100 the approximate rubber size is 100nm while in ASA1000 the rubber is significantly larger and approximately 1 micron or 1000nm. The variation in rubber shape throughout the thickness for each system can be related to residual stress from injection molding while inclusions can be seen in the midsection of each system which is expected. The HTA process is seen to cause some subtle changes in the surface morphology especially for ASA100 and ASA1000, and can lead to relief of thermal residual stresses while minimizing orientational effects.
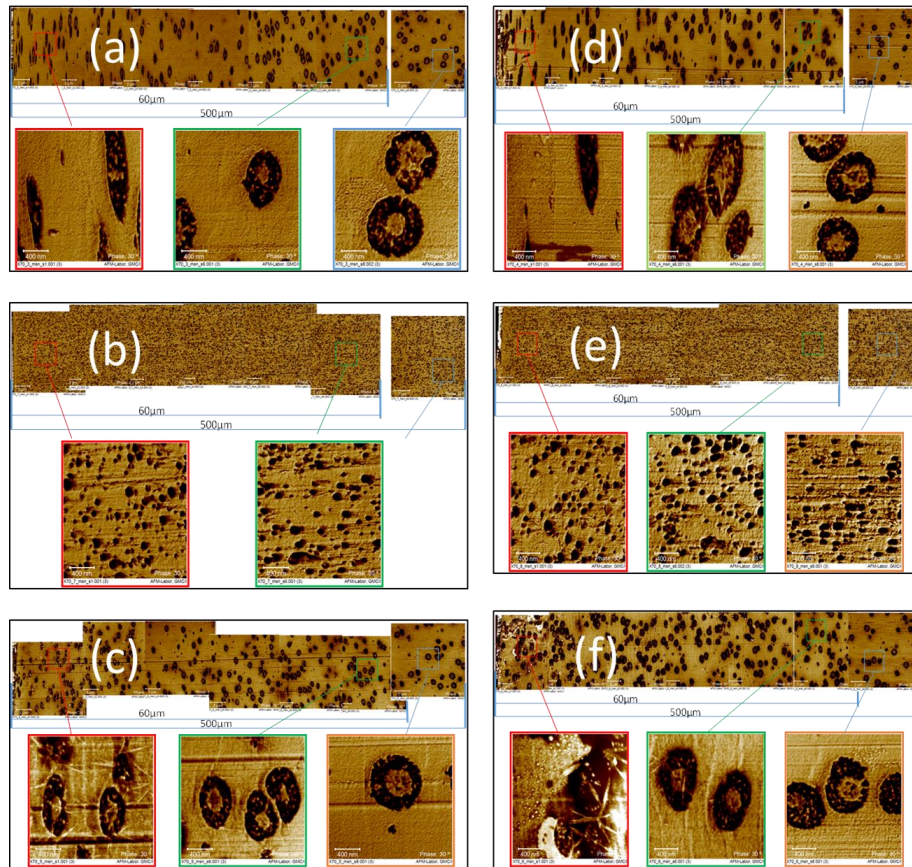
**Figure 34. AFM micrographs of cross-sections: close to the surface to middle of plaque: (a)ASA100 (b)ABS100 (c)ASA1000 (d)HTA-ASA100 (e)HTA-ABS100 and (f)HTA-ASA1000.**
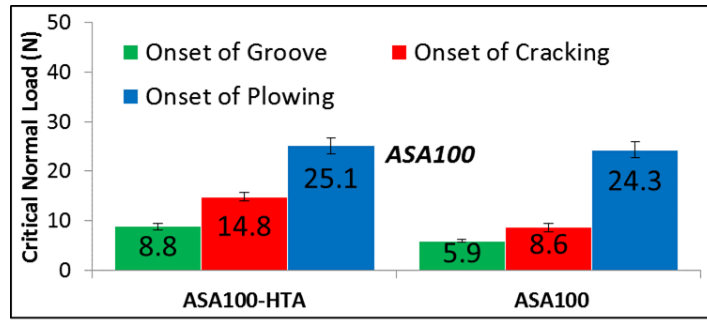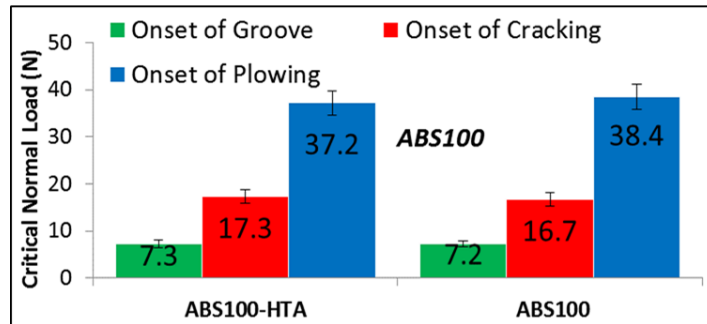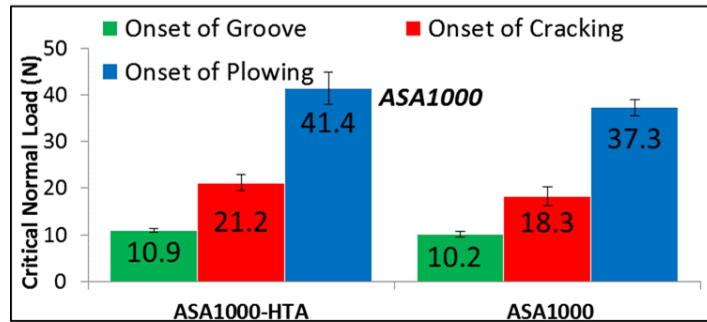
**Figure 35. Critical normal loads for onsets of crack formation and plowing before and after high temperature annealing in a) ASA100 b) ABS100 and c) ASA1000.**

The scratch resistance of model ASA and ABS systems under dry conditions before and after high temperature annealing were evaluated. The critical normal load results for onsets of crack formation and plowing for each system have been shown in Figure 35 (a)-(c). These damage criteria are the typical scratch deformation transitions

observed in SAN, ABS, and ASA type materials. Both onsets of cracking and plowing are indicators of material failure at the surface beyond which material fracture or removal will take place.

The onset of groove formation for ABS100 and ASA1000 are not affected by the HTA process while the critical load for groove formation in ASA100 increases noticeably due to the annealing process. The onset of cracking in ABS100 is seen to remain unchanged after the annealing process which can be attributed to the low oriented structure and mechanical isotropic behavior of ABS which can be an advantage during melt molding and processing [111,112]. Since it was found elsewhere [102] that the HTA process doesn't affect scratch resistance of single phase SAN, the presence of rubber phase in ASA is most likely the determining factor. The HTA process did not seem to affect the onset of plowing in any of the three cases while for the onset of cracking it appears that HTA process caused a noticeable increase in scratch resistance for ASA100 while showing much less of an effect on ASA1000.

At the late stages of the linearly increasing normal load scratch deformation a tensile stress component is developed in front of the tip leading to material removal or plowing. This tensile stress possesses the highest tensile magnitude among other developing stress components [122]. The tangential direction of this stress component relative to the scratch tip leads to the cutting of the piled up material ahead of the tip which also leads to a reduction in stick slip motion. As mentioned above the HTA process did not affect the onset of plowing in the studied systems, which will be subject to further investigations. In general an important attribute of ABS copolymers are their

minimum tendency to orient or develop mechanical anisotropy during processing and molding [128, 129] compared to other rubber modified systems such as ASA or HIPS. This ABS property is identified as the major reason behind the independence of scratch resistance to annealing process for ABS. However, for ASA the mechanical anisotropy due to processing must be taken into consideration which leads to the differences in scratch behavior due to annealing especially in ASA100.

During high temperature heat treatment of rubber/plastic blends the elastomeric phase is usually more vulnerable to decomposition, mainly due to the chemical composition i.e. having double bounds (C=C) in the backbone. Hence the importance of obtaining physical spectra prior to and after heat treatments to confirm the surface similarities. An FTIR spectrum of ASA100 before and after annealing has been shown in Figure 37. This spectrum, obtained under ATR mode, indicates the identical characteristics of the surface prior to and after annealing. Similar spectroscopy was also performed on ABS100 and ASA1000 with similar results which have been omitted here. The typical adsorption peaks [1] caused by C=O double bonds and C≡N triple bonds have been highlighted in Fig. 37. Even though long-term aging at 90°C in air causes butadiene to oxidize in the rubbery phase of ABS [2] the matching spectra suggest no degradation detected after HTA process. In general ASA holds up very well against annealing in extreme conditions due to its' lack of C=C double bonds and the vacuum environment [3].

Heat treatment of styrenic multiphase copolymers has been shown to yield different results for different types of copolymers as well as their treatment conditions. It

91

has been shown that in the case of long-term annealed ABS at temperatures below $T_g$, deterioration in mechanical properties, such as impact resistance and ductility, can be observed [128]. This is attributed to two factors. One is the presence of the C=C double bond on the butadiene segments resulting in change in chemical composition and degradation in properties [128]. Another is the physical changes occurred during the aging process which can lead to decreases in ductility [128, 134]. However, in the case of ASA copolymers it was shown that heat treatment close to $T_g$ for an extended period of time does not cause any major deterioration in mechanical properties [129]. The morphology of the rubber phase also appears to vary due to the heat treatment, where the rubber phase in the as-received samples is more elongated; while, after the annealing process, the rubber particles tend to become a more spherical-like morphology. This is due to the effect of heat treatment on relaxation of thermal stress or variations in molecular orientation caused by the injection molding process, which has been shown to occur in previous studies [134].

Alternatively, the above phenomena can also be caused by the relaxation of the highly oriented SAN molecules and retraction of PBA rubber near the skin of the injection-molded ASA samples. Upon high temperature annealing, the relaxation and retraction of the SAN molecules and PBA rubbers leads to exposure of the PBA rubber on the sample surface and roughens the surface somewhat, confirmed by the reported increase in surface roughness. It is reasonable to assume that the changes in scratch behavior in the ASA systems are due to either PBA migration toward the surface or relief of surface residual stresses and molecular orientation, or a combination of both.

However, the annealing conditions are seen to significantly alter the scratch performance of ASAs while having minimal effect on SAN. The sole difference between ASA and SAN copolymers is the presence of rubber phase in ASAs. Therefore, the changes in molecular orientation and relaxation of residual stress alone due to annealing are seen to have minimal effects on the scratch performance of these systems.
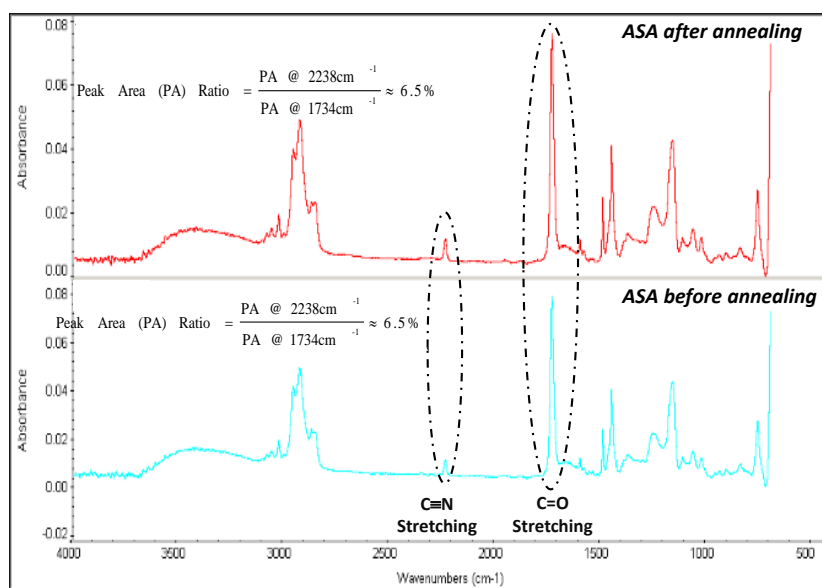


**Figure 36. ATR mode FTIR spectrum of sample surface before and after heat treatment.**

To assess the scratch performance of various polymer systems, the corresponding mechanical properties should be determined. As discussed elsewhere, various aspects of the mechanical properties can influence the scratch resistance exhibited depending on the performance criteria chosen, i.e., crack formation, visibility, or material removal. For crazing-prone polymers it has been shown that tensile strength and friction coefficient ($\mu_f$) are most critical to scratch resistance [128]. Tensile comparisons of the studied systems have been shown in Figure 37 where curves with solid lines represent non-

93

annealed systems while dashed .curves represent the HTA systems. It is seen that the annealing process does not impact any of the systems response to uniaxial tension while the same was observed for compression tests. The tensile behavior of the model systems before and after annealing were also seen to closely resemble each other as observed in Figure 37. Therefore bulk tensile and compressive properties do not explain the observed influence of HTA on scratch resistance.
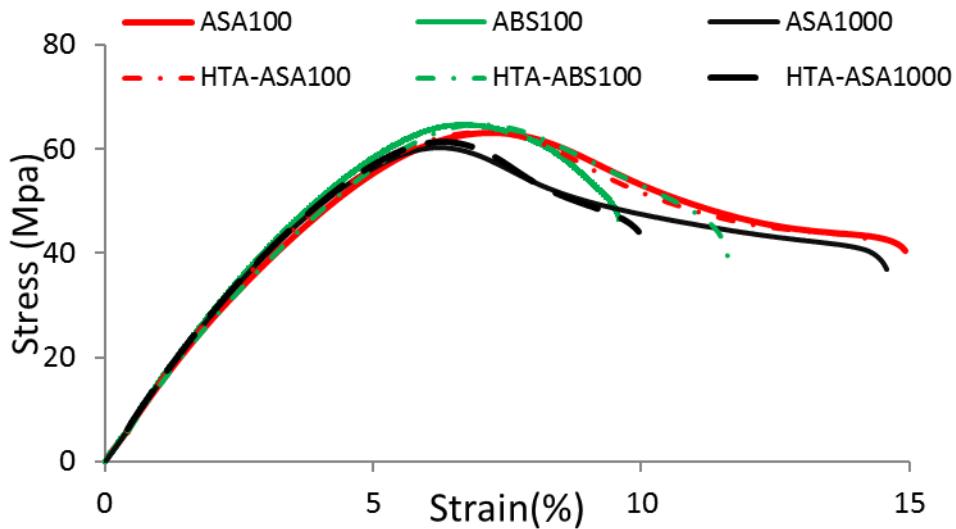


**Figure 37. Mechanical properties of ASA100, ABS100, and ASA1000 before and after annealing.**

Furthermore, it is evident that the onset of periodic cracking has been significantly delayed in the case of HTA treated ASA systems. The migration of the rubber particles to the surface as evidenced by the AFM images and supported by contact angle results can influence the scratch performance of the copolymer. While it has been shown that the bulk mechanical properties remain unchanged, the increase in rubber content at or near the surface can delay the cracking phenomena. Since periodic

94

cracking occurs at or near the surface of the ASA sample, the increased rubber content may lead to a localized toughening effect near the surface while maintaining the bulk properties of ASA. The possible change in rubber phase morphology due to stress relaxation must also be considered as a contributing factor in these phenomena. The fact that onset of crack formation for ASA systems is significantly affected by annealing conditions while in the case of SAN onset of cracking is independent of annealing conditions must be noted. The only variable between SAN and ASA is the presence of rubber particles in ASA systems. This in turn suggests that the improved scratch performance due to annealing significantly above $T_g$ in ASAs must be due to the presence of rubber particles, which can either migrate to the surface or facilitate relaxation of the SAN molecules and cause retraction of the stretched PBA rubber particles. However, to better comprehend the exact nature of this finding and also determine the influence and contribution of molecular orientation, further detailed studies are still needed.

The coefficient of friction for each system before and after annealing is shown in Figure 38 where it is evident that the annealing process causes a significant reduction in ASA100 surface friction while not affecting surface friction for the other systems. Based on previous studies [125], the onset of groove formation depends on multiaxial compressive yield stress and surface friction between the scratch tip and the sample surface. This in fact provides an explanation for the relative onset of groove formation loads before and after annealing.
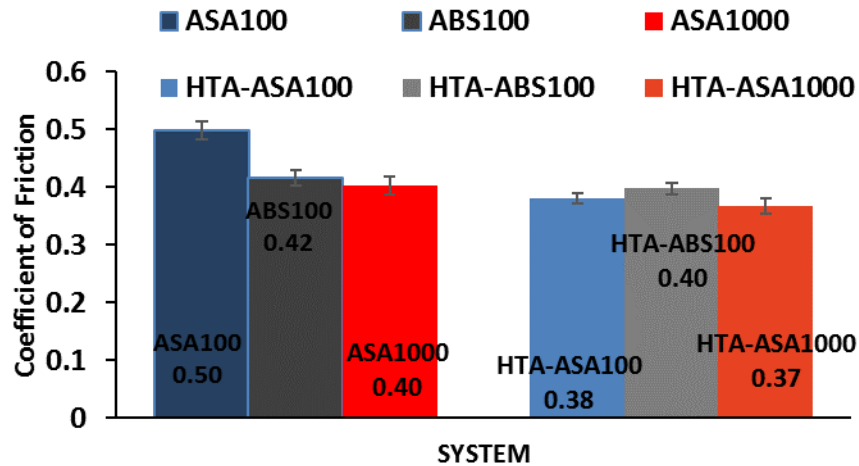
**Figure 38. Coefficient of friction comparison of model systems before and after annealing.**

PFQNM analysis done on the surface of dried and annealed samples during AFM measurements provides a surface mapping of modulus and hardness. The AFM micrographs and surface moduli values of SAN and ASA5 surfaces have been shown below in Figure 39 (a) and (b). It can be seen that SAN surface topography, modulus, height profile is not influenced by the HTA process (Fig. 39(a)) whereas in ASA5 the effect of annealing can easily be seen in Figure 39(b). Furthermore the HTA process is seen to cause surface roughening, morphology variation, and leads to observation of two separate modulus peaks in ASA while having little impact on SAN. Based on the size and shape of the soft phase observed by PFQNM coupled with surface modulus data including peak values and frequencies, a representative schematic of the rubber/plastic morphology at the surface can be drawn. The schematics shown in Figure 40 are based

on these AFM results and illustrate the variation in surface morphology before and after annealing for various systems.
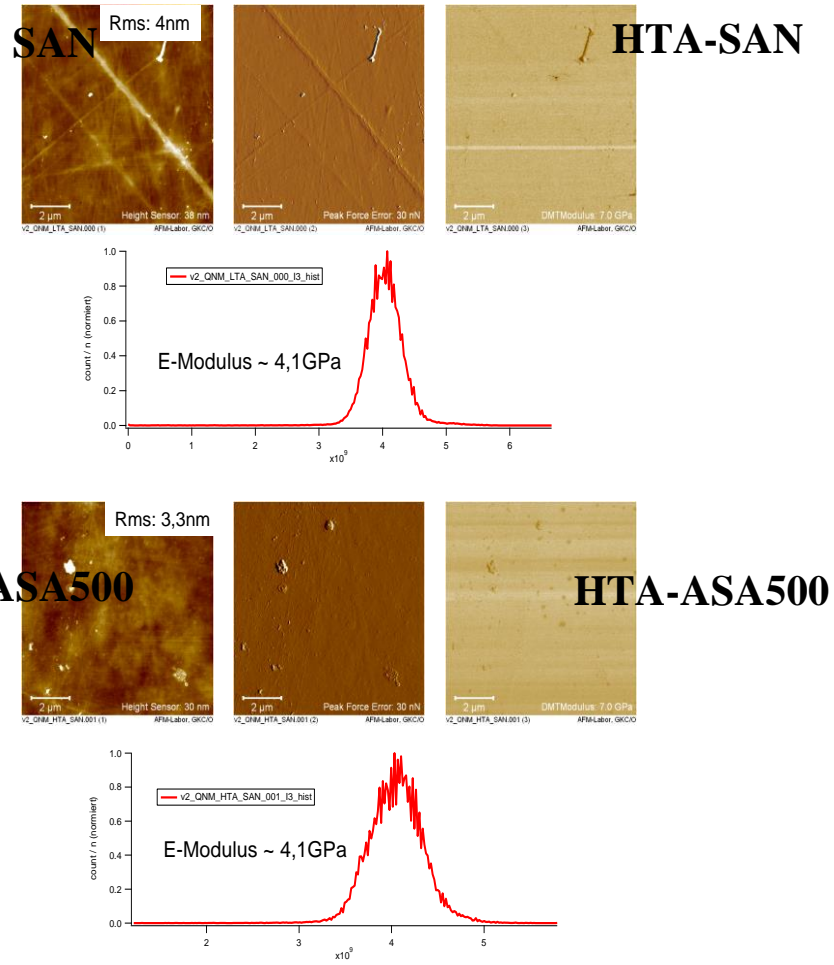


**Figure 39. PFQNM results and AFM micrographs of sample surfaces before and after high temperature annealing for a) SAN and b) ASA500.**
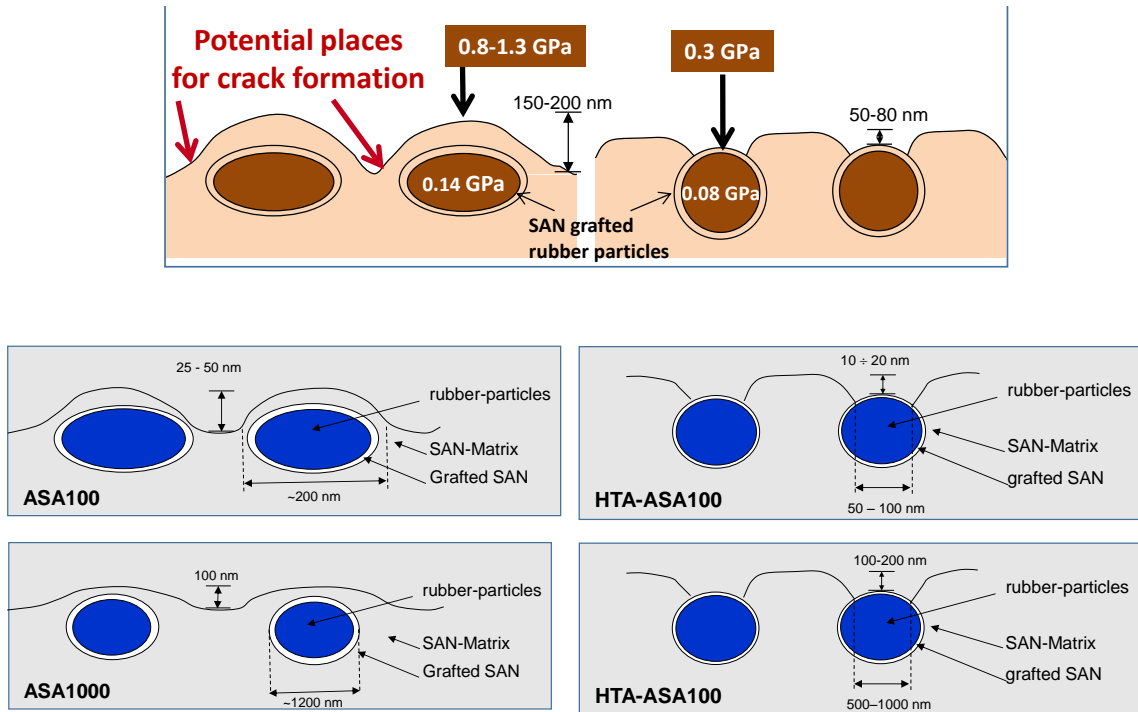
**Figure 40. Schematic representation of plastic/rubber morphology at ASA surfaces and alterations caused by annealing in different rubber sized systems a) ASA500 b) ASA100 and c) ASA1000.**

In Figure 40 it can be observed that in ASA100, ASA1000, and ASA500 the surface morphology of the plastic and rubber form hills and valleys with elongated rubber particles covered by the SAN matrix prior to HTA. After the annealing process the rubber particles are seen to appear at the surface and minimize their orientation in the melt flow or injection molding direction. However the surface hills and valleys in ASA100 and ASA500 seem to be more intense than ASA1000, where a thin layer of SAN plastic forms a topographical feature above the grafted PBA rubber particle. These thin layers of SAN plastic could be vulnerable to surface deformations such as scratch due to several factors including the interfacial bonding and adhesion between the rubber

and plastic matrix, which could lead to the observed flake like cracking which has been illustrated and discussed elsewhere [116].

The surface shear strength of ASA100 and ASA1000 under dry conditions, after HTA, and after moisture saturation can be seen below in Figure 41. It can be observed that in terms of surface shear strength ASA100 is affected positively from the HTA process while having no impact on ASA1000. Based on the scratch damage features observed in ABS and ASA copolymers, detailed elsewhere [116], where flake like cracks were observed in place of the more common tensile dominated parabolic shaped cracks [118] the surface shear strength findings can actually clarify some issues listed below.

The increase in surface shear strength after HTA will most likely cause the increased scratch resistance and delayed onset of cracking due to the flake like features of the original cracks which have been attributed to a more shear dominated failure mechanism due to the stress state exerted during a scratch deformation. The fact that surface shear strength of ASA1000 before and after annealing is constant explains the fact that HTA had little to no impact on scratch performance of ASA1000.
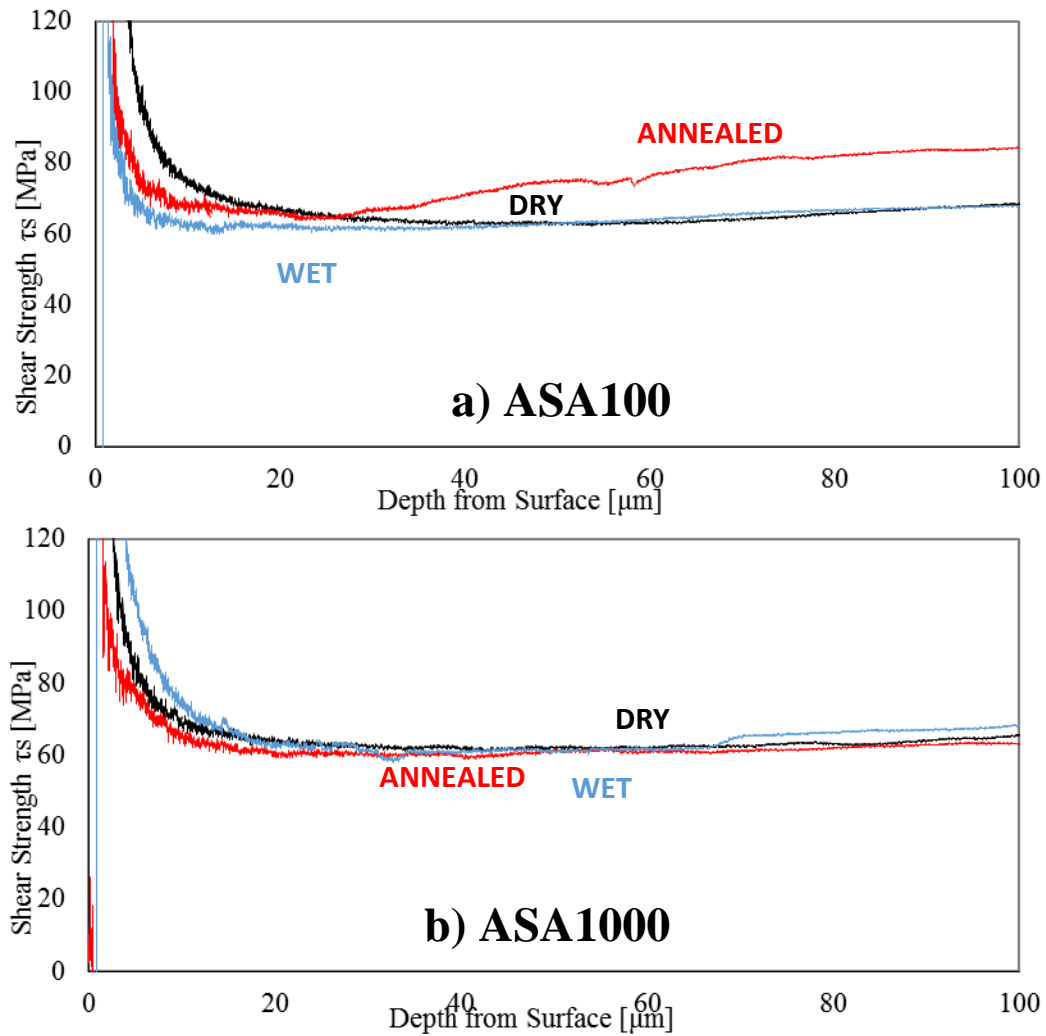
**Figure 41. Surface shear strength as a function of depth from surface for a) ASA100, and b) ASA1000 before and after annealing.**

Furthermore, the injection molding process of the model multiphase systems were carried out introducing another variable, the mold wall temperature (MWT) during injection molding, varying between 80, 100, 120, and 140°C. The effect of mold wall temperature on ASA scratch performance is examined and later correlated with the effects of ASA heat treatment through annealing on scratch behavior. Optical micrographs of the onset of crack formation along with the corresponding normal loads

for ASA100, ASA500, and ASA1000 are shown for the two extreme MWTs of 80 and 140°C in Figure 42. The critical loads for onset of crack formation for these systems at different MWTs are presented in Figure 43.
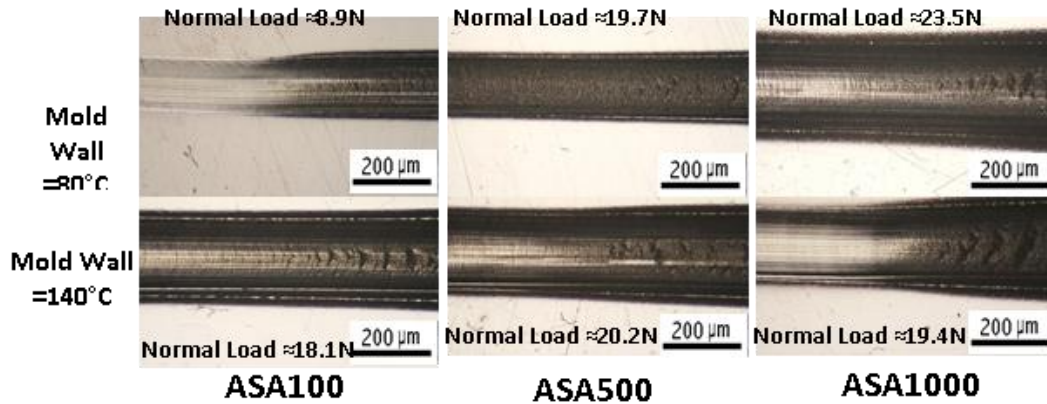


**Figure 42. Optical micrographs of the onset of crack formation for a) ASA100, b) ASA500, and c) ASA1000 with mold wall temperatures of 80°C and 140°C during injection molding process. Scratch direction is from left to right.**

Based on the normal loads at cracking shown in Figure 42 it seems that ASA100 is most influenced by MWT where increased mold wall temperatures lead to enhanced scratch resistance for ASA100 while ASA500 is seemingly not affected by MWT and interestingly ASA1000 scratch resistance is highest at lower MWTs although it is not as dependent as ASA100 on this heat treatment process. The bar graph shown below in Figure 43 confirms these observations regarding the scratch resistance of ASAs and the effect MWT will have. It should be noted that this behavior could be closely related to the effect of HTA on ASA scratch where the system (ASA100) which shows the highest impact from HTA also is influenced most by MWTs. This could simplify our quest for

101

designing scratch resistant materials through either processing conditions (MWT) or post processing heat treatments (HTA).
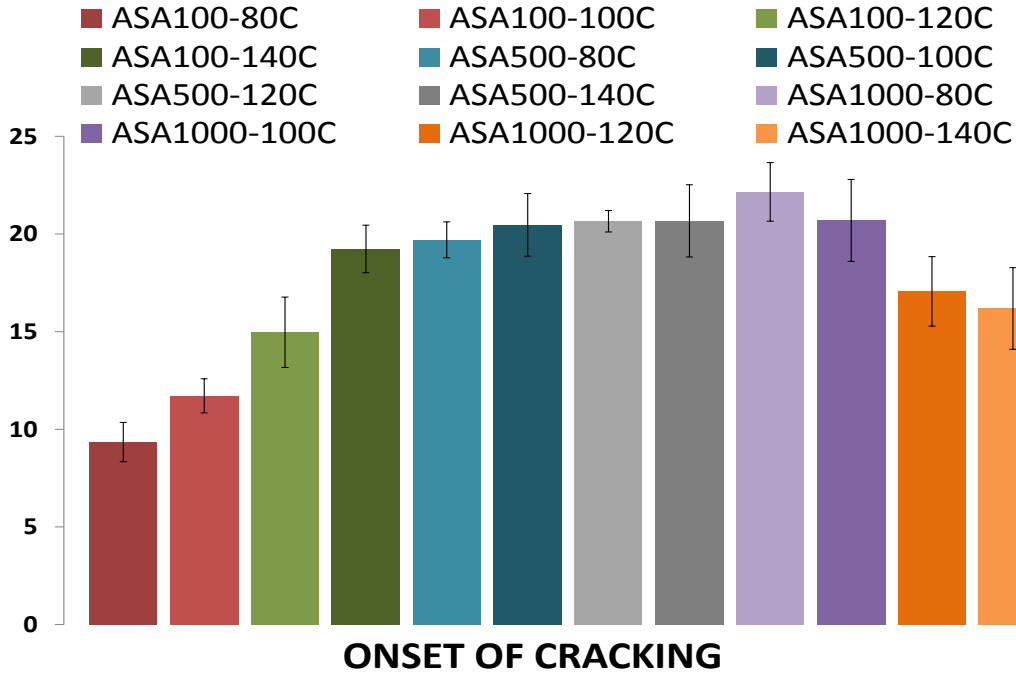


**Figure 43. Critical normal loads for onsets of crack formation and plowing for a) ASA100 b) ASA500 and c) ASA1000 at various injection mold wall temperatures of 80, 100, 120, and 140°C.**

## 4.5 Conclusion

In this study, the effects of two different environmental conditioning processes, heat treatment and water exposure on the scratch behavior of SAN and ASA systems were investigated. It is found that annealing well above Tg (HTA) caused a relative migration of rubber particles to the surface, which, in turn, leads to enhancement of the scratch behavior of ASAs. This improved scratch performance is evidenced by delays in the onset of periodic cracking, plowing deformation. Interestingly, it is also shown that the bulk mechanical properties of the systems remain the same after annealing, which

102

leads us to conclude that the improvements in scratch performance resulted from surface properties alteration. The surface shear strength results support this argument showing the localized effect in this case. These findings suggest that while keeping the bulk properties of a polymeric system unscathed, altering surface characteristics, such as phase morphology or molecular orientation, can lead to improved scratch behavior. This, in turn, introduces an interesting possibility of manipulating surface properties in order to achieve optimum scratch performance. Moisture and water exposure was seen to influence the scratch resistance of systems containing rubber particles to a higher extent which were explained through the local lubricating effect caused by the formation of water clusters.

# CHAPTER V

# EFFECT OF MOISTURE EXPOSURE ON SCRATCH RESISTANCE OF PMMA

## 5.1 Synopsis

Effect of environmental conditioning on scratch performance of polymethylmathacrylate (PMMA) is investigated. Three different grades of PMMA with varying levels of polarity were chosen and their scratch resistance compared in both dry and moist conditions. Linear increasing normal load scratch tests were performed according to ASTM D7027/ISO 19252 standards. Results indicate a drop in scratch resistance with initial exposure to moisture in all three systems. In the two highly polar PMMA systems, the scratch resistance recovers to that of the dry condition after long exposure to moisture.  It is proposed that the moisture absorbed initially acts as a plasticizer causing weakening of the surface mechanical integrity. In the case of more polar systems this moisture absorption continues until saturation where water molecules cluster and impart a degree of lubrication and consequently improves scratch resistance.

## 5.2 Introduction

Polymeric materials are widely utilized for durable goods applications due to their low cost, weight to strength ratio, and ease of fabrication. However, the scratch resistance of polymers is seen to be considerably less than that of rivaling materials such as ceramics and metals. Hence, polymer scratch resistance is a topic of major research interest.

Environmental exposure may lead to considerably changes in properties through different mechanisms including moisture absorption/desorption, ageing/annealing, morphology evolution, and composition alteration in bulk or surface. Environmental exposure of polymers typically includes ultraviolet (UV) radiation, cyclic heating, and humidity. Some thermoplastic polymers are known to undergo stress cracking due to UV exposure through sunlight [142–145]. Significant recent efforts have focused on investigating the effects of environmental conditioning on tribology and surface behavior of polymers [146–152]. For instance, it was found [149] that increasing temperature causes an increase in friction and affects the deformation during the sliding process. An increase in temperature was also found to have a detrimental effect on the scratch resistance of coated automobile polymer systems [150].

One of the most common environmental factors that may greatly influence the retention of surface quality and its resistance to deformation is the humidity to which a polymer is exposed to after being fabricated. Polar thermoplastic polymers are especially susceptible to moisture absorption and diffusion due to their affinity to moisture. The absorbed moisture behaves as a plasticizer for the polymer chains to exert a greater

degree of freedom for movement, thus weakening the polymer. To our best knowledge, no systematic efforts have been undertaken to directly link the effect of absorbed moisture and material parameters on the scratch performance of polymers. Plasticization is known to have a detrimental effect on properties like glass transition temperature, modulus, tensile strength, etc. [153–155]. There has been a great deal of work focused on the moisture absorption of cross-linked epoxy-based polymer matrices [156–158]. On the other hand, moisture absorption of many thermoplastic polymers like polyethylene, polypropylene, and polystyrene is considered largely negligible due to their highly non-polar nature in contrast to other thermoplastics, such as nylon, which contain stronger polar groups.

For over 50 years, acrylic plastics based on polymethylmethacrylate (PMMA) have been used for automotive taillight applications due to its high clarity and superior weathering characteristics. Other clear plastics, such as styrenics and polycarbonate, contain an aromatic structure that will interact with UV wavelengths. These plastics degrade and turn yellow, and experience gloss reduction upon outdoor exposure to sunlight. PMMA does not contain aromatic structures and is not susceptible to UV damage in sunlight. PMMA chemistry remains unchanged after outdoor exposure [159-162].

The effects of environmental conditioning on various physical and mechanical properties of PMMA have been previously examined [161, 163-179]. Ishiyama and Higo [169] found that increased moisture content leads to lower elastic modulus and tensile strength in various PMMAs. Absorbed water to PMMA causes swelling of the acrylic

polymer and reduction in glass transition temperature ($T_g$) [169-171] through decreased cohesive forces between polymer chains. Increased moisture content in PMMA causes a linear increase in coefficient of thermal expansion (CTE) [172], a noteworthy fact in thermal and mechanical applications. Effects of PMMA moisture content on diffusion coefficient and density have been examined extensively [173-176]. It was found that diffusion coefficient of water in PMMA decreases and the polymer density increases along with moisture concentration, in contrast to exposure to organic vapors which show an opposite trend [173, 179]. The difference observed in diffusion rate due to water/solvent presence depends on the polymer-solvent interaction as well as the physical properties of the penetrant. Lowered diffusion rates have been attributed to low solvent latent heat such as water in ethylcellulose [173, 175], which leads to formation of water clusters. Thus, if polymer-solvent interaction is weaker than solvent-solvent interaction, clustering of the solvent molecules within the polymer matrix is expected [173, 177, 178].

The current study investigates the influence of moisture exposure on the scratch behavior of a set of model PMMA systems with varying polarity using a standardized progressive load scratch testing and analysis methodology (ASTM D7027/ISO 19252) [180, 181]. The onsets of scratch deformation mechanisms like scratch visibility, and periodic micro-cracking within the scratch path are identified as metrics for scratch resistance evaluation. It is hoped that the current study can shed light on how an environmental factor, such as moisture uptake resulting from exposure to a humid environment, can influence the scratch behavior of polymers.

## 5.3 Experimental

### 5.3.1 Materials

Three grades of PMMA, including impact modified grade (PMMA-1), V-grade (PMMA-2), and scratch resistant grade (PMMA-3), were used for this study. The PMMA-3 has the highest polarity, followed by PMMA-2, and PMMA-1. Injection molded plaques of each grade with dimensions of 150mm x 150mm x 3mm were provided by Arkema Inc. All plaques are black in color and have smooth surfaces consistent with one another. Description of each grade was provided by the manufacturer as displayed in Table 5. Elastic modulus, tensile strength and other physical properties are given elsewhere [182].

**Table 5. Basic physical properties of each PMMA grade.**

|  | Melt Flow Rate (@ 230°C, 3.8Kg) | Glass Transition Temp.($T_g$) | Color | Relative Polarity |
|---|---|---|---|---|
| **PMMA-1** | 1.8 | 114°C | Black | Low |
| **PMMA-2** | 2.8 | 116°C | Black | Medium |
| **PMMA-3** | 3.4 | 105°C | Black | High |

### 5.3.2 Environmental Conditioning

The PMMA plaques were initially dried by placing in a vacuum oven for 24 hours at 80°C and a vacuum pressure of 30 mmHg. After drying, the various plaques were weighed using a high precision digital scale and then placed into a moisture chamber with a controlled relative humidity of 75% at 23°C. Over a period of 28 days,

the samples were removed from the chamber and weighed accordingly. After studying the moisture absorption behavior of the PMMA plaques, several plaques of each PMMA system were also periodically scratch tested over a two-week period. Each plaque was placed into the moisture chamber to allow for moisture absorption, then removed and scratch tested accordingly at various conditioning times ranging from one day to two weeks.

*5.3.3 Scratch Testing*

Scratch tests were carried out according to the ASTM D7027/ISO 19252 standard by using a progressive load range of 1–100 N at a constant scratch speed of 100 mm/s for a length of 100 mm. A stainless steel scratch tip with a spherical geometry was used. The diameter of the scratch tip is 1mm. A minimum of five scratch tests were performed on each PMMA scratch plaque oriented in the same direction as the melt flow.

*5.3.4 Scratch Performance Analysis*

After completion of scratch tests, 24 hours was allowed for any viscoelastic recovery before carrying out scratch analysis. For analysis purposes, the plaques were scanned using an Epson Perfection Photo 4870 PC scanner set at a resolution of 300 dpi along with a Munsell minicolor checker for color correction purposes. Automatic Scratch Visualization (ASV) software (http://www.surfacemachines.com) was used to analyze the scanned images and obtain scratch visibility of each scratch which has been detailed in earlier studies [183]. Since the orientation of the scratch path with respect to the illumination source can affect visibility assessment, the samples were scanned with

the scratch path oriented perpendicular and parallel to the direction of light source travel in the scanner.

The critical load for the onset of any scratch deformation mechanism is found by first noting the distance along the scratch path where the damage first appears and then extracting the applied normal load at that point from the data file. The onset points for micro-cracking and plowing were directly observed under a microscope. The microscope used for these observations was a Keyence VK9700 VLSCM under 10X magnification.

*5.3.5 Contact Angle Measurements*

All three PMMA systems were evaluated to assess contact angle changes as a function of conditioning time in the hygroscopic conditioning chamber. After drying and consequently throughout conditioning, the plaques were periodically removed from the moisture chamber and placed on a flat, level surface with proper lighting for contact angle measurements. Several individual droplets of deionized water were deposited on each surface using a 1 ml syringe fitted with a 27.5 gauge needle at atmospheric pressure, ambient temperatures, and 50% relative humidity. The distance between droplets was maintained at a minimum of 20mm to prevent interference.

Images were obtained using the super macro mode of a 10-megapixel Olympus SP-570UZ digital camera. Images were subsequently processed (inverted and sharpened) with ImageJ software (http://rsbweb.nih.gov/dij). Using the angle measuring tool in ImageJ, contact angles were measured for both sides of each droplet with respect to the sample surface. A minimum of six droplets was used to obtain average values.

*5.3.6 Coefficient of Friction Measurement*

To determine the coefficient of friction, $\mu_f$ at the interface between the PMMA plaques and stainless steel surface, a flat smooth stainless steel surface with dimensions of $10 \times 10$ mm$^2$ was used and tested using 5 N constant normal load for a distance of 60 mm at a velocity of 100 mm/s [193]. Three tests were conducted for each system to obtain an average value of $\mu_f$.

## 5.4 Results

Moisture absorption and diffusion behavior of each PMMA type plaque has been investigated up to four weeks and shown in Figure 44. The absorption of moisture was carried out until equilibrium was reached for each of the three model PMMA systems, which took approximately 14 days. The relative polarity of the PMMA grades can be directly related to the amount of moisture uptake at equilibrium as shown in previous studies [182]. However, the results of contact angle measurements in dry conditions also support this fact.
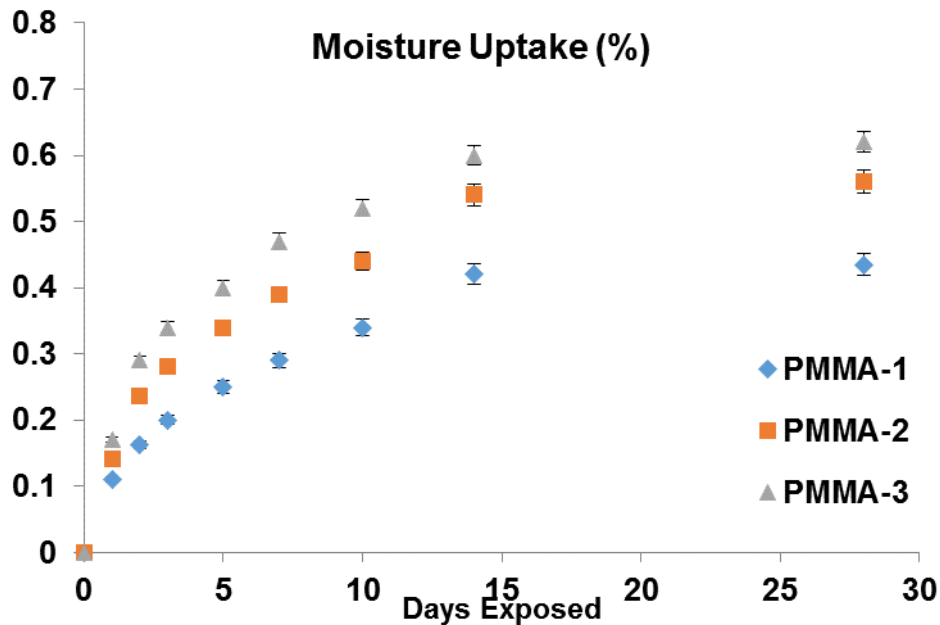
**Figure 44. Moisture uptake of various PMMA grades by weight %.**

The contact angle of water droplets on each PMMA grade as a function of conditioning time is shown in Figure 45. Contact angle measurements reported at day 0 correspond to the dry condition. The relative comparison of each system contact angle with water exposure against the dry condition is an indicator of their relative polarity. As expected, PMMA-3 has the lowest contact angle while PMMA-1 exhibits the highest contact angle. The effect of conditioning in a moist environment can be seen as a function of time for each system. While all three systems show reductions in contact angle from dry condition to equilibrium moisture saturation, the observed trends are different. In both PMMA-2 and PMMA-3 after approximately 5 days, a noticeable drop is apparent while this sudden change is absent in PMMA-1.
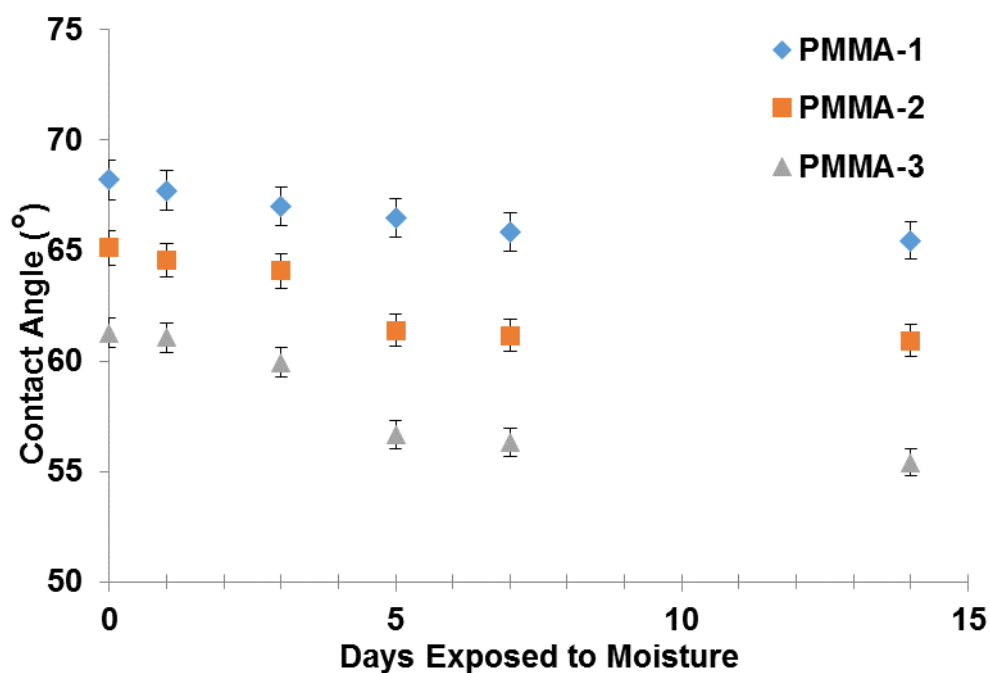
**Figure 45. Contact angle measurements as a function of conditioning time for all three PMMA grades.**

To assess the scratch performance of various polymer systems, the corresponding mechanical properties before and after moisture exposure should be determined. As discussed previously, various aspects of the mechanical properties can influence the scratch resistance exhibited depending on the performance criteria chosen, i.e., crack formation, visibility, or material removal. For crazing-prone polymers, such as PMMA, it has been shown that tensile strength and friction coefficient are most critical to scratch resistance [194]. As a result, the tensile strength values of the model PMMA systems are reported. As shown in Figure 46, the tensile strength of each PMMA grade is reduced with exposure to moisture. However, it should be noted that the moisture exposure can also noticeably reduce the friction coefficient, thus compensating for the

negative impact of tensile strength reduction in PMMA on scratch performance, as will be discussed below.
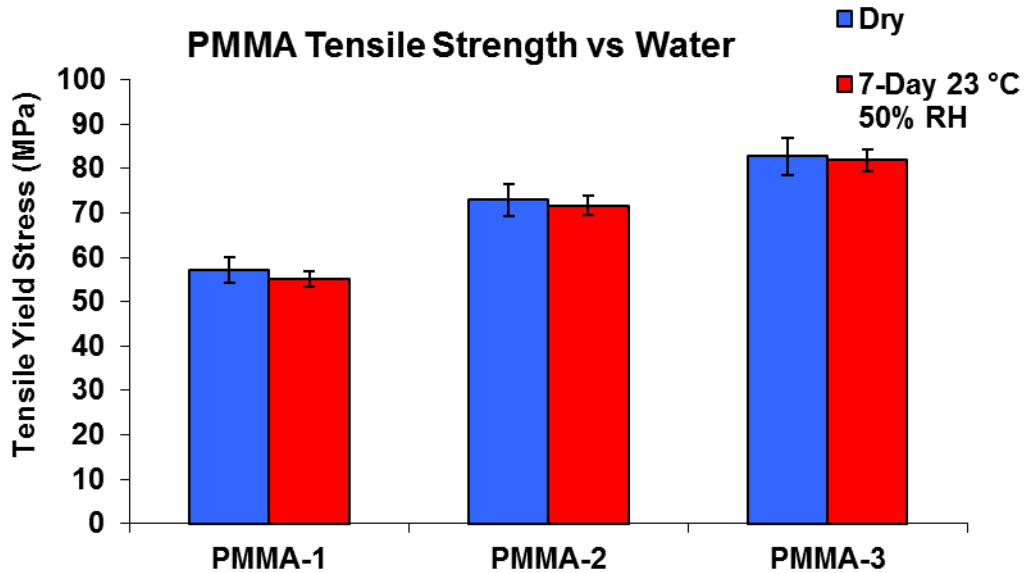


**Figure 46. Tensile strength of PMMA grades in dry condition and after moisture exposure.**

In Figure 46, it can also be seen that the tensile strength of PMMA-2 is higher than PMMA-1 in both dry and moisture absorbed conditions while PMMA-3 has the highest tensile strength. This is in agreement with the average critical load for onset of crack formation observed for the PMMA grades, where higher tensile strength leads to higher scratch resistance [184].

Periodic crack formation along the scratch path is a known scratch damage mechanism in PMMA [183]. As shown in Figure 47, the cracking transitions for each PMMA system in dry condition are shown with the corresponding normal load, where the scratch direction is from left to right.
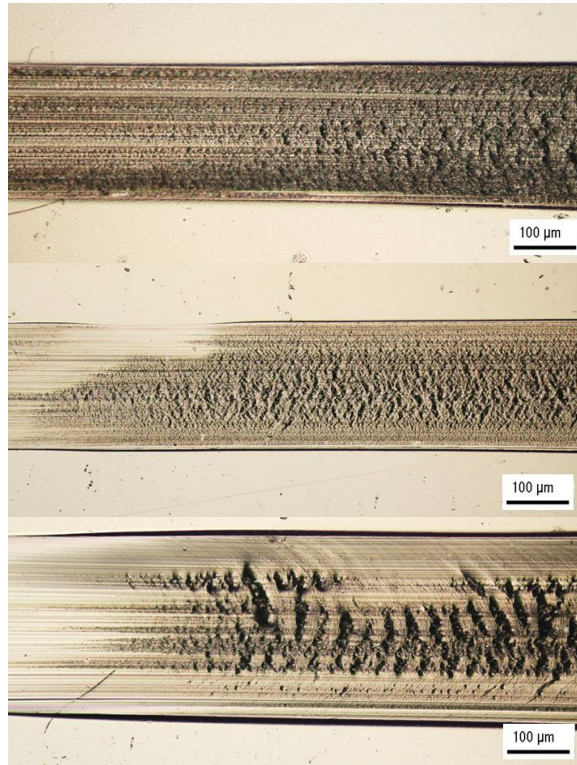
**Figure 47. Onset of crack formation micrographs and corresponding normal loads for a) PMMA-1, b) PMMA-2, and c) PMMA-3.**

The critical normal loads for onset of crack formation in PMMA systems are summarized in Figure 48. The onset of cracking is compared in dry and moisture exposed samples through various exposure days. In all three systems, it can be observed that the first days of moisture exposure leads to a reduction in scratch resistance independent of the PMMA type. In the case of the more polar PMMA systems, i.e., PMMA-2 and PMMA-3, recovery of scratch resistance can be seen after a short moisture exposure period. Interestingly, an improvement in the scratch resistance is observed after two weeks, the moisture exposure for these systems.
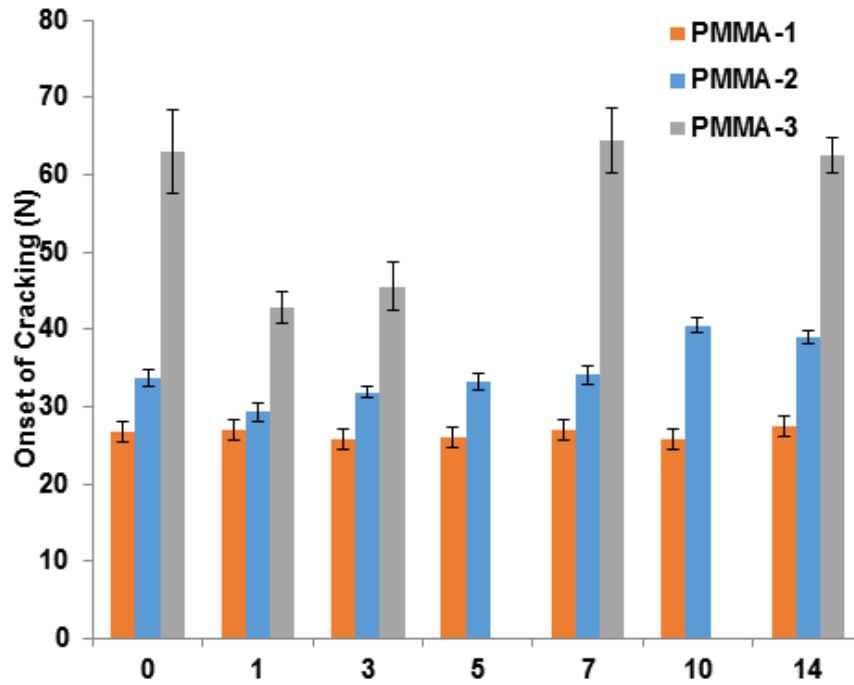
**Figure 48. Onset of crack formation vs. exposure days to moisture chamber for PMMA.**

The critical normal loads for onset of scratch visibility observed in both parallel and perpendicular orientations [183] can be seen in Figure 49. It can be observed that the onset of visibility results show the same trend as those observed in the onset of cracking for PMMAs and their moisture exposure effect. Also, in all three cases, the scratch visibility results in parallel and perpendicular orientations are in agreement with each other.

116
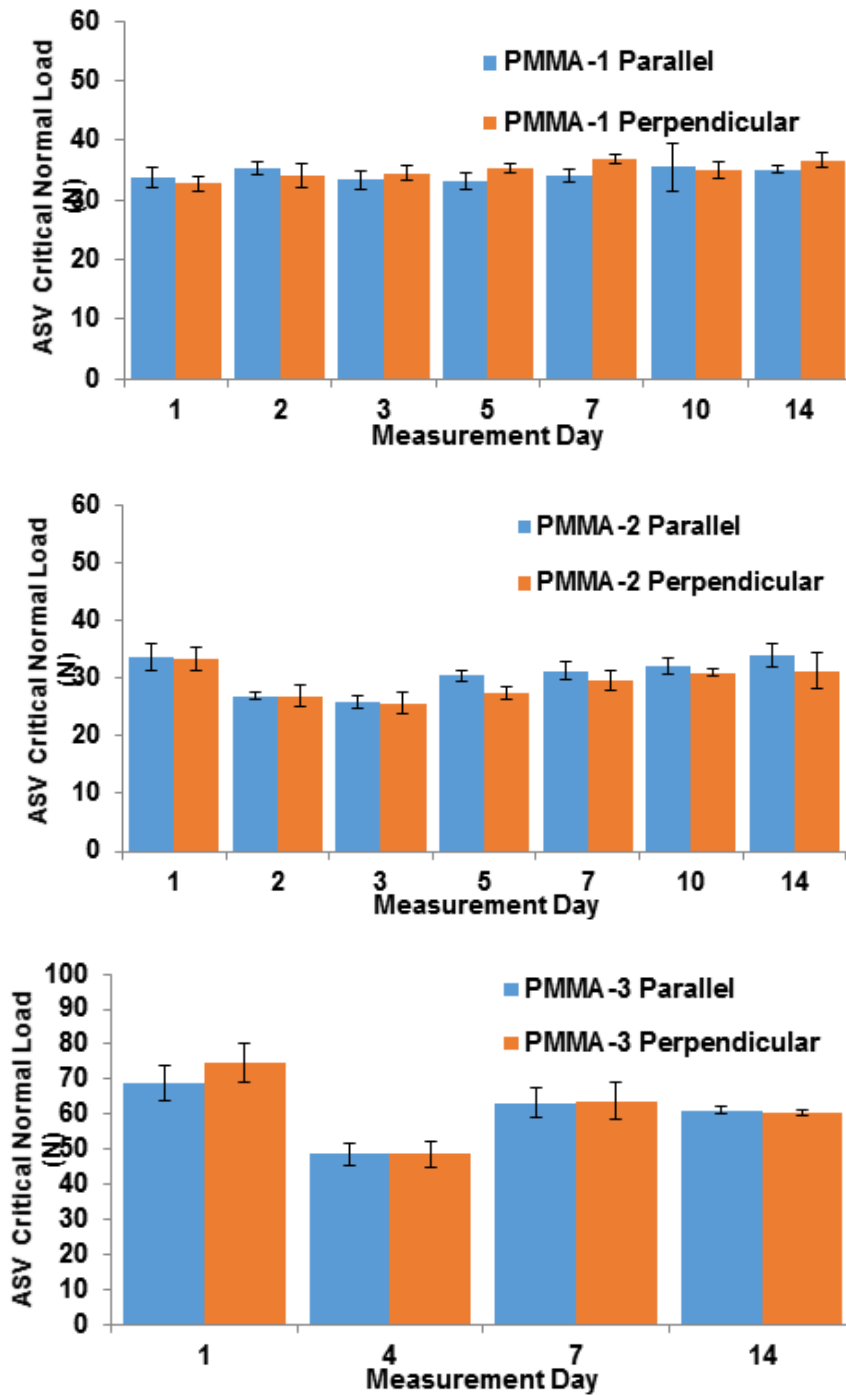
**Figure 49. Onset of scratch visibility for (a) PMMA-1 (b) PMMA-2 and (c) PMMA-3 in both parallel and perpendicular orientations.**

117

Coefficient of friction measurements were performed for each PMMA surface in dry condition and various moisture conditioning time intervals. The friction coefficient values for the three PMMA grades are shown in Figure 50.
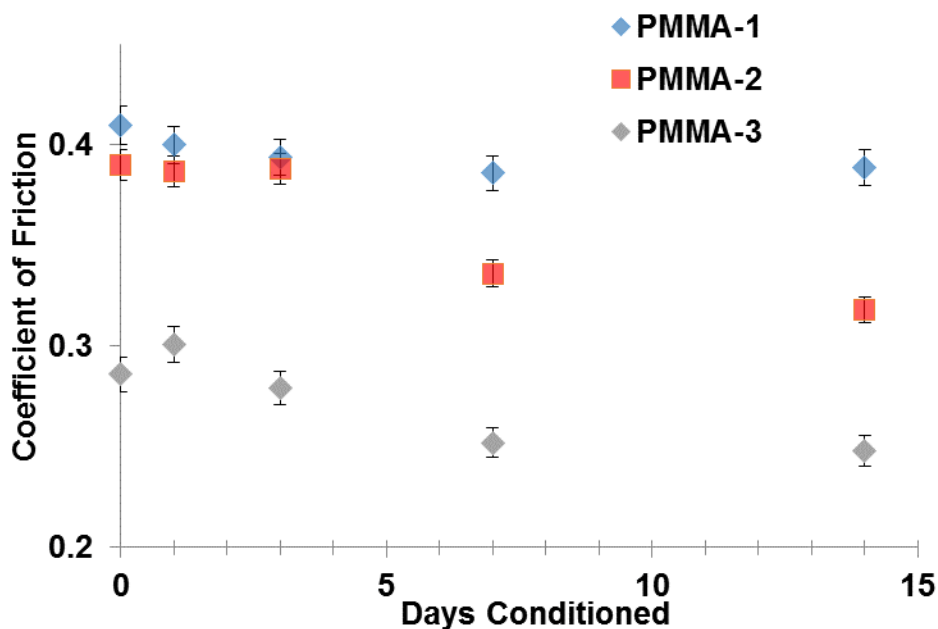


**Figure 50. Coefficient of friction as a function of conditioning time for all three PMMA grades.**

It can be seen that the first day of moisture exposure did not lead to any significant changes in the measured coefficient of friction. However, further exposure to moisture leads to a noticeable reduction in the friction coefficient for two more polar PMMA systems. PMMA-2 and PMMA-3 show a reduction in friction after 7 and 14 days, respectively. Interestingly, the duration at which reduction in friction is observed coincides with the enhancements in scratch resistance. This finding is in good agreement with observation made by Browning et al. [185] previously regarding the formation of water clusters on styrene acrylonitrile surface and their lubrication effect.

118

To further support this argument, attention can be drawn to the contact angle measurement results shown in Figure 45. It can be seen that, for the PMMA grades with higher relative polarity, a noticeable drop in contact angle is observed after five days; while for the less polar PMMA-1, no such effect is found. To better understand the changes observed in contact angle with environmental conditioning, the dominating mechanisms of water absorption and diffusion into the PMMA matrix must first be discussed.

The polarity of a polymer is known to not only affect the amount of moisture that can be absorbed at equilibrium conditions but also influence the moisture absorption and diffusion mechanisms [186-189]. There are two basic theories in regards to absorption and diffusion of any solvent molecules, i.e., water, within a polymeric system: the "free space theory" and the "polar site bonding theory" [190-192]. A schematic representation of a polar polymer structure containing chains and free volume is shown in Figure 51. Potential water bonding sites based on each mechanism are indicated in the image. Based on the polarity of the side groups shown in the figure, diffused water molecules will be located at either the free volume sites or the polar sites in the vicinity of the chain.

In the free space theory, several assumptions are made including minimal bonding between polymer and water molecules and a preferred affinity of water molecules within the free volume. Based on the free volume theory, water absorption should lead to increase in density while no changes in dimensions. On the other hand, the polar site bonding theory is based on bonding between water molecules and the polar

119

sites of the polymer chain, i.e., the carbonyl groups of PMMA. In this case, the diffused water affects the intermolecular bonding between polymer chains which lowers the glass transition temperature, while density remains unchanged leading to variation in the observed dimensional change [191, 192]. In the polar site bonding theory, based on polymer-water affinity compared to polymer-polymer affinity, the preferred hydrogen bonding at polar sites makes the formation of water clusters possible for certain systems. For instance, depending on the affinity of the polymer functional groups to water molecules, diffusion of moisture can either distribute uniformly throughout the polymer matrix or be drawn to form water clusters to a size as large as sub-micron sized particles. The former usually leads to plasticization of the matrix, but the latter can cause degradation of mechanical properties near the surface or throughout the bulk.
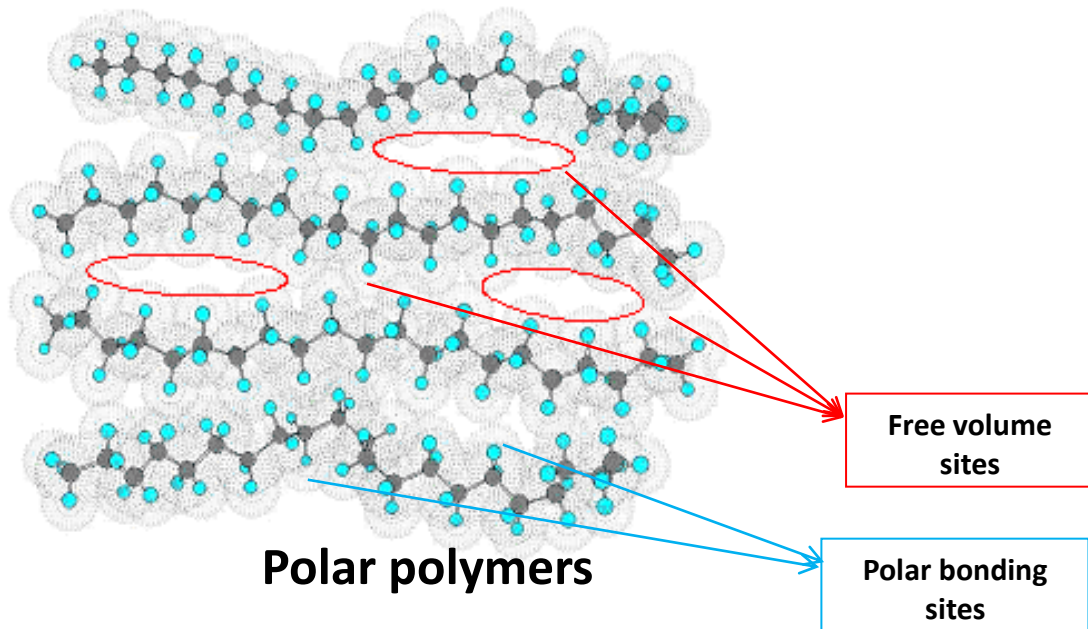


**Figure 51. Schematic representation of water absorption mechanisms and different bonding sites.**

Presence of water clusters is known to influence the interaction between various polymer chains possibly leading to changes in adhesion/cohesion, wettability (and thus contact angle), glass transition temperature, surface coefficient of friction, and numerous other properties of a polymeric system [186]. In this case the reductions observed in contact angle after five days of moisture exposure is directly related to the formation of water clusters in the two polar PMMA grades; while in the PMMA-1 grade, uniform moisture distribution minimizes effect on contact angle. Furthermore, the coefficient of friction of each PMMA grade shown in Figure 50 also supports this finding. The noticeable drops in surface friction coefficients in both polar PMMA grades against PMMA-1 indicate the two different mechanisms of water absorption.

Based on polymer surface polarity, environmental conditioning can greatly influence the scratch resistance of a polymer. In this study, the scratch test findings indicate that moisture can influence PMMA scratch resistance through two different mechanisms. In low polarity PMMA, water absorption is dominated by the "free volume theory" where water molecules diffuse and distribute uniformly in the polymer matrix. The uniformly distributed water molecules within the PMMA act as a plasticizer to degrade the bulk mechanical properties gradually. In high polarity PMMA grades, water diffusion follows the "polar site bonding theory" where diffused water molecules interact with polar sites and form water clusters through hydrogen bonding. In this case, the water molecules can aggregate on the surface and serve as slip agent to reduce surface friction. The results from coefficient of friction and surface contact angle

measurements support the above proposed mechanisms for the model PMMA investigated.

The resistance of a polymer to scratch deformation is an important property especially for polymers used in durable goods applications, e.g., car exteriors and interiors, appliance housing, cell phone, etc., where aesthetics are of significant importance. Retention of scratch resistance after exposure to an environment depends on the susceptibility of the polymer structure to the environment and the time of exposure. The present study indicates that humidity can both weaken the polymer surface mechanical integrity and lower surface friction, which improves scratch performance, at the same time. It is thus rather difficult to predict whether or not humidity exposure can positively impact scratch performance of a given polymer unless testing is performed. Careful assessment is definitely warranted for determining scratch performance of polymers upon extended environmental exposure.

## 5.5 Conclusion

To investigate the long-term scratch behavior of a polymer, the susceptibility of the polymer to environmental factors, such as moisture, must be investigated. In polar polymers or polymers containing polar segments, moisture absorption will greatly affect scratch resistance. Based on the polarity of the system, it is observed that water can act as a plasticizer to cause a reduction in strength, thus leading to a lowered scratch resistance. However, depending on the polarity and exposure time, the formation of water clusters may lead to a beneficial lubrication effect on the polymer surface leading to enhanced scratch resistance.

CHAPTER VI

CONCLUSIONS AND CONSIDERATIONS FOR FUTURE RESEARCH

**6.1 Summary and Conclusions**

Scratch behavior of multiphase (plastic and rubber) Styrenic copolymers have been investigated to determine rubber size and type influence on scratch resistance. It appears ASA1000 is superior to ASA100 while ABS100 is similar to ASA1000 in dry conditions while closer to ASA100 after moisture exposure in terms of scratch performance. Mechanical properties including uniaxial tension and compression for these systems were determined to be almost identical, which rules out a straightforward explanation for the observed differences in scratch resistance. Thus our focus was shifted to a more detailed examination of the damage transitions and features for the three systems. SEM top view analysis showed differences in crack types developed in the scratch path from tensile cracking to a type of flaking or shear cracking. The subsurface damage observed from the longitudinal sections of each scratch groove also pointed to varied crack types from one system to another based on rubber size and type.

In addition to SEM and OM analysis, cross sectional views of the scratch were evaluated using AFM which can be useful in characterizing the subsurface morphology after scratching for each case. These results will be added in hopes of further understanding their behavior. Evidence of variations in crack type ranging from tensile to shear based must also be found using microscopy techniques in order to further support our argument. Furthermore, a surface mechanical characterization of each

system will be carried out in hopes of determining and comparing the relative surface shear strength for each system. This surface shear strength may be correlated with the possibility of flake formation or the competition between tensile and mixed mode cracking during the scratch process.

The effect of heat treatments at two different temperatures on the scratch behavior of ASA systems with varying rubber content, type, and size were investigated. It was found that, in comparison to annealing slightly higher than Tg (LTA), annealing well above Tg (HTA) caused a relative migration of rubber particles to the surface, which, in turn, leads to enhancement of the scratch behavior of ASAs. This improved scratch performance is evidenced by delays in the onset of periodic cracking, plowing deformation, along with scratch visibility. Interestingly, it is also shown that the bulk mechanical properties of the systems remain the same after annealing, thus leading to the conclusion that the change in surface properties alone lead to this improved scratch resistance. These findings suggest that while keeping the bulk properties of a polymeric system unscathed, altering surface characteristics, such as phase morphology or molecular orientation, can lead to improved scratch behavior. This, in turn, introduces an interesting possibility of manipulating surface properties in order to achieve optimum scratch performance. The HTA process was seen to improve the scratch resistance of copolymers containing 100 nm spherical rubber particles compared to 1000 nm particles. This was attributed to the surface morphology and orientation of the rubber phase before and after annealing, which lead to higher surface shear strengths.

The effect of moisture exposure at different relative humidity conditions on scratch performance was investigated in a variety of polymeric systems. Our findings indicate an initial drop in scratch resistance due to the plasticization effect of absorbed water molecules while continued exposure was seen to have varying results. In highly polar systems, after a certain duration the diffusing water molecules tend to aggregate and form water clusters, which can be concentrated near the surface. Water diffusion and absorption follows the polar site bonding theory, which in turn leads to a lubrication effect by the water clusters reducing the surface friction and improving the scratch resistance. In less polar systems, this improvement in scratch performance was not observed and the absorption and diffusion of water into the polymer was noted to follow the free volume bonding theory.

## 6.2 Considerations for Future Research

The findings presented in this dissertation, specifically, the effects of a soft dispersed phase on scratch performance of polymers and the corresponding environmental conditioning influence opens up new horizon of research to further our understanding in the field.

*6.2.1 Extended Study on Quantitative Modeling of Multiphase Systems*

The results of our experimental scratch evaluations can be further examined and understood by the assistance of numerical simulations in a complementing study. In this case, a detailed stress distribution map comparing the effects of rubber size, shape, and content on the surface deformation is desired.

125

*6.2.2 Determining Defined Parameters for Moisture/Water Influence*

The influence of moisture/water exposure on polymer scratch can be an advantage in production/design factor. If this phenomenon is fully understood, the application of specific polymers can be specifically tailored based on geographical locations, weather conditions, and type of use. For instance, the exterior coating of a car manufactured for use in Europe where weather conditions often mimic water immersion, can be designed from polymers with a high affinity for water cluster formation. However, a more general approach must be taken in order to properly predict moisture effect on any polymer system. This will require a more systematic approach and understanding of the thermodynamic process and related factors involved in water absorption theories.

*6.2.3 Examining the Interface and Interphase between Rubber and Plastic*

The interface between the rubber and plastic phases stemming from their interactions and adhesive affinity can also be explored to better comprehend subsurface damage in a scratch deformation. While this research has focused on the macro-scale observations of scratch research, the interphase between the two phases may also play a role, especially at lower length scales using an AFM or other nano-scale devices.

REFERENCES

[1]     Browning, R.L., Jiang, H., Sue, H.-J., *Scratch behavior of polymeric materials*, in *Tribology of Polymeric Nanocomposites*, K. Friedrich, Schlarb, A.K., Editor. **2008**, Elsevier: Oxford. p. 354-373.

[2]     Lim, G.T., *Scratch behavior of polymers*, Dissertation in *Mechanical Engineering* **2005**, Texas A&M University: College Station, Texas.

[3]     Wong, M., Lim, G.T., Moyse, A., Reddy, J.N., Sue, H.-J., *A new test methodology for evaluating scratch resistance of polymers. Wear*, **2004**. 256**,** 1214-1227.

[4]     Wong, M., *The Development of Scratch Test Methodology and Characterization of Surface Damage of Polypropylene*, in *Mechanical Engineering,* **2003**, Texas A&M University: College Station, Texas.

[5]     ASTM D7027-05, *Standard Test Method for Evaluation of Scratch Resistance of Polymeric Coatings and Plastics using an Instrumented Scratch Machine*, **2005**, ASTM International: Pennsylvania.

[6]     Jiang, H., Browning, R.L., Hossain, M.M., Sue, H.-J., Fujiwara, M., *Quantitative evaluation of scratch visibility resistance of polymers. Applied Surface Science*, **2010**. 256 (21): 6324-6329.

[7]     Jiang, H., Browning, R.L., Sue, H.-J., *Understanding of scratch-induced damage mechanisms in polymers. Polymer*, **2009**. 50(16): 4056-4065.

[8]     Browning, R.L., Sue, H.-J., Minkwitz, R., Charoensirisomboon, P., *Effects of acrylonitrile content and molecular weight on the scratch behavior of styrene-acrylonitrile random copolymers. Polymer Engineering & Science*, **2011**. 51(11): p. 2282-2294.

[9]     Jiang, H., Lim, G.T., Reddy, J.N., Whitcomb, J.D., Sue, H.-J., *Finite element method parametric study on scratch behavior of polymers. Journal of Polymer Science Part B: Polymer Physics*, **2007**. 45(12): 1435-1447.

[10]    Hossain, M.M., Jiang, H., Sue, H.-J., *Effect of constitutive behavior on scratch visibility resistance of polymers-A finite element method parametric study. Wear*, **2011**. 270(11-12): 751-759.

[11]    Hossain, M.M., Browning, R.L., Minkwitz, R., Sue, H.-J., *Effect of asymmetric constitutive behavior on scratch-induced deformation of polymers. Tribology Letters*, **2012**. 47(1): 113-122.

[12]    Bucaille, J.L., Gauthier, C., Felder, E., Schirrer, R., *The influence of strain hardening of polymers on the piling-up phenomenon in scratch tests: Experiments and numerical modelling. Wear*, **2006**. 260(7-8): 803-814.

[13] Hossain, M.M., Minkwitz, R., Sue, H.-J., *Minimization of surface friction effect on scratch-induced deformation in polymers. Polymer Engineering & Science*, **2013**. 53(7): 1405-1413.

[14] Hossain, M.M., Jiang, H., Sue, H.-J. *Correlation between constitutive behavior and scratch visibility resistance of polymers-A finite element method parametric study*. in *SPE TPO Global Conference*. **2011**. Detroit, Michigan.

[15] Reddy, J.N., *An Introduction to the Finite Element Method. 2nd ed.* **1993**, New York: McGraw-Hill.

[16] Mackerle, J., *Finite element and boundary element simulations of indentation problems: A bibliography (1997–2000). Finite Elements in Analysis and Design*, **2001**. 37(10): 811-819.

[17] Lee, J.H., Xu, G.H., Liang, H., *Experimental and numerical analysis of friction and wear behavior of polycarbonate. Wear*, **2001**. 251(1-12): 1541-1556.

[18] Bucaille, J.L., Felder, E., Hochstetter, G., *Mechanical analysis of the scratch test on elastic and perfectly plastic materials with the three-dimensional finite element modeling. Wear*, **2001**. 249(5-6): 422-432.

[19] Subhash, G., Zhang, W., *Investigation of the overall friction coefficient in single-pass scratch test. Wear*, **2002**. 252(1-2): 123-134.

[20] Jiang, H., Browning, R.L., Whitcomb, J.D., Ito, M., Shimouse, M., Chang, T.A., Sue, H.-J., *Mechanical modeling of scratch behavior of polymeric coatings on hard and soft substrates. Tribology Letters*, **2010**. 37(2): 159-167.

[21] Lim, G.T., Wong, M., Reddy, J.N., Sue, H.-J., *An integrated approach towards the study of scratch damage of polymer. JCT Research*, **2005**. 2(5): 361-369.

[22] Jiang, H., *Experimental and numerical study of polymer scratch behavior*, in *Mechanical Engineering* **2009**, Texas A&M University: College Station, Texas.

[23] Pelletier, H., Gauthier, C., Schirrer, R., *Influence of the friction coefficient on the contact geometry during scratch onto amorphous polymers. Wear*, **2010**, 268(9-10): 1157-1169.

[24] Pelletier, H., Durier, A.-L., Gauthier, C., Schirrer, R., *Viscoelastic and elastic–plastic behaviors of amorphous polymeric surfaces during scratch. Tribology International*, **2008**. 41 (11): 975-984.

[25] Schirrer, R., Gauthier, C., Pelletier, H., *Experimental and finite-element analysis of scratches on amorphous polymeric surfaces. Proceedings of the Institution of Mechanical Engineers, Part J: Journal of Engineering Tribology*, **2008**. 222(3): 221-230.

[26] Pelletier, H., Gauthier, C., Schirrer, R., *Strain and stress fields during scratch tests on amorphous polymers: Influence of the local friction. Tribology Letters*, **2008**. 32(2): 109-116.

[27]   Bucaille, J.L., Felder, E., Hochstetter, G., *Experimental and three-dimensional finite element study of scratch test of polymers at large deformations. Journal of Tribology*, **2004**. 126(2): 372-379.

[28]   Briscoe, B.J., Pelillo, E., Sinha, S.K., *Scratch hardness and deformation maps for polycarbonate and polyethylene. Polymer Engineering & Science*, **1996**. 36(24): 2996-3005.

[29]   Briscoe, B.J., Evans, P.D., Pellilo, E., Sinha, S.K., *Scratching maps for polymers. Wear*, **1996**. 200(1-2): 137-147.

[30]   Briscoe, B.J., Pelillo, E., Ragazzi, F., Sinha, S.K., *Scratch deformation of methanol plasticized poly(methylmethacrylate) surfaces. Polymer*, **1998**. 39(11): 2161-2168.

[31]   Browning RL, Jiang H, Moyse A, Sue HJ, Iseki Y, Othnari K, *Journal of Material Science* **2008**, 43, 1357-1370.

[32]   Moghbelli E, Sun L, Jiang H, Boo WJ, Sue H-J, *Polymer Engineering and Science* **2009**, 36, 483-494.

[33]   Xiang C, Sue HJ, Chu J, Masuda K. *Polymer Engineering and Science* **2001**; 41: 23 − 31.

[34]   Jardret V, Morel P. *Progress in Organic Coatings* **2003**; 48: 322 − 331.

[35]   Browning R, Jiang H, Moyse A, Sue HJ, Iseki Y, Ohtani K, Ijichi Y. *Journal of Materials Science* **2008**; 43: 1357 − 1365.

[36]   Jiang H, Browning R, Fincher J, Gasbarro A, Jones S, Sue HJ. *Applied Surface Science* **2008**; 254: 4494 − 4499.

[37]   Hadal R, Misra RDK. *Materials Science and Engineering A − Structures* **2004**; 398: 252 − 261.

[38]   Moghbelli E, Sun L, Jiang H, Boo WJ, Sue HJ. *Polymer Engineering and Science* **2009**; 49: 483 − 490.

[39]   Mudaliar A, Yuan Q, Misra RDK. *Polymer Engineering and Science* **2006**; 46: 1625 − 1634.

[40]   Yuan Q, Ramisetti N, Misra RDK. *Acta Materialia* **2008**; 56: 2089 − 2100.

[41]   Dasari A, Yu ZZ, Mai YW. *Materials Science and Engineering* **2009**; 63: 31 − 80.

[42]   Browning R, Sue HJ, Minkwitz R, Charoensirisomboon, P, *Polymer Engineering and Science* **2011**; 51, 2282-2293.

[43]   Liang YL; Sue H.J.; Minkwitz R.; *Journal of Applied Polymer Science* **2012**, 126, 1088-1096.

[44]   Tabor D, Briscoe BJ, *Journal of Applied Physics* **1956**, 7, 159-170.

[45]   Guevin PR, *Journal of Coatings Technology* **1995**, 67, 61-66.

[46]   Kody RS, Martin DC, *Polymer Engineering and Science* **1996**, 36, 298-309.

[47]   Chu J, Rumao L, Coleman B, *Polymer Engineering and Science* **1998**, 38, 1906-11.

[48]   Krupicka A, Johnansson M, Hult A, *Progress in Organic Coatings* **2003**, 46, 32-40.

[49]   Wong M, Lim GT, Moyse A, Reddy JN, Sue HJ, *Wear* **2004**, 256, 1214-22.

[50]   ASTM International. ASTM D7027-05, *Annual Book of ASTM Standards*; **2005**.

[51]   Browning R, Lim GT, Moyse A, Sue HJ, Chen H,Earls JD,,*Surface Coatings Technology* **2006**; 201, 2970-77.

[52]   Jiang H, Lim GT, Whitcomb J, Sue HJ, *Journal of Polymer Science Polymer Physics* **2007**, 45, 1435-44.

[53]   Jiang H, Browning R, Fincher J, Gasbarro A, Jones S, Sue HJ, *Applied Surface Science* **2008**; 254, 4494-54.

[54]   Browning RL, Jiang H, Moyse A, Sue HJ, Iseki Y, Othtani K, Ijichi Y, *Journal of Materials Science* **2008**, 43, 1357-64.

[55]   Moghbelli E, Browning RL, Boo WJ, Hahn SF, Feick LJE, Sue HJ, *Tribology International* **2008**, 41, 425-37.

[56]   Jiang H, Browning RL, Sue HJ, *Polymer* **2009**, 50, 4056-61.

[57]   Moghbelli E, Sun L, Jiang H, Boo WJ, Sue HJ, *Polymer Engineering and Science* **2009**, 36, 483.

[58]   Hossain MM, Browning RL, Minkwitz R, Sue HJ,  *Tribology Letters* **2012,** *47*, 113-122.

[59]   Hossain MM, Jiang H, Sue HJ, *Wear.* **2011,** *270*, 751.

[60]   Hossain MM, Minkwitz R, Sue HJ, *Polymer Engineering Science* **2013,** *53*, 1405.

[61]   Briscoe BJ, *Tribology International* **1998**, 31, 121.

[62]   Briscoe BJ, Pelillo E, Sinha SK, *Polymer Engineering and Science* **1996**, 36, 2996.

[63]   Maeda K, Bismarck A, Briscoe BJ, *Wear* **2005**, 259, 651.

[64]   Kim H, Keskkula H, Paul DR, *Polymer* **1990**, 31, 869.

[65]   Pelletier HA, Durier L, Gauthier C, Schirrer R, *Tribology International* **2008**, 41 975–984.

[66]   Pelletier H, Gauthier C, Schirrer R, *Journal of Engineering Tribology* **2008**, 222, 221–230.

130

[67]    Pelletier H, Gauthier C, Schirrer R, *Tribology Letters* **2008**, 32, 109–116.

[68]    Bucaille JL, Gauthier C, Felder E, Schirrer R, *Wear* **2006**, 260, 803–814.

[69]    Steebrink AC, Litvinov VM, Gaymans RJ, *Polymer* **1998**, 39, 4817.

[70]    McKee GE, Kistenmacher A, Goperrissen H, Breulmann M, In Modern Styrenic Polymers; Scheirs, J.; Priday, D., Ed.; Wiley, **2002**.

[71]    Kang MS, Kim CK, Lee JW, *Journal of Rheology* **2006**, 18, 1, 1-14.

[72]    Bucknall CB, Smith RR, *Polymer* **1965**; 6: 437-44.

[73]    Schmitt JA, *Journal of Applied Polymer Science* **1968**; 12, 533-46.

[74]    Bucknall CB, Ayre DS, Dijkstra DJ, *Polymer* **2000**; 41: 5937-50.

[75]    Bucknall CB, *Toughened Plastics*, Applied Science Publishers, London **1977**; Ch.7-10.

[76]    Katime I, Quintana JR, Price C, *Material Letters* **1995**; 22: 297-306.

[77]    Beguelin PH, Plummer JG, Kausch HH, *Polymer Blends and Alloys*, New York **1999**, 549.

[78]    Heckmann W, Mckee GE, Ramsteiner F, *Macromolecules Symposium* **2004**; 214: 85-92.

[79]    Tang H, Martin DC, *Journal of Materials Science* **2003**; 38, 803-809.

[80]    Blaga A, Yamasaki RS, *Durability Building Materials* **1986**; 4: 21–34.

[81]    Ramsteiner F, Mckee GE, Heckmann W, Fischer W, Fischer M, *Acta Polymer* **1997**; 48: 553-561.

[82]    Chang MCO, Nemith RL, *Journal of Applied Polymer Science* **1996**; 61:1003-1011.

[83]    Ramteke AA, Maiti SN, *Journal of Applied Polymer Science* **2010**; 116(1): 486–492.

[84]    Ramsteiner F, Heckmann W, McKee GE, Breulmann M, *Polymer* **2002**; 43: 5995.

[85]    Huang JJ, Keskkula H, Paul DR, *Polyme*r **2004**; 45: 4203-4215.

[86]    J. K. Fink, *Acrylonitrile/Styrene/Acrylate Polymers, in Handbook of Engineering and Specialty Thermoplastics: Polyolefins and Styrenics* **2010**, John Wiley & Sons, Inc., Hoboken, NJ, USA.

[87]    ASTM International, ASTM D7027-05, *Annual Book of ASTM Standards*, **2005**.

[88]    M. Wong, G. T. Lim, A. Moyse, J. N. Reddy, H. J. Sue, *Wear* **2004**; 256: 1214-1227.

[89]   R.L Browning, G.-T. Lim, A. Moyse, H.-J. Sue, H. Chen and J.D. Earls, *Surface & Coatings Technology* **2006**; 201: 2970-2976.

[90]   H. Jiang, G.T. Lim, J.D. Whitcomb, and H.-J. Sue**,** *Journal of Polymer Science Polymer Physics* **2007**; 45: 1435-1447.

[91]   H. Jiang R. Browning, J. Fincher, A. Gasbarro, S. Jones, H. J. Sue, *Applied Surface Science* **2008**; 254: 4494-4499.

[92]   R. L. Browning, H. Jiang, A. Moyse, H. J. Sue, Y. Iseki, K. Othtani, Y. Ijichi, *Journal of Material Science* **2008**; 43: 1357-1365.

[93]   E. Moghbelli, R. L. Browning, W. J. Boo, S. F. Hahn, L.J.E. Feick, H. J. Sue, *Tribology International* **2008**; 41: 425-433.

[94]   H. Jiang, R. Browning, H. J. Sue, *Polymer* **2009**; 50: 4056-4065.

[95]   E. Moghbelli, L. Sun, H. Jiang, W. J. Boo, H. J. Sue, *Polymer Engineering & Science* **2009**; 36: 483-490.

[96]   B. J. Briscoe, *Tribology International* **1998**; 31: 121-126.

[97]   B. J. Briscoe, E. Pelillo, S. K. Sinha, *Polymer Engineering & Science* **2006**; 36: 2996-3005.

[98]   K. Maeda, A. Bismarck, B. J. Briscoe, *Wear* **2005**; 259: 651-660.

[99]   H. Jiang, R. L. Browning, M. M. Hossain, H. J. Sue, *Applied Surface Science* **2010**; 256: 6324-6329.

[100]  T. Scherzer, *Vibrational Spectroscopy* **2002**; 29: 139-143.

[101]  M. Akay, S. Ozden*, Journal of Material Science* **1995**; 30: 3358-3368.

[102]  Y.L. Liang, H.J. Sue, R. Minkwitz, "Rubber Content Effect on Scratch Behavior in Acrylonitrile Styrene Acrylate Copolymers *Journal of Applied Polymer Science*, accepted.

[103]  Chi-san Wu, "*Handbook of size exclusion chromatography and related techniques*" **2001**; 91: 19.

[104]  L. Zhang, J. C. M. Li, *Material Science & Engineering* **2003**; 44: 182-189.

[105]  ASTM International, ASTM D638, *Annual Book of ASTM Standards*, **1998**.

[106]  R. Browning, H. J. Sue, R. Minkwitz, P. Charoensirisomboon, *Polymer Engineering & Science* **2011**; 51: 2282-2294.

[107]  G. T. Lim, M. Wong, J.N. Reddy, H. J. Sue, *Journal of Coatings Technology and Research* **2005**; 25: 361-369.

[108]  M. Sargent, J. L. Koenig, and N. L. Maecker, *Applied Spectroscopy* **1991**; 45: 1726-1732.

[109]  Modern Styrenic Polymers book J. Scheirs, D. Priddy, "*Modern Styrenic Polymers*" Wiley: West Sussex, **2003**.

[110]  L. D. Coxon, and J. R. White, *Polymer Engineering & Science* **1980**; 20: 230–236.

[111]  M. M. Hossain, H. Jiang, H. J. Sue, *Wear* **2011**; 270: 751-759.

[112]  K. Hirano, S. Tamura, and T. Kanai, *Journal of Applied Polymer Science* **2007;** 105: 2416-2426.

[113]  K. Hirano, S. Tamura, Y. Obata, and T. Kanai, *Journal of Applied Polymer Science* **2008**; 108: 76-84.

[114]  J. K. Fink, Acrylonitrile/Styrene/Acrylate Polymers, in *Handbook of Engineering and Specialty Thermoplastics: Polyolefins and Styrenics*, John Wiley & Sons, Inc., Hoboken, NJ, USA, **2010**.

[114]  ASTM International, ASTM D7027-05, *Annual Book of ASTM Standards*, **2005**.

[115]  M. Wong, G. T. Lim, A. Moyse, J. N. Reddy, H. J. Sue, *Wear* **2004**; 256: 1214-1227.

[116]  R.L Browning, G.-T. Lim, A. Moyse, H.-J. Sue, H. Chen and J.D. Earls, *Surface & Coatings Technology* **2006**; 201: 2970-2976.

[117]  H. Jiang, G.T. Lim, J.D. Whitcomb, and H.-J. Sue**,** *Journal of Polymer Science* **2007**; 45: 1435-1447.

[118]  H. Jiang R. Browning, J. Fincher, A. Gasbarro, S. Jones, H. J. Sue, *Applied Surface Science* **2008**; 254: 4494-4499.

[119]  R. L. Browning, H. Jiang, A. Moyse, H. J. Sue, Y. Iseki, K. Othtani, Y. Ijichi, *Journal of Material Science* **2008**; 43: 1357-1365.

[120]  E. Moghbelli, R. L. Browning, W. J. Boo, S. F. Hahn, L.J.E. Feick, H. J. Sue, *Tribology International* **2008**; 41: 425-433.

[121]  H. Jiang, R. Browning, H. J. Sue, *Polymer* **2009**; 50: 4056-4065.

[122]  E. Moghbelli, L. Sun, H. Jiang, W. J. Boo, H. J. Sue, *Polymer Engineering & Science* **2009**; 36: 483-490.

[123]  B. J. Briscoe, *Tribology International* **1998**, 121-126.

[124]  B. J. Briscoe, E. Pelillo, S. K. Sinha, *Polymer Engineering & Science* **2006**; 36 (2996) 2996-3005.

[125]  K. Maeda, A. Bismarck, B. J. Briscoe, *Wear* **2005**; 15:651-660.

[126]  H. Jiang, R. L. Browning, M. M. Hossain, H. J. Sue, *Applied Surface Science* **2010**; 256: 6324-6329.

[127]  T. Scherzer, *Vibrational Spectroscopy* **2002;** 29: 139-145.

[128]  M. Akay, S. Ozden, *Journal of Material Science* **1995**; 30: 3358-3368.

[129]  Y.L. Liang, H.J. Sue, R. Minkwitz, "Rubber Content Effect on Scratch Behavior in  Acrylonitrile Styrene Acrylate Copolymers" *Journal of Applied Polymer Science*, accepted.

[130]  Chi-san Wu, "*Handbook of size exclusion chromatography and related techniques*" **1991**; 21: 19-21.

[131]  L. Zhang, J. C. M. Li, *Material Science & Engineering* **2003;** 344: 182-189.

[132]  ASTM International, ASTM D638, *Annual Book of ASTM Standards*, **1998**.

[133]  R. Browning, H. J. Sue, R. Minkwitz, P. Charoensirisomboon, *Polymer Engineering & Science* **2011**; 51: 2282-2294.

[134]  G. T. Lim, M. Wong, J.N. Reddy, H. J. Sue, *Journal of Coatings Technology and Research* **2005**; 25: 361-369.

[135]  M. Sargent, J. L. Koenig, and N. L. Maecker, *Applied Spectroscopy* **45**, 1726-1732 (1991)

[136]  Modern Styrenic Polymers book J. Scheirs, D. Priddy, "Modern Styrenic Polymers" Wiley: West Sussex, **2003**.

[137]  L. D. Coxon, and J. R. White, *Polymer Engineering & Science* **1980**; 20: 230–236.

[138]  M. M. Hossain, H. Jiang, H. J. Sue, *Wear*, **2011**, 270:751-759.

[139]  K. Hirano, S. Tamura, and T. Kanai, *Journal of Applied Polymer Science* **2007**, 105: 2416-2426.

[140]  Keskkula H, Simpson GM, Dicken FL, *Society of Plastics Engineers Preprints Annual Technology Conference* **1966**; 12: XV-12.

[141]  Namiro B, Mozeli H; *Plastics* **1965**; 38: 708-711.

[142]  Nakamura H, Nakamura T, Noguchi T, Imagawa K. Photodegradation of PEEK sheets under tensile stress. *Polymer Degradation* **2006**;91:740.

[143]  Timoteo GAV, Fechine GJM, Rabello MS. Stress cracking and photodegradation behavior of polycarbonate: The combination of two major causes of polymer failure. *Polymer Engineering Science* **2008**;48:2003-10.

[144]  Sousa AR, Amorim KLE, Medeiros ES, Melo TJA, Rabello MS. Evaluation of photodegradation in LDPE-modified starch blends. *Polymer Degradation* **2006**;91:1504-1510.

[145]  Jiang H, Browning R, Liu P, Chang TA, Sue H-J. Determination of Epoxy Coating Wet-Adhesive Strength Using a Standardized ASTM/ISO Scratch Test, *Journal of Coating Technology* **2011**;8:255-63.

[146] Brostow W, Kovacevic V, Vrsaljko D, Whitworth J. Hydroxyapatite based hybrid dental materials with controlled porosity and improved tribological and mechanical properties. *Journal of Materials Education* **2010**;32:273-280.

[147] Rabek JF. *Polymer photodegradation: mechanisms and experimental methods*. London: Chapman and Hall; **1995**.

[148] Brostow W, Deborde J-L, Jaklewicz M, Olszynski P. Tribology with emphasis on polymers: friction, scratch resistance and wear. *Journal of Materials Education* **2003**;25:119-32.

[149] Myshkin NK, Petrokovets MI, Kovalev AV. Tribology of polymers: Friction, wear and mass transfer. *Tribology International* **2005**;38:910.

[150] Hainsworth SV, Kilgallon PJ. Temperature-variant scratch deformation response of automotive paint systems. *Progress in Organic Coatings* **2008**;62:21-33.

[151] Van der Heide E, Lossie CM, van Bommel KJC, Reinders SAF, Lenting HBM. Experimental Investigation of a Polymer Coating in Sliding Contact with Skin-Equivalent Silicone Rubber in an Aqueous Environment. *Tribology* **2010**;53:842-7.

[152] Starczewski L, Szumniak J. Mechanisms of transferring the matter in a friction process in a tribology system: polymeric composite-metal. *Surface Coating Technologies* **1998**;100:33-7.

[153] Wilenski M. The improvement of the hygrothermal and mechanical properties of bismaleimide and K3B/IM7 carbon fiber. *PhD Thesis*. Michigan State University, **1997**.

[154] Cinquin J, Abjean P. Moisture diffusion behavior in bismaleimide resin subjected to hygrothermal cycling. *International SAMPE Symposium* **1993**;38:1539-51.

[155] Biney PO, Zhong Y, Zhou J. *International SAMPE Symposium* **1998**;43:120-126.

[156] Lin YC, Chen X. Moisture sorption-desorption-resorption characteristics and its effect on the mechanical behavior of the epoxy system. *Polymer* **2005**;46:1994-2003.

[157] Li Y, Miranda J, Sue H-J.Morphology and Mechanical Properties of Blown Film of LDPE/LLDPE blend. *Polymer Engineering and Science* **2002;** 42: 375-81.

[158] Li Y, Miranda J, Sue H-J. Hygrothermal Diffusion Behavior in Bismaleimide Resin. *Polymer* **2001**;42:7791-9.

[159] Banyay R. Weathering Performance Advantages of Mold-In-Color Acrylic Versus coated Plastics for Exterior Trim Applications. *SPE ANTEC Technical Paper* **2009**;2009-01-0350.

[160] Banyay R. Weathering Performance Advantages of Mold-In-Color Acrylic Versus Coated Plastics for Exterior Trim Applications-2. *SAE Technical Paper* **2009**;2009-01:1292-99.

[161]    Banyay R. Physical Property Retention of Exterior Automotive Mold-In-Color Plastics After UV Exposure. *SAE Technical Paper* **2011**; 2011-01:1495-99.

[162]    Banyay R & Pope T. Optimization of Acrylic Capped ABS Coextruded Systems for Sheet Applications. *SPE Thermoforming Quarterly* **2004**; 23:2: 111-117.

[163]    Smith LSA, Chen C C, Sauer JA. The effect of water on the tensile yield of polystyrene. *Polymer* **1982**; 23: 1540–3.

[164]    Shen J, Chen CC, Sauer JA. Effects of sorbed water on properties of low and high molecular weight PMMA:1. Deformation and fracture behavior. *Polymer* **1985**; 26: 511–8.

[165]    Smith LSA, Sauer JA. Sorbed water and mechanical behavior of poly(methyl methyacrylate). *Plastics Rubbers Composites Processing and Application* **1986**: 6; 57–65.

[166]    Hill RG, Bates JF, Lewis TT, Rees NJ. The fracture of acrylic polymers in water. *Material Science* **1984**; 19: 1904–16.

[167]    Hunt DG, Darlington MW. Accurate measurement of creep of nylon-6,6 at constant temperature and humidity. *Polymer* **1978**: 19; 977–983.

[168]    Chen CC, Shen J, Sauer JA. Effects of sorbed water on properties of low and high molecular weight PMMA: Fatigue performance. *Polymer* **1985**; 26: 89–93.

[169]    Ishiyama C, Higo Y. Effects of humidity on Young's modulus in poly(methyl methacrylate). *Journal of Polymer Science Part B*: *Polymer Physics* **2002**; 40: 460-5.

[170]    Masai P, Nicodemo L, Migliaresi C, Nicolais L. *Polymer Communications* **1984***; 25: 331–3.*

[171]    Smith LSA, Shmitz V. The effect of water on the glass transition temperature of poly(methyl methacrylate) *Polymer* **1988***; 29: 1871–8.*

[172]    Drotning WD, Roth EP. Effects of moisture on the thermal expansion of PMMA; *Journal of Materials Science* **1989**; 24: 3137 –40.

[173]    Barrie JA, Platt B. The diffusion and clustering of water vapour in polymers. *Polymer* **1963**; 4: 303-13.

[174]    Masko U, et al. Water absorption of poly(methyl methacrylate) containing 4-methacryloxyethyl trimellitic anhydride. *Biomaterials* **2003**; 24; 8:1381-87.

[175]    Rouse PE. Diffusion of Vapors in Films. *Journal of American Chemical Society* **1947**; 69: 1068-1082.

[176]    Barrer RM, Barrie JA. Sorption and diffusion in ethyl cellulose. Part IV. Water in ethyl cellulose. *Journal of Polymer Science* **1958**; 28: 377-86.

[177]    Rogers CE, Stannett V, Szwarc M. The sorption, diffusion, and permeation of organic vapors in polyethylene. *Journal of Polymer Science* **1960**; 45: 61-70.

[178] Zimm BH, Lundberg JL. Sorption of Vapors by High Polymers. *Journal of Physical Chemistry* **1956**; 60: 425-433.

[179] Turner DT. Polymethyl methacrylate plus water: sorption kinetics and volumetric changes. *Polymer* **1982**; 23: 197-202.

[180] ASTM D7027, **2005**, *ASTM International*.

[181] ISO 19252, **2008**, *ISO International*.

[182] Barnay R. Improved Scratch and Chemical Resistance Acrylic for Automotive Mold-In-Color Applications. *SPE ANTEC* 2012; 126-135.

[183] Jiang H, Browning R, Fincher J, Gasbarro A, Jones S, Sue H-J. Influence of surface roughness and contact load on friction coefficient and scratch behavior of thermoplastic olefins. *Applied Surface Science* **2008**; 254: 4494-99.

[184] Hossain MM, Browning R, Minkwitz R, Sue H-J. Effect of Asymmetric Constitutive Behavior on Scratch-induced Deformation of Polymers. *Tribology Letter* **2012**; 47: 113-122.

[185] Browning R, Minkwitz R, Charoensirisomboon P, Sue H-J. Influence of Humidity Exposure on the Scratch Behavior of Polystyrene-Acrylonitrile Random Copolymers. *Journal of Material Science* **2011**; 46: 5790-7.

[186] Mittal KL, Ed. *Contact Angle, Wettability and Adhesion*. Utrecht: VSP; **1993**.

[187] Dias CR, Rosa MJ, Norberta de Pinho M. Structure of water in asymmetric cellulose ester membranes—and ATR-FTIR study. *Journal of Membrane Science* **1998**; 138:2: 259-67.

[188] Saijo K, Arimoto O, Hashimoto T, Fukuda M, Kawai H. Moisture sorption mechanism of aromatic polyamide fibres: diffusion of moisture into regular Kevlar as observed by time-resolved small-angle X-ray scattering technique. *Polymer* **1994**; 35:3: 496-503.

[189] Kitano H, Ichikawa K, Ide M, Fukuda M, Mizuno W. Fourier Transform Infrared Study on the State of Water Sorbed to Poly(ethylene glycol) Films;, *Langmuir* **2001**; *17* (6), 1889-95.

[190] Drotning WD, Roth EP. Effects of moisture on the thermal expansion of poly(methylmethacrylate). *Journal of Materials Science*, **1989**; 24: 3137–40.

[191] Thomas AM. Moisture permeability, diffusion and sorption in organic film-forming materials. *Journal of Applied Chemistry*, **1951**; 1: 141-58.

[192] Masko U, et al. Water absorption of poly(methyl methacrylate) containing 4-methacryloxyethyl trimellitic anhydride. *Biomaterials* **2003**; 24: 1381-7.

[193] Jiang H, Browning RL, Fincher J, Gasbarro A, Jones S, Sue H-J. "Influence of Surface Roughness and Contact Load on Friction Coefficient and Scratch Behavior of Thermoplastic Olefins. *Applied Surface Science* **2008**; 254: 4494-9.

[194]   Jiang H, Browning RL, Sue H-J. Understanding Scratch Damage Mechanisms of Polymers. *Polymer* **2009**; 50:4056-65.